Georg Spanring

Structural analysis and determination of charge carrier properties of semiconductor devices by measurements of optical beam induced currents created by near infrared radiation

MASTER THESIS

For obtaining the academic degree
Diplom-Ingenieur

Master Programme of
Technical Physics

Graz University of Technology

Supervisor:
Univ.-Prof. Ph.D. Peter Hadley
Institute of Solid State Physics

Graz, December 2014

Abstract

In the semiconductor industry high demands on the quality and reliability of devices are made. At the same time the requirements for the efficiency in fabrication processes constantly increase. To maintain and improve the high quality level, methods to analyze and characterize semiconductors have to be refined systematically and new methods have to be developed.

Optical beam induced current (OBIC) measurements can be used to determine the structure of semiconductor devices and obtain charge carrier properties. In this method the device is illuminated with light, which leads to a measureable current, taking advantage of the photovoltaic effect. Radiation created by a near infrared laser is used. If a device is scanned point by point, the position of pn-junctions can be revealed and abnormalities can be identified. The method has been applied on several devices to visualize their structure. Furthermore the vertical position of pn-junctions buried in the substrate was determined. In this method usually laser light with photon energies above the band gap of the investigated semiconductor is used. In this thesis it could be demonstrated that the experiment is practicable also by using laser light with photon energies slightly beneath the band gap energy and this offers additional possibilities.

Moreover, the behavior of reverse biased junctions was investigated. From these measurements, conclusions about the doping concentrations were made. That delivers additional options in qualification. Advanced analysis allow the determination of charge carrier properties like the diffusion length of minority charge carriers, which was obtained.

EIDESSTATTLICHE ERKLÄRUNG

AFFIDAVIT

Ich erkläre an Eides statt, dass ich die vorliegende Arbeit selbstständig verfasst, andere als die angegebenen Quellen/Hilfsmittel nicht benutzt, und die den benutzten Quellen wörtlich und inhaltlich entnommenen Stellen als solche kenntlich gemacht habe. Das in TUGRAZonline hochgeladene Textdokument ist mit der vorliegenden Masterarbeit/Diplomarbeit/Dissertation identisch.

I declare that I have authored this thesis independently, that I have not used other than the declared sources/resources, and that I have explicitly indicated all material which has been quoted either literally or by content from the sources used. The text document uploaded to TUGRAZonline is identical to the present master's thesis/diploma thesis/doctoral dissertation.

____________________________ ________________________________

Datum / Date Unterschrift / Signature

Acknowledgement

I would like to thank Univ.-Prof. Ph.D. Peter Hadley for guiding me through the thesis. I also want to thank my Infineon supervisor Dipl.-Ing. Werner Heincz and the whole failure analysis team of Infineon Villach for providing me help and support. I want to thank Dipl.-Ing. Stefan Kirnstoetter and Dipl.-Ing. Martin Facinelli of the TU Graz for their scientific advice. I also want to thank my family and friends for supporting me during the whole time of my studies.

Georg Spanring, Graz December 2014

Contents

1 List of symbols and abbreviations **7**

2 Fundamentals **10**
- 2.1 Interaction of light with matter . . . 10
  - 2.1.1 Reflection, refraction, transmission . . . 10
  - 2.1.2 Absorption . . . 11
- 2.2 Gaussian laser beam . . . 13
- 2.3 Semiconductor fundamentals . . . 14
  - 2.3.1 Generation, diffusion, (surface) recombination and carrier lifetime . . . 15
  - 2.3.2 pn-junction . . . 18
  - 2.3.3 Photovoltaic effect . . . 19
  - 2.3.4 Seebeck effect . . . 20
- 2.4 Determination of the diffusion length of minority charge carriers . . . 21
- 2.5 Important semiconductor devices . . . 22
  - 2.5.1 Metal-oxide-semiconductor fieldeffecttransistor (MOSFET) . . . 22
  - 2.5.2 Insulated gate bipolar transistor (IGBT) . . . 23
  - 2.5.3 Micro electro mechanical systems (MEMS) . . . 23

3 Methods **24**
- 3.1 Equipment . . . 24
- 3.2 PHEMOS-1000 . . . 25
  - 3.2.1 Tool specifications . . . 27
  - 3.2.2 Optimum configuration of the PHEMOS-1000 parameters for OBIC experiments . . . 28
  - 3.2.3 Manually oparated stage control . . . 32
  - 3.2.4 Data evaluation from OBIC images . . . 33
- 3.3 Sample preparation . . . 34
  - 3.3.1 Preparation of wafers . . . 34
  - 3.3.2 Preparation of cross sections . . . 34

4 Measurements on TPMS devices **36**
- 4.1 Revealing structures . . . 37
  - 4.1.1 Depth sensitive measurements . . . 39
- 4.2 Diffusion length measurements . . . 45
  - 4.2.1 Comparison of two possibilities to obtain the diffusion length . . . 48
  - 4.2.2 Comparison of diffusion length measurements with the 1064 nm and the 1300 nm laser . . . 50
  - 4.2.3 Line scans with various intensities . . . 52
  - 4.2.4 Comparison of line scans done at different positions of the p-well . . . 53
  - 4.2.5 Deriving a function including the laser spot size . . . 53

5 OBIC measurements on proton doped samples **55**
5.1 EDMR . . . 55
5.1.1 Determination of the depletion width and the concentration of dopants of EDMR8 (not proton doped) . . . 55
5.1.2 Determination of the diffusion length of minority charge carriers on EDMR8 (not proton implanted) . . . 58
5.1.3 Determination of the depletion width and the concentration of dopants of proton doped samples . . . 59
5.2 P116 . . . 62

6 OBIC measurements on an EMCON diode **63**

7 Structure visualization on various devices using OBIC **65**
7.1 CoolMOS^{TM} . . . 65
7.2 Insulated gate bipolar transistor (IGBT) . . . 68
7.3 S-FET2 . . . 70
7.4 S-FET3 . . . 72

8 Conclusive discussion and perspectives **73**
8.1 Structural analysis of semiconductor devices . . . 73
8.2 Determination of charge carrier properties . . . 74

Chapter 1

List of symbols and abbreviations

List of symbols

α	Absorption coefficient
$\tilde{\alpha}$	Surface recombination parameter
ϵ_0	Vacuum permittivity $[F/m]$
ϵ_r	Relative permittivity
Θ	Angle of propagation direction in relation to the vertical
κ	Extinction coefficient
μ	Mobility $[m^2/Vs]$
μ_g	Expected value of Gaussian function
ν	Frequency $[1/s]$
λ	Wavelength$[nm]$
σ	Standard deviation
τ_n	Minority carrier lifetime (electrons in p-semiconductor) $[s]$
τ_p	Minority carrier lifetime (holes in n-semiconductor) $[s]$
ω	angular frequency $[rad/s]$
c	Phase velocity $[m/s]$
D	Diffusion constant $[m^2/s]$
e	Elementary charge $[C]$
E_C	Maximum conduction band energy $[eV]$
E_F	Fermi energy $[eV]$
E_g	Band gap energy $[eV]$
E_p	Phonon energy $[eV]$
E_V	Minimum valence band energy $[eV]$
G	Generation term at non-equilibrium $[1/m^3s]$
G_{therm}	Generation term at thermal equilibrium $[1/m^3s]$
h	Planck constant $[Js]$
I	Instensity $[W/m^2]$
I_0	Initial intensity $[W/m^2]$
I_{diff}	Diffusion current $[A]$
I_{max}	Maximum Current $[A]$
I_{spot}	Laser spot size related current $[A]$
j_n	Electron current density $[A/m^2]$
k	Fitting parameter diffusion length $[A]$
k_B	Boltzmann constant $[J/K]$
L	Minority charge carrier diffusion length [μm]
m^*	Effective mass $[kg]$
n	Index of refraction
$\tilde{n}$	Complex index of refraction

N_a	Number of acceptors
N_C	Effective density of states for electrons in the conduction band
N_d	Number of donors
n_n	Electron density
n_i	Intrinsic charge carrier density
n'_n	Change in the number of electrons from equilibrium
n_{n0}	Number of electrons at thermal equilibrium
N_V	Effective density of states for holes in the valence band
p_n	Hole density
p'_n	Change in the number of holes from equilibrium
p_{n0}	Number of holes at thermal equilibrium
P_r	Recombination probability
r	Distance to the pn-junction [μm]
R	Recombination term at non-equilibrium [$1/m^3s$]
r_p	Reflection coefficient, parallel
r_s	Reflection coefficient, perpendicular
R_p	Reflectance, parallel
R_s	Reflectance, perpendicular
R_{therm}	Recombination term at thermal equilibrium [$1/m^3s$]
t	Time [s]
T	Temperature [K]
t_p	Transmission coefficient, parallel
t_s	Transmission coefficient, perpendicular
T_p	Transmittance, parallel
T_s	Transmittance, perpendicular
V	Voltage [V]
V_{bi}	Built in voltage [V]
v_s	Surface recombination velocity [m/s]
V_{th}	Threshold voltage [V]
w	Width of Gaussian laser beam [m]
W	Depletion width [m]
w_0	Beam waist of a Gaussian laser beam [m]
z	Distance in z-direction [m]

List of abbreviations

BS	Backside
CA	Current amplifier
CCD	Charge coupled device
Com	Computer
CS	Cross section
Det	Detector
DU	Driving unit
DUT	Device under test
EBIC	Electrical beam induced current
EDMR	Electrically detected magnetic resonance
EMCON	Emitter controlled
EPI	Epitaxially grown layer
FET	Field effect transistor
FIB	Focused ion beam
FOX	Field oxide
FS	Frontside
GaN	Gallium nitride
HSCA	High sensitivity current amplifier
IC	Integrated circuit
IGBT	Insulated gate bipolar transistor
InGaAs	Indium Gallium Arsenide
NA	Numerical aperture
LSM	Laser scanning microscope
MEMS	Micro electro mechanical system
MOSFET	Metal-oxide-semiconductor fieldeffecttransistor
OBIRCH	Optical beam induced resistance change
OBIC	Optical beam induced current
OL	Objective lens
PEM	Photo emission microscopy
SCA	Standard current amplifier
SEM	Scanning electron microscopy
Si	Silicon
SRP	Scanning resistance probing
STM	Semi transparent mirror
TPMS	Tire pressure monitoring system
ZWOX	Interlayer dielectric (Zwischenoxid)

Chapter 2

Fundamentals

2.1 Interaction of light with matter

2.1.1 Reflection, refraction, transmission

If the surface of a material is illuminated, the incident light will partially be reflected. The transmitted part gets refracted. While passing through the medium, some of the light is absorbed. Therefore, the index of refraction $\tilde{n}$ contains a complex factor corresponding to the absorption.

$$\tilde{n} = n + i\kappa \tag{2.1}$$

The index of refraction is related to the relative permittivity ϵ_r by equation 2.2.

$$\sqrt{\epsilon_r} = n + i\kappa \tag{2.2}$$

The change in the propagation direction due to refraction dependent on the indices of refraction n_1 and n_2 of the involved media is expressed by Snell's law, where Θ_1 and Θ_2 are the angles of the propagation direction of the incident and the refracted beam measured from a line normal to the surface.

$$n_1 \cdot \sin(\Theta_1) = n_2 \cdot \sin(\Theta_2) \tag{2.3}$$

From Snell's law the angle Θ_2 can be expressed. The reflection r and the transmission t is then given by the Fresnel equations, where r_p, r_s and t_r, t_s describe the reflection and the transmission. The indices s and p indicate the polarization of the incident beam (perpendicular s or parallel p) to the surface.

$$r_p = \frac{E_{rp}}{E_{ip}} = \frac{\sqrt{\epsilon_2}\cos(\Theta_1) - \sqrt{\epsilon_1}\cos(\Theta_2)}{\sqrt{\epsilon_2}\cos(\Theta_1) + \sqrt{\epsilon_2}\cos(\Theta_2)}, \qquad t_p = 1 - r_p \tag{2.4}$$

$$r_s = \frac{E_{rs}}{E_{is}} = \frac{\sqrt{\epsilon_2}\cos(\Theta_2) - \sqrt{\epsilon_1}\cos(\Theta_1)}{\sqrt{\epsilon_1}\cos(\Theta_1) + \sqrt{\epsilon_2}\cos(\Theta_2)} \qquad t_s = 1 - r_s \tag{2.5}$$

The transmission is given by $t = 1 - r$ due to conservation of energy for both contributions. The reflection and transmission coefficients are then given by equation 2.6.

$$R_p = |r_p|^2, \qquad T_p = 1 - R_p, \qquad R_s = |r_s|^2 \qquad T_s = 1 - R_s \tag{2.6}$$

2.1.2 Absorption

For the light which is transmitted through the surface and propagates through the material, the wavelength of the beam and the optical properties of the material will determine the absorption. The decay of the intensity $I(r)$ of the incident beam I_0 due to absorption as it covers a certain distance r inside a material is described by the Beer-Lambert Law:

$$I(r) = I_0 \exp(-\alpha r) \tag{2.7}$$

The absorption coefficient α is dependent on the present absorption processes. It is related to the imaginary part of the complex index of refraction κ by the relationship 2.8.

$$\alpha = -\frac{2\kappa\omega}{c} \tag{2.8}$$

In this thesis measurements on silicon semiconductor devices using two infrared lasers emitting light at wavelengths of 1064 nm and 1300 nm were done. In this case absorption depends on two main contributions.

The first is the inner photoelectric effect, a process that involves interband absorption. If the energy of the photon is higher than the band gap it can be absorbed by creating an electron hole pair. Silicon is an indirect semiconductor with a band gap of 1.12 eV at 300 K. This absorption process will therefore be present only for the first laser as its wavelength of 1064 nm corresponds to a photon energy of 1.16 eV while the photons emitted by the 1300 nm laser exhibit an energy of 0.92 eV. However, it is also possible that the 1300 nm laser is absorbed by interband absorption in silicon, e.g. at surface states. In an indirect semiconductor, the crystal momentum of the minimum energy of the conduction band and the maximum energy of the valence band differ. This means that in an absorption process momentum has to be transferred to the crystal lattice and therefore a phonon has to be generated or annihilated as conservation of momentum has to be fulfilled. For this reason the probability of the indirect, phonon assisted absorption process is lower than for the direct absorption process occurring in direct semiconductors like GaN[1]. A relationship between the Photon Energy and the absorption coefficient α for an indirect semiconductor is given by [Pan10]:

$$\alpha \propto \frac{(h\nu - E_g + E_p)^2}{exp(\frac{E_p}{k_B T}) - 1} + \frac{(h\nu - E_g - E_p)^2}{1 - exp(-\frac{E_p}{k_B T})} \tag{2.9}$$

Besides the energy of the incident beam $h\nu$, the band gap E_g and the phonon E_p it depends on the temperature T. This equation ignores all other sources of absorption.

The second process involved is intraband absorption, where transitions within the same band occur. In the case of an extrinsic semiconductor (e.g. n-doped) the photon is absorbed by conduction band electrons which will - in a further step - relax to the minimum conduction band energy by phonon interaction. This process becomes important especially if the silicon is highly doped. In this case a relationship is given by [Bar99] where the absorption coefficient exhibits a quadratic dependence on the wavelength λ but also depends on the doping concentration n (as it increases the number of free charge carriers at a certain temperature), the effective mass m^* and the mobility μ:

$$\alpha \propto \frac{\lambda^2 n}{m^* \mu} \tag{2.10}$$

An absorption spectrum of silicon at various doping levels for electrons and holes at 300 K can be found in [Sor87]. A graph for the transmission, which is related to the absorption as it is defined by the ratio between the transmitted and the initial intensity $T = \frac{I_T}{I_0}$, versus the

[1] Gallium nitride

wavelength for silicon at several doping levels is shown in figure 2.1. It can be seen that the transmittance is best for energies close beyond the band gap. It decreases rapidly as the wavelength of the photons gets beyond a certain value close to 1 μm. However, at a wavelength of 1064 nm silicon still exhibits a good transmittance. This can be a useful fact for some experiments done later in this thesis but also cause problems at others. The transmittance for the 1300 nm laser depends on the doping level, especially for high doping levels it decreases appreciably. In figure 2.1 it can be seen that at a doping level close to $10^{17}\,cm^{-3}$ there is already a strong effect of the doping concentration to the transmittance. If, instead of a semiconductor, a metal is illuminated both lasers will cause local heating. The metal will, of course, screen the layers below.

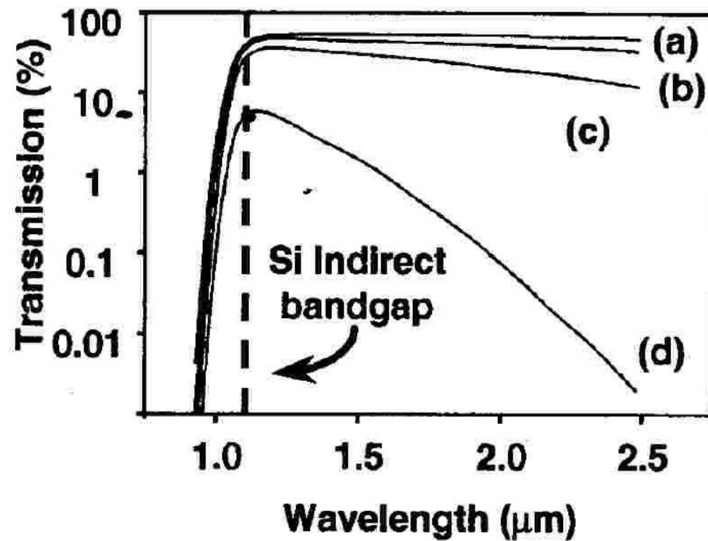

Figure 2.1: Transmission through 625 μm, p-doped Si of various doping concentrations x 10^{16} of (a) $1.5\,cm^{-3}$, (b) $33\,cm^{-3}$, (c) $120\,cm^{-3}$ and (d) $730\,cm^{-3}$ [Bar99]

Absorption at boundary surfaces

The surface of the semiconductor is an important parameter for absorption processes. It will be explained later while explaining recombination processes that it exhibits lots of surface defects, like dangling bonds and crystal defects and therefore states within the band gap, which lead to a shift in the Fermi energy. If there are occupied states within the band gap for which the distance to the conduction band is beyond the energy of the 1300 nm laser its photons can be absorbed via interband absorption processes. This leads to a higher absorption at the surface than in the bulk.

2.2 Gaussian laser beam

The lasers exhibit a Gaussian intensity distribution. An exact description can be found in reference [Hec02]. As the name suggests, the intensity profile perpendicular to the direction of propagation is Gaussian and given by the relationship

$$I = I_0 e^{-\frac{2r^2}{w^2}} \tag{2.11}$$

In equation 2.11 w is chosen to be 2σ, where σ is the standard deviation. Thus, the intensity will decay slowly above a certain distance to the center of the beam while within a defined cylinder most of the energy propagates. Therefore the half width, which is the distance to the center where the electric field is decayed from its maximum value E_0 to $\frac{E_0}{e}$, is defined as the boundary. As the intensity is the square of the electric field strength the condition is fulfilled for $w = r$ and equation 2.11 becomes

$$I = I_0 e^{-2} \tag{2.12}$$

For a Gaussian beam propagating in z direction in free space, the spot size $w(z)$ of the beam with respect to the distance z, the initial spot size ω_0 and a wavelength λ is given by

$$w(z) = w_0 \left[1 + \left(\frac{\lambda z}{\pi w_0^2} \right)^2 \right]^{\frac{1}{2}} \tag{2.13}$$

It exhibits a minimum $w(z)$ at $z = 0$ which is defined as beam waist. The beam will therefore broaden as it propagates inside a sample. Furthermore the ratio between the intensity and illuminated area will have a maximum at a certain position which is important for later measurements. Figure 2.2 shows the Gaussian intensity distribution in xy-, as well as the spot width in z-direction of the propagating beam.

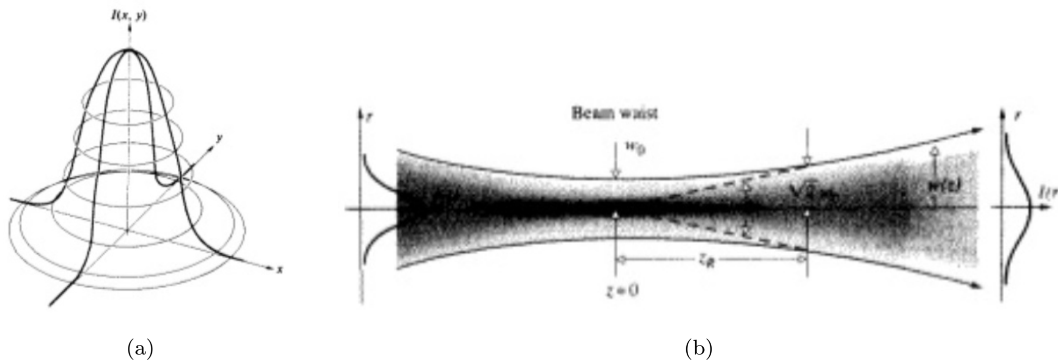

(a) (b)

Figure 2.2: (a) Intensity distribution of a Gaussian beam in the xy-plane (b) Broadening of the Gaussian beam when propagating in z-direction (beam waist w_0), figure reproduced from reference [Hec02]

2.3 Semiconductor fundamentals

As described in 2.1, semiconductors are materials which exhibit a gap in the band structure between the valence and the conduction band. The Fermi Energy E_F lies within this band gap. In contrast to isolating materials, the band gap for semiconductors E_G lies beneath 3 eV [Sin01]. This leads to a temperature dependent conductivity due to an occupation of states in the conduction band described by the Fermi function. If the density of states is known, the electron- and the hole density can be calculated [Kit04]. For intrinsic semiconductors, the electron density equals the hole density.

The properties of semiconductors are modified by doping. In the doping process impurities are incorporated in the crystal lattice. In the most common case elements out of the group in the periodic system next to the semiconductor are used, like boron or phosphorus in silicon. Those elements can be added in the course of the fabrication of the raw wafer (e.g. during the Czochralski process) or in a later production step using e.g. by implantation of ions or by adding the dopant during the epitaxial growth of new layers onto the substrate. The implanted elements exhibit the property that the number of valence electrons is different to the base material. If the elements are incorporated into the crystal structure they can act as donors or acceptors. A donor like phosphorus in silicon has an additional valence electron. This electron is only loosely bound and can be excited to the conduction band with low thermal energy (n-doping). An acceptor like boron in silicon has one electron less. In that case, the number of holes in the valence band is increased (p-doping). Doping introduces additional states in the band structure. The donor states are located close to the conduction band and the acceptor states close to the valence band. Therefore, the Fermi energy of the material is shifted from almost the middle of the band gap close to the conduction or the valence band, respectively.

While in an intrinsic semiconductor the electron- and hole density is equal, it strongly differs in extrinsic semiconductors at room temperature as nearly all of the additional charge carriers are excited. Therefore, in an n-type semiconductor, the concentration of electrons will exceed the concentration of holes by magnitudes. In a p-type semiconductor, the opposite behavior is found. It is distinguished between majority (electrons in an n-type or holes in a p-type semiconductor) and minority (holes in a n-type or electrons in a p-type semiconductor) charge carriers. The number of electrons in the conduction band and holes in the valence band (thus the number of majority charge carriers) is given by equation 2.14.

$$n = N_c \exp\left(\frac{E_F - E_C}{k_B T}\right), \qquad p = N_v \exp\left(\frac{E_V - E_F}{k_B T}\right) \tag{2.14}$$

N_c and N_v are the effective density of states. For extrinsic semiconductors under normal conditions $n \approx N_d$ and $p \approx N_a$ (N_d...concnetration of donors, N_a...concentration of acceptors). The number of minority charge carriers can be estimated by using the mass action law given by equation 2.15 which declares that the product of the number of electrons and holes equals the square of the intrinsic carrier concentration n_i.

$$np = N_v N_c \exp\left(-\frac{E_g}{k_B T}\right) = n_i^2 \tag{2.15}$$

As the number of majority charge carriers almost equals the number of dopants at room temperature, the number of minority charge carriers is then given by equation 2.16.

$$p = \frac{n_i^2}{N_d}, \qquad n = \frac{n_i^2}{N_a} \tag{2.16}$$

It should not go unnoticed that besides the described states a wide range of, desired and undesired, states can appear inside the band gap. Deep level defects are located near the middle of the band gap. For those defects, the thermal energy is not sufficient to move an electron or

hole to the conduction- or valence band. They can be used to compensate the dominant charge carrier type as they act as recombination centers. In silicon iron or copper impurities can cause those defects. Deep level defects can trap and release electrons or holes and can therefore act as donors or acceptors. Also crystallographic defects can be a source of such additional states. An overview of energy levels of states located within the band gap of silicon caused by several impurities is given in figure 2.3.

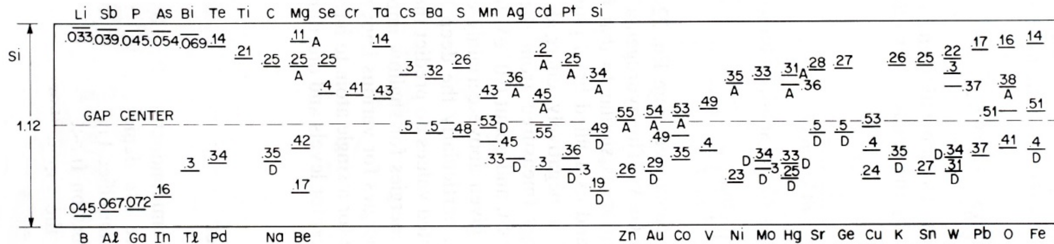

Figure 2.3: Overview of states localized within the band gap of silicon. Figure reproduced from reference [Sze85]

The previous considerations describe a semiconductor inside the bulk. The surface (or a phase interface) has to be considered separately. In general the surface exhibits numerous states within the band gap. They are caused by e.g. crystal defects, but also by the fact that atoms directly at the surface are not bound to bonding partners on all sides like inside the crystal. These are called dangling bonds. The Fermi energy lies in the middle of these states. This can be explained as it indicates the position where half of the states are occupied and electrons will occupy these additional states if they are present. As the surface states cause this shift in the Fermi energy, band bending and thus an electric field will occur at the surface. The presence of these surface states has an actual influence on measurements done in this thesis. This will be described more exactly in 2.4.

2.3.1 Generation, diffusion, (surface) recombination and carrier lifetime

Generation always indicates the creation of an electron hole pair in this chapter, thus the excitation of an electron from the valence band to the conduction band. In a semiconductor generation and recombination processes are always present. Without external perturbation, the concentration of charge carriers will assume a constant value, as a dynamic equilibrium, where the generation processes compensate the recombination processes, appears. For n and p semiconductors, the concentration of majority and minority charge carriers is given by the equations 2.14 and 2.15. Later experiments will add up to the fact that the carrier concentration is modified locally by generation processes. It is important to keep in mind that the majority carrier concentration strongly exceeds the number of minority carriers and therefore the semiconductor will be highly sensitive to a change in the minority carriers, which will be measured.

The generation of a minority charge carrier requires energy transfer. Two relevant ways of achieving this were already used in 2.1 and previously in this chapter. A local temperature change will lead to a change in the carrier density. The temperature dependence of the number of minority charge carriers comes with the value of n_i. Furthermore, light with an energy greater than the band gap can create electron hole pairs. In this process, the photon energy is transferred to the electron [Ein05]. This relationship is given by 2.17 where ν is the frequency of the incident photon.

$$h\nu \geq E_g \tag{2.17}$$

It has already been mentioned that for indirect semiconductors this process is phonon assisted. The charge carrier will, afterwards, diffuse through the material for a certain distance, performing a random walk, till it recombines. The length L covered is the 'diffusion length of minority charge carriers' and an important parameter in semiconductor industry. It is clear that the diffusion length is a statistical quantity which gives information about which distance an average minority charge carrier will cover before it recombines. It is related to the minority carrier lifetime τ with the diffusion coefficient D by equation 2.18:

$$L = \sqrt{D\tau} \tag{2.18}$$

The diffusion coefficient D is a material parameter and connected to the mobility by the Einstein relation [Ash88]. The diffusion length L cannot be measured directly, but can be obtained using the method described exactly in 2.4, which is one of the goals of this thesis. It is a key parameter in the semiconductor industry as it strongly depends on the presence of defects, which will lead to a decrease of L, undesirable e.g. for solar cells.

For the recombination, three processes are relevant. Radiative recombination occurs mainly in direct semiconductors, which do not exhibit a momentum difference between the maximum of the valence- and the minimum of the conduction band in their band structure. In this case a photon, corresponding to the energy difference between the two states, is emitted. In Auger recombination, the energy is transferred to another electron in the conduction band. For indirect semiconductors like silicon, Shockley-Read-Hall recombination is the dominant process ([Sho52],[Hal52]). The recombination process is assisted by a localized state within the band gap, which absorbs the electron momentum. The energy is transferred to phonons (thermal energy). The process is therefore radiationless. The energy levels in the crystal lattice come from defects, like dopants, but also deep level traps, which were referred to as recombination centers before. A graphical illustration of a generation-, diffusion- and recombination process is given by figure 2.4.

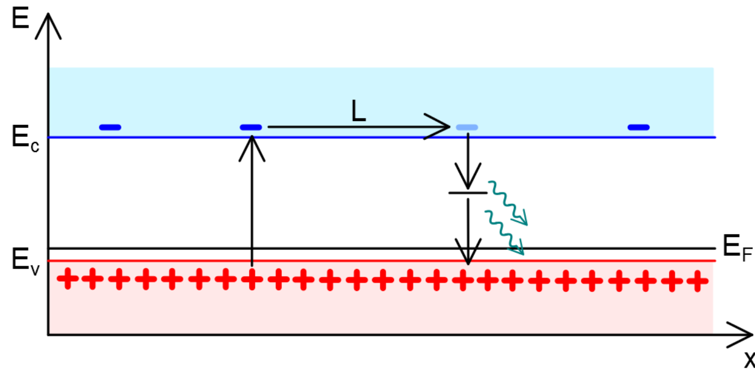

Figure 2.4: Generation- and recombination process in a p-type semiconductor. A minority charge carrier (electron) is created, diffuses the distance L and recombines with a hole via Shockley-Read-Hall recombination under phonon emission

Surface recombination

Surface recombination plays an important role in recombination and therefore practically determines the diffusion length. It is usually described by the surface lifetime τ_s which is a function of the surface recombination velocity. This parameter can be understood as the surface exhibits a high recombination rate due to surface defects and depletes it of minority carriers. As therefore their concentration will be lower on the surface than in the bulk, minority charge carriers will flow towards the surface. At the border case of no surface recombination, the recombination

velocity will be zero, while if the surface recombination is infinite, it will assume the maximum velocity the carriers can achieve.

General considerations about the lifetime of injected minority charge carriers

In equilibrium, generation and recombination equalize each other: $G_{therm} = R_{therm}$, where G_{therm} is the generation- and R_{therm} is the recombination term. A derivation of the behavior of a semiconductor which is illuminated with light is given by [Sch06]: The light pulse of a duration Δt causes an increase in carrier generation ($G > R_{therm}$). The charge carrier densities of electrons and holes are increased by Δn_n and Δp_n, respectively. Before the light pulse the semiconductor is in equilibrium state

$$G_{therm} = R_{therm} = P_r \cdot n_{n0} \cdot p_{n0} \tag{2.19}$$

P_r is the recombination probability. The product of the concentrations has a constant value according to the mass action law given in equation 2.15. The increase in the majority charge carriers will be small compared to their total number while the number of minority charge carriers is increased by an important factor. The continuity equation for charge carriers is given by

$$\frac{\delta n}{\delta t} = -\nabla \vec{j_n} + G - R + \frac{\delta N_D}{\delta t} \tag{2.20}$$

for electrons. The same equation is valid for holes if the charge carrier type n is replaced by p and the number of donors N_D by the number of acceptors N_A. With negligible current (if it is considered that charge carriers recombine at their generation point) and if the change in the carrier concentration is n'_n and p'_n, respectively equation 2.20 becomes

$$\frac{\delta n'_n}{\delta t} = \frac{\delta p'_n}{\delta t} = G - R. \tag{2.21}$$

The number of donors doesn't change over time. If the number of charge carriers after illumination is n_n and p_n and is put in equation 2.19 and Shockley Read Hall recombination is considered (so the released energy is only converted into phonons, thus heat) equation 2.22 is received:

$$G - R = G_{therm} - P_r \cdot n_n \cdot p_n = G_{therm} - P_r \cdot (n_{n0} + n'_n) \cdot (p_{n0} + p'_n) \tag{2.22}$$

If the equation is expanded most terms cancel out as $G_{therm} = P_r \cdot n_{n0} \cdot p_{n0} (= R_{therm})$ and due to the fact that the number of minority charge carriers is by magnitudes smaller than the majority charge carriers so that, in the case of an n-doped semiconductor, $n_{n0} >> n'_n \approx p'_n$ and $n_{n0} >> p_{n0}$. The equation then simplifies to

$$G - R = \frac{\delta p'_n}{\delta t} \approx -r \cdot n_{n0} \cdot p'_n \tag{2.23}$$

If the equation is solved for p'_n, the solution given in 2.24 is received

$$p'_n = p'_n(t = 0) \cdot \exp\left(\frac{-t}{\tau_p}\right) \tag{2.24}$$

It includes the minority carrier lifetime τ which is given by equation 2.25 for holes τ_p and electrons τ_n.

$$\tau_p = \frac{1}{P_r \cdot n_{n0}}, \qquad \tau_n = \frac{1}{P_r \cdot p_{n0}} \tag{2.25}$$

2.3.2 pn-junction

A pn junction is the most fundamental semiconductor element. At the transition from the p- to the n-doped semiconductor diffusion of majority charge carriers into the opposite region where they recombine occurs, driven by a concentration gradient, leaving back donator- and acceptor ions. This leads to an electric field that counteracts the diffusive force. The process continues till equilibrium is reached and leads to the formation of a depleted region at the pn-junction where charge carriers are almost absent, known as space charge region.

In the band diagram, band bending occurs since the Fermi energy, which lies near the valence band for the p-doped and near the conduction band for the n-doped semiconductor has to adapt to the same level. The width of the depletion region can be seen in the band diagram by the distance in which the band bending occurs. A higher doping level will lead to a smaller depletion region. The arising electric potential inside the pn-junction can be directly seen in the band diagram as it is the vertical height between the particular energy levels. Electrons in the conduction band have to apply energy to reach a higher-, holes to reach a lower state. The band diagram of a pn junction and a scheme where the space charge region is sketched is shown in figure 2.5.

Under normal conditions generation- and recombination processes as well as diffusion and drift currents are always present as it is also sketched in the figure. On the one hand, majority charge carriers will diffuse as described before. On the other hand, minority charge carriers are constantly created, performing a random walk through the material. Majority charge carriers near the pn junction will see a potential barrier. They will be able to diffuse into the opposite region only if their energy is sufficient. In contrast the minority charge carriers are, provided that they reach the pn junction before they recombine, accelerated through the space charge region by the electric field into the opposite region, where they arrive as majority charge carriers. The minority charge carrier current depends on the generation rate (temperature) as well as on the diffusion length L. If the pn junction is in an equilibrium state, the described currents compensate each other.

With these considerations the behavior of a biased pn-junction (thus a diode IV characteristics) can be explained. If the pn-junction is forward biased (p-positive, n-negative), the electric potential of the space charge region becomes lower. More majority charge carriers will have sufficient energy to overcome the barrier, the current will rise rapidly. The critical voltage is given by the built in voltage V_{bi}, which is dependent of the material and the doping. In this regime, new charge carriers from the external source flow towards the device, continuously recombinating in the depletion region. Reverse biasing the pn-junction will lead to a broadening of the depletion region, thus an increase of the electric potential. Only a small reverse current is measured, provided by the minority charge carriers dependent on their generation rate and therefore limited to a saturation value. Above a critical voltage, reverse breakdown occurs due to the high electric fields.

The depletion width for a reverse biased pn-junction can be calculated. In the most simple case of a linear pn-junction, the depletion width W as a function of the applied voltage V is given by equation 2.26 [Pie96].

$$W \approx \sqrt{\left[\frac{2\epsilon_r\epsilon_0}{e}\frac{N_A+N_D}{N_AN_D}(V_{bi}-V)\right]} \tag{2.26}$$

The direction of propagation is dependent on the doping concentration. If p- and n-region are not equally doped it will broaden towards the lightly doped region. At the boarder case e.g. if $N_A >> N_D$ almost all the broadening will proceed into the lightly doped n-region. In this case, the depletion width will be dependent mainly on the doping concentration of the lightly doped

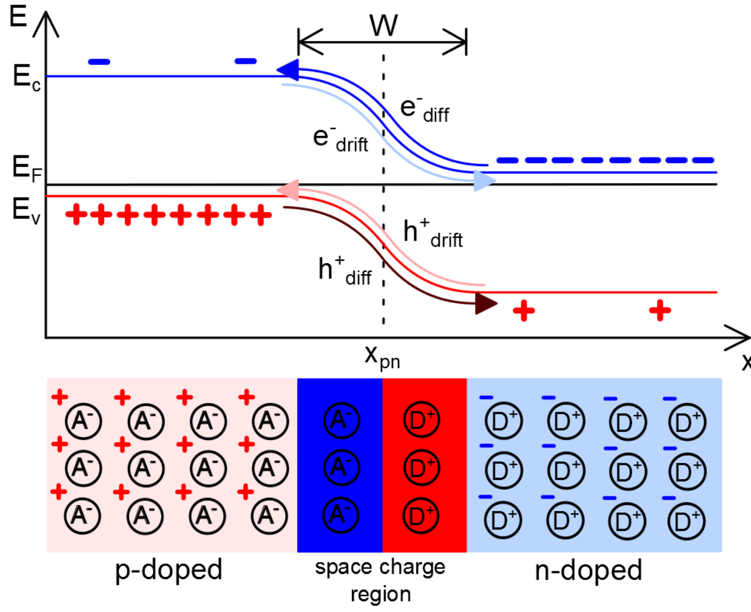

Figure 2.5: Upper image: Band diagram of a pn-junction, including the involved drift- and diffusion currents. Lower image: Scheme of a pn-junction, including the space charge region

region, which can also be seen when observing equation 2.26: The middle term of the equation including the concentrations then simplifies for e.g. heavily doped p- and lightly doped n-region to $1/N_D$:

$$W \approx \sqrt{\left[\frac{2\epsilon_r\epsilon_0}{e}\frac{1}{N_D}(V_{bi} - V)\right]} \tag{2.27}$$

The total width at a certain voltage is dependent from the doping concentration. The more lightly the doping concentration, the bigger the space charge region and the more the increase of the depletion width when voltage is applied.

2.3.3 Photovoltaic effect

The photovoltaic effect is the key phenomenon on which all OBIC measurements are based and, by the way, the functional principle of solar cells. It describes the arise of a photocurrent if a pn-junction is illuminated with light.

If the depletion region of a pn-junction is illuminated with light greater than the band gap electron hole pairs are created at a certain probability. The electric field inside the depletion region then separates the electrons and holes as it accelerates the electrons towards the n-, the holes towards the p-type semiconductor where they remain as majority charge carriers. This will cause an electric potential. If the n- and the p-region are connected and an amperemeter is inserted current will be detected. Comparing the process to the previous chapter, where the currents inside a pn-junction were described makes it obvious that the relevant charge carrier type for the photovoltaic current are minority charge carriers as they have the property to be accelerated by the electric field of the pn-junction into the opposite area.

If a minority charge carrier is created somewhere outside the pn-junction, the diffusion length L will determine the measured current as it has to reach the pn-junction before recombination.

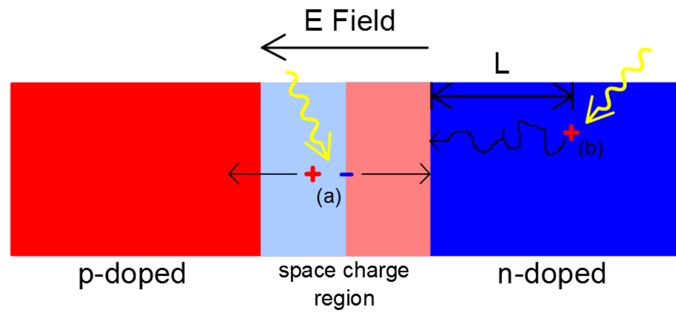

Figure 2.6: An incident photon creates an electron hole pair (a) in the depletion region (b) in the n-bulk. While the electron-hole pair created in the depletion region is immideately separated, the minority charge carrier created in the n-bulk has to cover a certain distance L without recombining.

Creation of the minority charge carriers with light which exhibits an energy greater than the band gap is not the only way. In 2.1 the absorption process for the 1300 nm laser was described, heating up the sample at a certain position, which leads to a local fluctuation in the carrier concentration, which, as will be seen in the measurements, also leads to an OBIC signal. Furthermore, for very high light intensities two photon absorption causes a not negligible current. Not only interaction with light creates electron hole pairs. Electrical beam induced current (EBIC) measurements take advantage of an electron beam created in a scanning electron microscope (SEM) and is a very common method that exhibits advantages over OBIC like the higher spatial resolution, which is limited by the minimum spot size of the beam for OBIC measurements, and the possibility to exactly adjust the electron beam to the requirements of the experiment. However OBIC offers possibilities for experiments that cannot be done with EBIC like depth sensitive measurements. Several EBIC measurements on semiconductor devices can be found in [Fac13].

2.3.4 Seebeck effect

The Seebeck effect describes a voltage between two conducting materials arising from a temperature gradient. It is mentioned as it can appear as an undesired side effect in OBIC measurements. However, other measurement methods in failure analysis use the effect for defect localization.
If the metal of a (e.g. metal semiconductor heterojunction) is heated up its free electrons increase their thermal energy, while the energy of those in the cold region stays the same. Therefore, electrons flow from the hot to the cold end which causes a contrarily voltage that compensates the diffusion. A more detailed view and a description how laser stimulation can be used to perform Seebeck effect measurements in failure analysis is given by [Glo10].

2.4 Determination of the diffusion length of minority charge carriers

The relationship between the measured current and the distance to the position where minority charge carriers are created depends on several factors like the surface recombination velocity and the geometrical shape of the pn-junction. A general relationship is given by [Ong94], where I_{diff} is the measured diffusion current, r is the distance to the pn-junction and L is the diffusion length.

$$I_{diff} \propto e^{-\frac{r}{L}} \tag{2.28}$$

For a linear pn-junction parallel to the incident beam and perpendicular to the surface the general relationship is given by 2.29

$$I_{diff} = k \cdot r^{\tilde{\alpha}} \cdot e^{-\frac{r}{L}} \tag{2.29}$$

In this case, k is a proportional constant and $\tilde{\alpha}$ if a fitting parameter which takes the surface recombination velocity v_s into account. $\tilde{\alpha} = 0$ for $v_s = 0$ and $\tilde{\alpha} = -1/2$ for $v_s = \infty$ [Ong94]. If the surface recombination is neglected, equation 2.29 simplifies to:

$$I_{diff} = k \cdot e^{-\frac{r}{L}} \tag{2.30}$$

For the extraction of the diffusion length, $ln(J \cdot r^{-\tilde{\alpha}})$ is plotted versus $-\frac{r}{L}$. Then, the diffusion length L can be estimated as it is given by the inverse of the linear slope of the function.

$$ln(I_{diff} \cdot r^{-\tilde{\alpha}}) = -\frac{r}{L} + ln(k) \tag{2.31}$$

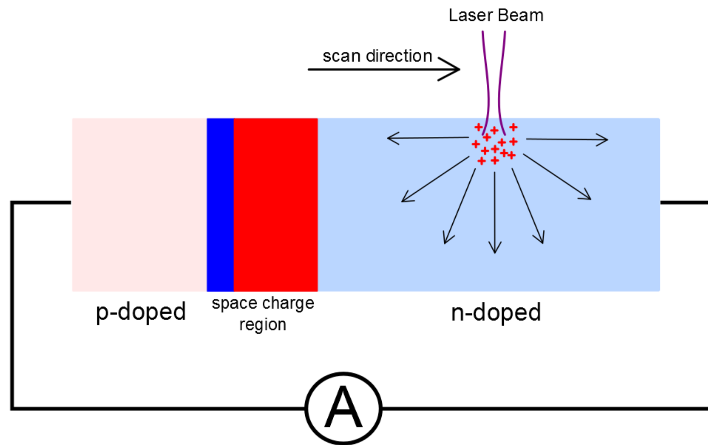

Figure 2.7: OBIC measurement on a pn junction

The choice of the parameter $\tilde{\alpha}$ will determine the estimated diffusion length. It can be estimated, using the method described in [Ong94]. For the measurements in this thesis it was not obtained but estimated dependent on the sample properties- and preparation.

2.5 Important semiconductor devices

This section gives a short overview of the devices on which measurements were done during this thesis. The behavior of the most fundamental element, the diode, on which all other devices are based, was already discussed in detail previously.

2.5.1 Metal-oxide-semiconductor fieldeffecttransistor (MOSFET)

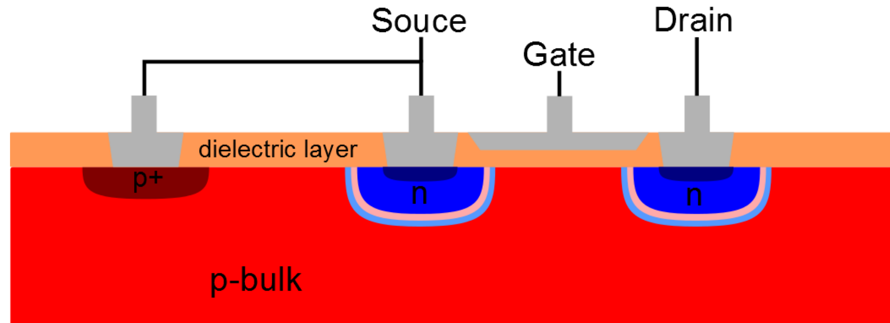

Figure 2.8: Structure (cross section) of an n-channel MOSFET

A field effect transistor is a device in which a current between source and drain is controlled by the voltage which is applied on an isolated gate. In a MOSFET (metal-oxide-semiconductor field-effect transistor) a metal gate is isolated by an oxide layer from the bulk. Although in most actual MOSFETs the gate is made of conductive polysilicon the name remained. It can either be designed as n- or p-channel MOSFET. A sketched cross section of an n-channel MOSFET is shown in figure 2.8. Two n-wells are doped into the p-bulk. On top a dielectric layer (oxide) has been grown and etched where the metal contacts, drawn in gray color are placed for the source, the drain and the body contact. Usually the body contact is connected to the source. The dark red/blue color next to the metal contacts indicates a higher doping which is usually done to create an ohmic contact. The gate contact is isolated from the bulk by the oxide. If a voltage is applied between source and drain no current flows as the device exhibits two contrarily connected diodes. To turn the device on (which means that a current can flow from the source to the drain) a positive voltage has to be applied on the gate to achieve inversion in the region beyond the gate, between the two n-wells. In inversion, the dominant charge carrier type in a certain region is inverted, which means that between the n-wells, a conducting n-channel occurs. This happens as the positive potential of the gate contact pulls minority charge carriers (electrons) out of the p-bulk to the region beyond the oxide. The threshold voltage V_{th} is the voltage that has to be applied on the gate to reach charge carrier inversion. In a p-channel MOSFET the doping type of the doped areas is inverted, which means that a negative voltage has to be applied to turn the transistor on. While in figure 2.8 a horizontal n-channel is drawn, high power transistors as they are analyzed in this thesis are usually constructed vertical. Usually the frontside of the chip is the source-, the backside is the drain contact.

2.5.2 Insulated gate bipolar transistor (IGBT)

In an IGBT (Insulated gate bipolar transistor) the base of a bipolar transistor is controlled by the drain of a fieldeffect transistor. The basic structure is drawn in figure 2.9. The bipolar transistor can be seen in the middle of the image, where the p-well is acting as emitter and the p-region at the backside as collector. The fieldeffect transistor consists of the n-well, which is acting as source, the p-well, which is the bulk and the n-region in the middle, which is the drain. The n-channel will be established beyond the gate in the p-well. To turn the bipolar transistor (which is a pnp-transistor in the drawing) on, the n-base has to be set to a negative potential to the p-emitter, thus the pn-junction is forward biased. In this case, majority charge carriers from the base are injected into the p-region and holes are injected into the n-region. The n-region, which is usually by far more narrow than the p-region is depleted from majority charge carriers. Thus holes emitted from the p-region drift through the n-region. The same time the collector is put on negative potential. The holes which do not recombine in the n-region drift through it and are collected, the transistor is turned on. In case of an IGBT the n-region is biased via the drain of a fieldeffect transistor. If a positive voltage is applied on the emitter and the gate, electrons will flow through the n-channel into the emitter, which leads, the same way, to a depletion of the n-region of majority charge carriers so the holes can drift through it and turn the transistor on.

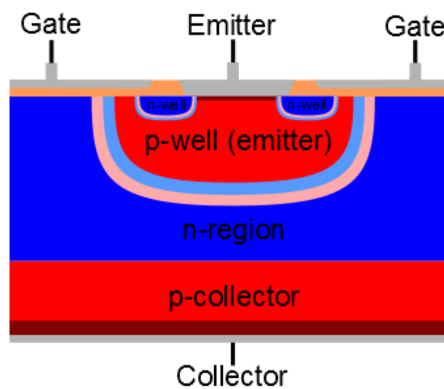

Figure 2.9: Structure (cross section) of an IGBT

2.5.3 Micro electro mechanical systems (MEMS)

Micro electro mechanical systems are mechanical devices which exhibit dimensions in the micrometer range. Usually sensors or actuators are designed in semiconductor applications. The systems in general contain a driving chip and the sensor. In this thesis various measurements will be done on a sensor chip containing a pressure- and an acceleration sensor. They both take advantage of the piezo-resistive effect, which describes a change in the resistivity of a material due to a mechanical deformation. An exact description of the examined device is given in chapter 4.

Chapter 3

Methods

3.1 Equipment

Emission microscope	Hamamatsu PHEMOS-1000 (configuration see 3.2)
Picoamperemeter	Keithley 6485 PICOAMMETER
Silver glue	Acheson Silver Dag 1415
Micromanipulators	Karl Suss PH 120/150
Micromanipulator tips	Micromanipulator 7A-M, Picoprobe T-4-22
Grinding machine	Stuers Roto Pol-35
Grinding machine (embedded samples)	Struers Planopol V
Grinding papers	Allied 800 (P-2400) Grit Silicon Carbide Paper
	Allied 1200 (P-4000) Grit Silicon Carbide Paper
	Allied 550-30065
Synthetic resin	Araldite AY 103-1
Laser Power/Energy Meter	Coherent FieldMax II-TOP

3.2 PHEMOS-1000

All measurements in this thesis were done on the PHEMOS-1000 by Hamamatsu, shown in figure 3.1. The PHEMOS-1000 is an emission- and/or laser-scan microscope including several features. It is conceived for failure analysis applications in the semiconductor industry and is available in various configurations. The configuration which was used in this thesis includes the emission microscopy setup as well as the laser-scan microscope. The system includes two lasers which emit light in the infrared at wavelengths of 1300 nm and 1064 nm. The laser scanning application usually uses the 1300 nm laser. The 1064 nm laser is included for backside emission microscopy analysis.

Figure 3.1: PHEMOS-1000

Photo emission microscopy (PEM) is a failure analysis method used to detect defects where radiation is emitted, like a diode with an early reverse breakdown voltage inside an integrated circuit. This method was not used in this thesis but a short description is given as it gives the explanation why the 1064 nm laser is included in the tool. For the detection of the light the PHEMOS-1000 gives the opportunity to choose between an InGaAs-[1] and a Si-CCD[2] camera which differ in the sensitivity for the emitted wavelength, InGaAs- is used for long, Si-CCD for short wavelengths. To relate the detected spot to a certain position in the IC an ordinary optical image of the investigated area is taken before the actual measurement. This image is then overlaid with the PEM-image. However, the frontside of an IC, is often covered by a metal. In this case light that is emitted inside the IC will not be visible as the light cannot penetrate the metal. In this case one has the possibility to remove the backside metallization and perform the analysis through the backside. The devices, however, usually have a thick silicon substrate on the backside which can in fact be penetrated by the emitted light, but not by the visible light with which the overlay image is taken. In this case the 1064 nm laser can be used to take an image to be used for the overlay as it has quite a high transmittance through silicon as can be seen in the fundamentals in figure 2.1. The laser is therefore focused through the backside onto

[1]Indium Gallium Arsenide
[2]Charge-coupled device

the frontside. Afterwards, the image is being mirrored by the software.

The laser-scan microscope is intended for optical beam induced resistance change (OBIRCH) analysis. OBIRCH analysis methods are described in [Hab06]. This method is used to detect an undesired current in a device, e.g. resistive connections between metal lines in an IC. The setup for an OBIRCH measurement is very similar to an OBIC measurement and can therefore be mostly adopted, although the essential phenomena are different. For an OBIRCH measurement voltage is applied between two pins on an IC and the current is measured. The 1300 nm laser is then scanned over the selected area of the device point by point and the current change is stored for every coordinate. As already described in 2.1 the laser beam heats up the illuminated area. It is focused on a specific point using an optical system including objectives for various magnifications, which are specified in table 3.2. Greater areas on the chip can be investigated with the lower magnification objectives. Usually they are used to obtain the rough position of the failure which is then located exactly with the higher magnifications. By scanning over the device, the laser will cause a decrease of the resistivity when scanned over a section where current flows due to the heating. The detected current changes for every point are converted to a grayscale on a scale from 0 to 255 and afterwards merged to an image. They are therefore distributed proportional to their value around the mean current value. A local decrease of the resistivity will be visible as a white spot (or black spot if the pins are connected in reverse) and can be localized as the position of the irregularity on the chip. As well as the previously described PEM analysis, OBIRCH can be executed from the backside as well. Figure 3.2 shows a sketch of the basic components for an OBIC analysis on the PHEMOS-1000.

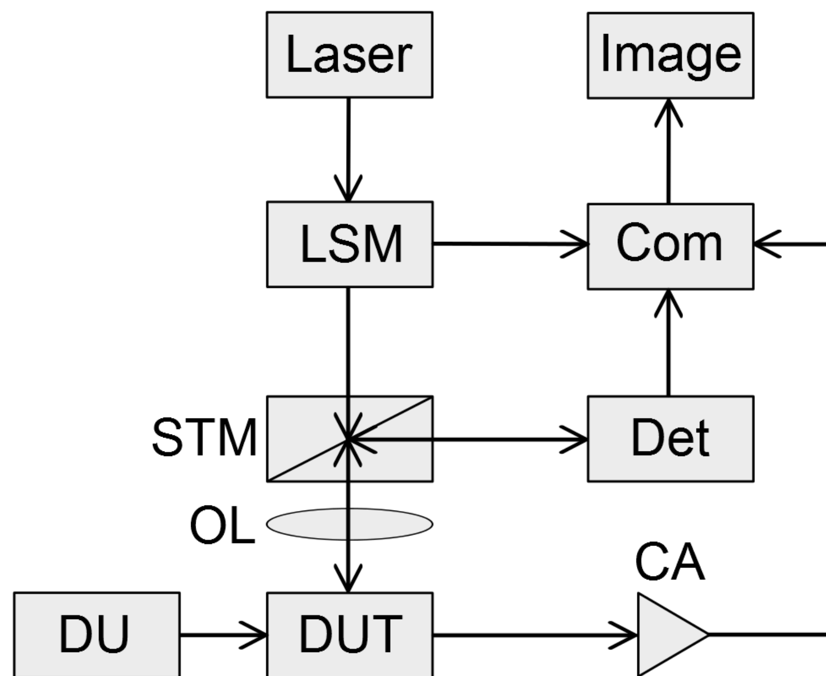

Figure 3.2: OBIC Setup, LSM: Laser scanning microscope, STM: Semi-transparent mirror, Det: Detector, OL: Objective lens, DU: Driving unit, DUT: Device under test, CA: Current amplifier, Com: Computer

An OBIC measurement can be executed with basically the same setup. However, the main difference is that in this case not a change in the current flowing across the device from pin A

to pin B, but the current that is induced by the laser beam is detected. Therefore no voltage is applied (in the basic experiment). As the induced current reaches its highest value if the charge carriers are created within the depletion region of a pn-junction, those will appear as spots. Usually the detected currents will be comparatively small for OBIC analysis. The maximum OBIC currents detected at suitable laser powers are in the range of 100 to 200 nA in a typical experiment as will be seen in the later measurements. To detect also very low current changes the PHEMOS-1000 is equipped with two current amplifiers. The specifications of the current amplifiers are summarized in table 3.3. The standard current amplifier is used for OBIRCH analysis where the device exhibits large leakage currents. Therefore the maximum voltage that can be applied is lower. It is usually not suitable for OBIC measurements, although it can be as will be seen later and also delivers useful results. However, the highly sensitive current amplifier is the tool that is usually used as the currents are usually low. Furthermore, when voltage has to be applied for some OBIC experiments, it provides the possibility to apply a voltage up to 25 V, compared to the 10 V which is the maximum voltage that can be applied using the other amplifier. As can be seen in the table, currents in the pA range are detectable. The same as for OBIRCH analysis the low magnification objectives will be used for a visualization of large structures to get an overview. Experiments where it is important to have a high resolution like diffusion length measurements will be executed with the configuration that exhibits the lowest possible laser spot size.

3.2.1 Tool specifications

The specifications of the PHEMOS-1000 in the used configurations are summarized in this section. The information is provided by Hamamatsu.

Lasers

The PHEMOS-1000 gives the opportunity to choose between two infrared lasers with wavelengths of 1064 nm and 1300 nm. The laser power can be adjusted to the requirements from 0 to 100 % in steps of 0.1 %. It is dependent on the used objective and highest for the lowest magnification of 5x. For the used configuration the maximum laser power for the different objectives was determined during the installation of the tool by the manufacturer, which was shortly before the start of the thesis, and is given by table 3.1.

Laser wavelength	Laser Power 5x lens	Laser Power 20x lens	Laser Power NA 50x lens	Laser Power 100x lens
1064 nm	54 [mW]	34 [mW]	32 [mW]	3 [mW]
1300 nm	162 [mW]	114 [mW]	118 [mW]	13 [mW]

Table 3.1: Maximum laser power

Objectives

The available objectives are summarized in table 3.2. In the used configuration, the 50x lens is a nanolens used for special failure analysis cases. It would exhibit the smallest laser spot size of all but is, for practical reasons, not suitable for OBIC measurements and therefore not used for measurements done during this thesis.

Current amplifiers

The system includes two current amplifiers. Their properties are summarized in table 3.3.

Objective Magnification	Numerical apperture (NA)	1300 nm laser spot size [μm]	1064 nm laser spot size [μm]
5x	0.14	11.33	9.27
20x	0.42	3.78	3.09
High NA 50x	0.76	2.09	1.71
100x	0.5	3.17	2.6

Table 3.2: Microscope ojectives and laser characteristics

Mode	Standard current amplifier	High sensitivity current amplifier
Voltage range	10 mV - 10 V	10 mV - 25 V
Maximum current	100 mA	100 μA
Detectability	10 nA	10 pA
Amplification	10 e6 V/A	10 e7 V/A

Table 3.3: Current amplifier characteristics

3.2.2 Optimum configuration of the PHEMOS-1000 parameters for OBIC experiments

The PHEMOS-1000 is provided with a software that allows for the adjustment of a wide range of parameters to meet the measurement requirements. This section gives a summary of how those of the parameters that are important when an OBIC measurement is done have to be chosen to receive suitable results.

Laser

The choice if the 1064 nm or the 1300 nm laser is used for a certain experiment is dependent on the structure of the material and the parameters that shall be obtained during the measurement. Both lasers can create minority charge carriers and therefore an OBIC current but the area in which they are created differs. For both lasers a good transmission through (lightly) doped silicon is found as could also be seen in figure 2.1. However, for the creation of charge carriers there is a relevant difference. While the 1064 nm laser will create them on its whole path through the substrate by lifting electrons from the valence to the conduction band, the 1300 nm laser will create electron hole pairs mainly near the surface and therefore be responsible for a section on the chip near the surface where the carrier generation is increased. Although it does penetrate through the substrate too, a measurable effect can only be seen when the laser is focused onto the surface. This leads to several considerations for the revealed structures. Figure 3.3 (a-d) gives an overview of four idealized structures. The laser beam is sketched simplified wedge shaped in dark red.

Image (a) shows a pn-junction parallel to the surface and perpendicular to the incident beam. The laser beam is drawn in focus on the surface (1), in the middle of the depletion region (2) and somewhere in the n-region (3). If the experiment is done with the 1064 nm laser the detected photocurrent will be independent of the laser focus as the current is dependent on the total generation of charge carriers inside or near the depletion region only. No matter if the laser is focused or not, their total number will be the same, they only will be distributed over a bigger horizontal area. The vertical position of the pn-junction in theory has an influence on the measured current because it is dependent on the light intensity that reaches the pn-junction and therefore on the absorption. However, in practice a current difference for pn-junctions that exhibit a difference in the vertical position of, in general in the range of 10 μm is not measureable. In contrast, the 1300 nm laser creates charge carriers mainly near the surface. In this case, the

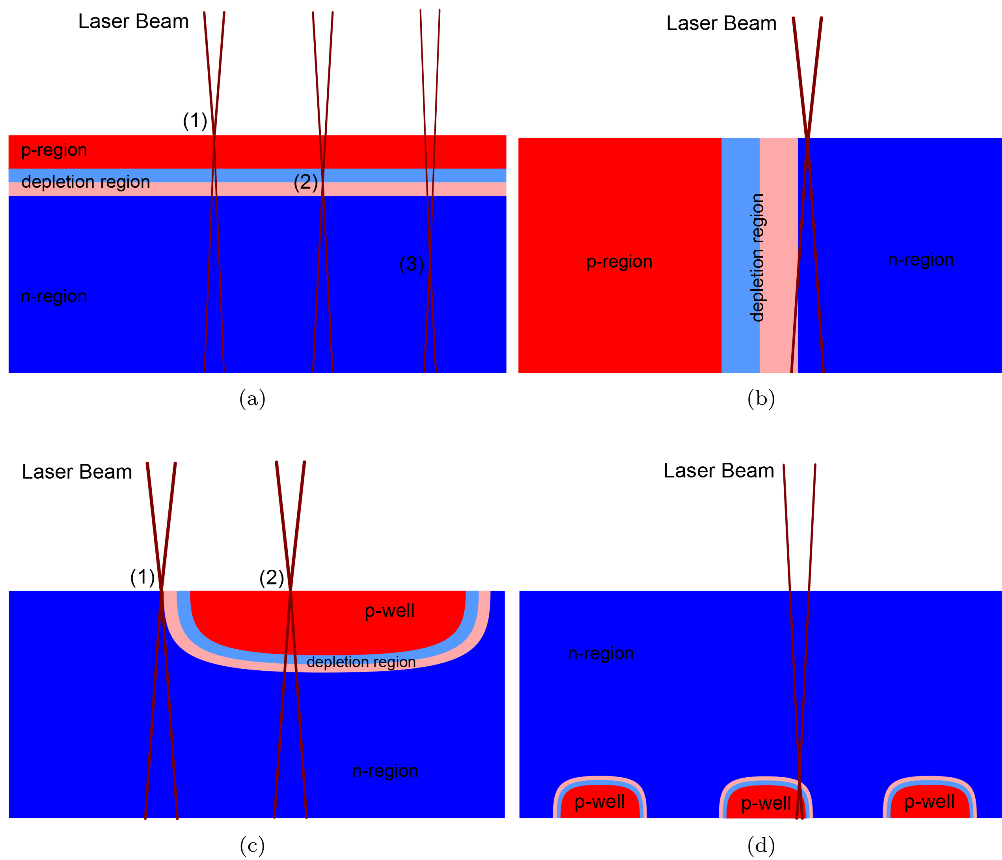

Figure 3.3: Laser scan over different structures: (a) Scan along a pn-junction parallel to the surface, perpendicular to the beam, (b) scan along a pn-junction perpendicular to the surface and parallel to the beam, (c) scan along a p-well, (d) scan along structures, buried deep in the substrate

vertical position of the pn-junction will have a measureable influence on the photocurrent. If the position is too far away from the surface, no current will be detected at all.

Image (b) shows a pn-junction parallel to the beam and perpendicular to the surface. Using the 1064 nm laser leads to problems in this case. As can be seen the spot size and so the area in which charge carriers are created broadens within the substrate if the laser is focused on the surface. This leads to additional, undesired currents, the signal will become blurred. Again, changing the focus will hardly lead to changes in the current. In case of such a structure, the 1300 nm laser is used. The limitation of the carrier generation on regions near the surface prevents the additional currents and leads to a sharp signal with a resolution close to the spot size in focus.

In image (c) a p-well at the surface is shown. In this case, the p-region is flat enough so that the pn-junction doesn't get blurred if the experiment is done with the 1064 nm laser (1). Both lasers resolve these flat p-wells very well. As seen in the description of the image (a) the current measured with the 1300 nm laser depends on the distance of the depletion region to the surface. As the depletion region reaches close to the surface at the edges of this structure (1) the current will differ to a scanning position in the middle of the p-well (2). This leads to peaks at the edges and can deliver information about the depth of the p-well.

Image (d) shows structures buried deep in the substrate. In this case only the 1064 nm laser can be used. It can resolve the structures if their horizontal distance is not smaller than the laser spot size. However, if the structures are not flat but extend in the vertical direction, the same problems as for the structure in image (b) occurs. This will, although, only happen if the vertical extension is very wide (the spreading of the beam is sketched exaggerated in the images). In chapter 7.1 e.g. p-wells in n-substrate are imaged from the backside which exhibt a vertical width of about 40 μm but hardly get blurred.

Laser power

To find the suitable laser powers for OBIC experiments a preparative measurement was done on a diode with a pn-junction close and parallel to the surface and perpendicular to the incident beam. In this case a constant current is detected, only dependent on the laser power. The position of the laser was fixed and the current was measured with a picoamperemeter while the laser power was increased step by step. The results are plotted in figure 3.4. For the 1300 nm laser, plotted in image (c) no significant current signal could be measured for powers beneath 30 %. The 1064 nm laser exhibits very high currents for high laser powers (a). The dependence is linear for most of the scale, except the section from 0 to 2 % at the 1064 nm laser. A detail look is given in image (b). At 1.6 % the behavior starts to get linear. It can be summarized that for experiments with the 1300 nm laser one usually has to set the power on high values above (at least) 30 %. For experiments with the 1064 nm laser a laser power value between 1.5 % and 2 % usually delivers the best results.

Scan mode

There are basically four scan modes available. In normal mode, the laser scans over the whole image. In slit mode the laser scans along a certain section of the image. The slit can be chosen horizontal or vertical in different widths. In line scan mode the laser is moved along a straight line from the top to the bottom or from the left to the right. In point scan mode the laser is fixed in the middle of the image. A graphical overview is given in figure 3.5.

Scan direction

In standard mode the laser scans from the top right to the bottom left corner, as it was indicated before. The direction can be rotated by 90°, 180° and 270°. Usually it is useful to choose the scan direction perpendicular to the pn-junction.

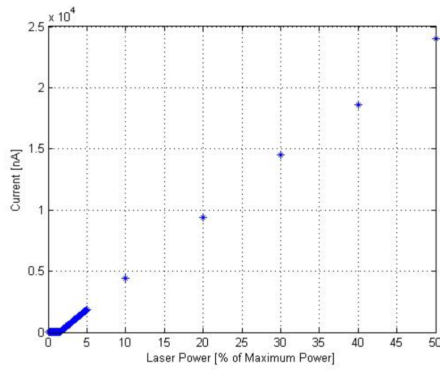

(a) 1064 nm

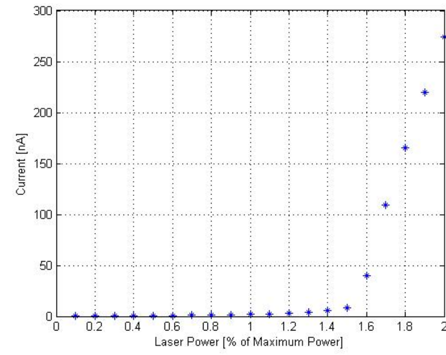

(b) 1064 nm (detail)

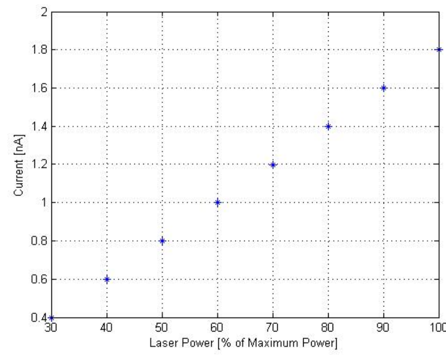

(c) 1300 nm

Figure 3.4: Measured photocurrent on a pn-junction, parallel to the surface and perpendicular to the indident beam, plotted against the laser power for the 1064 nm- and the 1300 nm laser. Image (b) shows the section between 0 and 2 % in detail for the 1064 nm laser

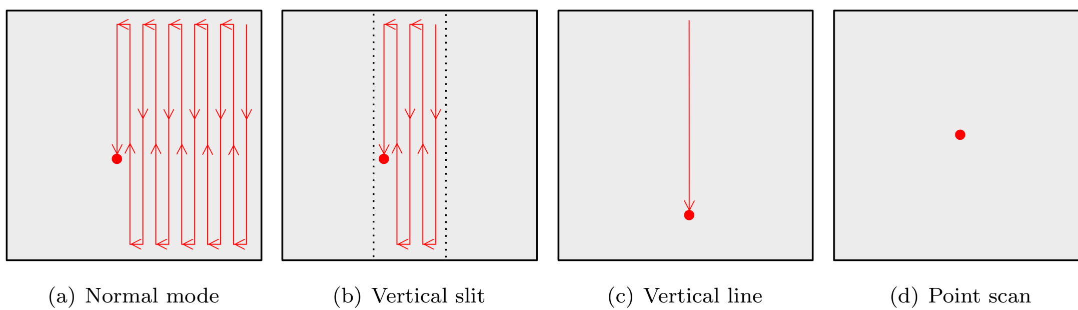

(a) Normal mode (b) Vertical slit (c) Vertical line (d) Point scan

Figure 3.5: Scan modes provided by the PHEMOS-1000 software: Gray indicates the scanned area, the red arrow the scan direction.

Laser scan speed

The scan speed is denoted in seconds and is the time in which the laser completes one image. If the scan speed is chosen too fast the spatial resolution will be worse compared to lower speeds. However, in practical experiments it could be found that a scan speed of 16 s delivers the optimum results. If the parameter is set on a very high value which corresponds to a low speed undesired side effects appear. Very low scan speeds are usually used to do Seebeck effect measurements.

Number of frames

The software offers a function to integrate over an optional number of OBIC images taken one after another. If an analysis is done where the relative values between the current maximum and minimum are important the number should be set to 1, thus no integration is done. Certainly, if the goal of an experiment is to visualize a doped structure on the chip with high accuracy, the function is useful to improve the quality of the image.

Current amplifier

Usually the high sensitivity current amplifier is chosen. Only for experiments on biased devices with high leakage currents the other amplifier has to be used (if the current exceeds the allowed maximum value of 100 μA).

Chuck

For general applications the sample is placed on a chuck as it can be seen in figure 3.6. It gives the possibility to place wafers with a maximum diameter of eight inches. The chuck is conductive and therefore the backside can be connected over the chuck. The frontside is connected conventionally with metering needles. For backside analysis of wafers the system gives the possibility to substitute the chuck and use a backside chuck. In this case the wafer is attached onto the chuck backwards (frontside down). An aperture in the middle gives the possibility to investigate the desired area. Again, the backside is connected over the chuck.

3.2.3 Manually oparated stage control

The objective system can be moved manually using the software in 1 μm steps in the xy-plane. Furthermore it can be moved in z-direction to adjust the focus. To receive an image as it was described before the focus is fixed manually and afterwards the image is obtained by the software. Figure 3.6 shows the objective system, the chuck on which the samples are placed and a micromanipulator placed on the right side of the image next to the chuck.

In this thesis manual line scans were done. In this case, not the provided software but an externally connected picoamperemeter was used to measure the current. This has the advantage over the acquisition with the PHEMOS-1000 software, that the measurement result includes current values, while the software only provides color values converted from current values. A measurement setup is sketched in figure 2.7. For these measurements, the point scan mode (3.2.2) was chosen. The focus was fixed in the desired vertical position. Afterwards the laser was activated and moved manually point by point into the desired direction (e.g. over a pn-junction). At every point the current value was read and noted. The received data was later analyzed in a computer program.

Furthermore depth sensitive measurements were done. In this case the vertical position of buried pn-junctions was obtained. Therefore the normal scan mode (3.2.2) was used to acquire images and the focus was varied manually. The laser was first focused onto the surface and then moved into the sample stepwise. For every step an OBIC image was taken which can be related

to a certain depth.

The depth sensitive measurement requires some considerations. To know the new position of the focus if the objective system is moved by one step (which corresponds to 1 μm), the index of refraction of the material has to be identified. The relationship between the propagation direction of the incident beam and the beam inside the material was described in 2.1.1. If it is not known, the factor can be obtained if the thickness of the chip is known (e.g. it can be measured on a cross section) and if the chip exhibits a metal structure on the backside. In this case, one needs to focus on the frontside and count the steps that are necessary till the metal structure on the backside is in focus. As one knows then the thickness and how much the objective system has been moved, the factor can be calculated. If the chip does not have a metal structure on the backside, one has no benchmark. In this case silver glue can be used.

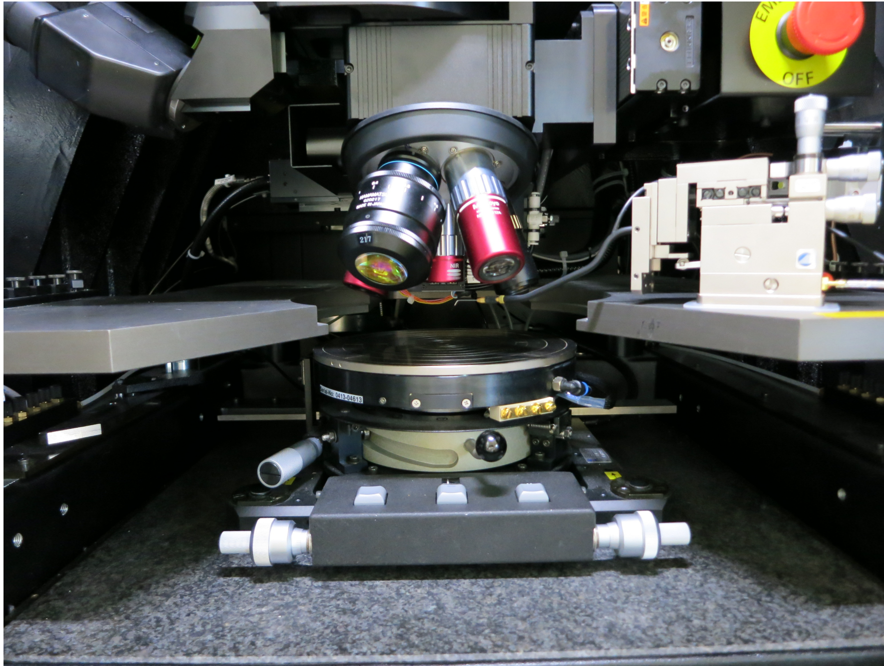

Figure 3.6: Chuck on which the samples are placed and objective system in a PHEMOS-1000. A micromanipulator is placed on the right side.

3.2.4 Data evaluation from OBIC images

As mentioned before, the PHEOMS-1000 software does not provide current values. The output of the measurements are images in which the current values are converted into gray levels. Dependent on how the junction is connected, a high current can either be seen as bright or dark area. To identify the structure of a sample this is sufficient. However if certain properties like the diffusion length should be obtained, a computer program has to be used to interpret the images. An image of a pn-junction can then be converted in e.g. a linear graph. In general the graph is then plotted in units of the maximum value (% of current maximum). This can be done as the investigated properties depend on the shape of the graph only. However, usually those measurements will be done with an externally connected amperemeter.

3.3 Sample preparation

3.3.1 Preparation of wafers

All experiments were done on wafers or wafer fractions from the front- or the backside or on cross sections of chips. If the wafer is taken out from production during a desired step and the experiment is executed from the front side, usually no further preparation has to be done. If the experiment is done from the backside usually the back side metallization has to be removed. This is done using a wet-chemical method. It can be done selectively for a desired area which is useful as in most cases the backside has to be connected during the measurements with a metering needle which can then be done on a position where the metallization is still present. Not all devices exhibit a metal back- or frontside, for instance if a wafer is taken from a certain production step or if the backside is removed completely to execute a failure analysis measurement. In that case, one may not get a good contact with the metering needle. This problem can be solved by placing silver glue on the substrate. If an analysis has to be done from the backside but the substrate is too thick or highly doped it may not be possible to receive an image as it gets intransparent for the laser beam. In this case the chip has to be thinned from the backside. This can either be done mechanically or by using reactive-ion etching. For both cases it is important to achieve a planar surface.

3.3.2 Preparation of cross sections

Many devices which were examined exhibit pn-junctions parallel to the surface which extend over the whole area of the chip as it has been shown in figure 3.3a. To obtain the desired parameters usually cross sections are prepared and investigated. The received structures then correspond to the structure shown in 3.3b.

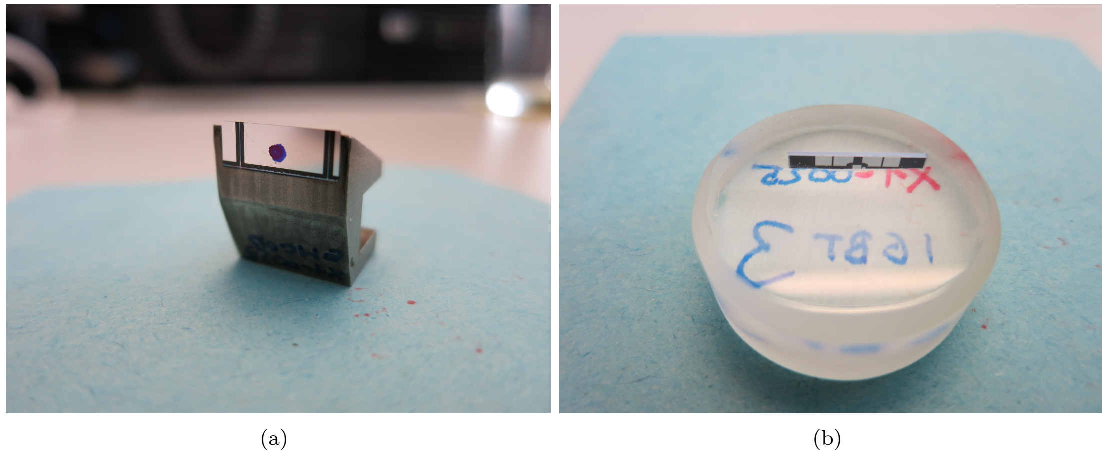

(a) (b)

Figure 3.7: Two possibilities to prepare samples before performing an OBIC analysis on cross sections: (a) Broken and polished chip, attached onto a metallic block, (b) cross section of a chip, embedded into synthetic resin.

In general the cross sections can be prepared in two ways. In one method the broken chip is embedded into synthetic resin and ground afterwards. An embedded and polished chip is shown in figure 3.7b. Embedding has advantages a as the handling during the grinding is easier and surfaces which are equally plane over the whole area of the cross section can be reached. For the grinding and the polishing step, the embedded sample can be put into the grinding machine which performs the grinding automatically. However, this method also has significant disadvantages. If the chip has large dimensions the deformation of the resin during tempering can cause cracks. Furthermore it will be more difficult to connect the chip as in most cases front- and

backside have to be connected. One can either try to bond both sides before embedding with metal wires and arrange them in a way that they stick out of the frontside of the resin, or try to put the metering needles onto the cross section if the device has a metallization. Sometimes it is useful to perform ion polishing after the grinding step to decrease the leakage current caused by chip material which is blurred during grinding.

The second preparation method is abandoned cross sections. In this case the chips are not embedded and have to be grinded manually (as they cannot be fixed in the grinding machine). A cross section prepared with this method is shown in figure 3.7a. It is therefore more difficult to achieve a surface which is completely planar over the whole area (especially for large samples with a width in the range of centimeters and thicknesses above 200 μm it is almost impossible). However it is usually sufficient for the measurements to have a section of the chip which is planar. After the grinding the chip is attached onto a metallic block using glue. For very thin samples with a thickness beneath 100 μm and thus a low stability during grinding it is useful to attach the sample onto another, thicker chip before the grinding. To improve the electrical parameters it can be useful to drop hydrogen fluoride onto the surface before the measurements are done. In contrast to the embedded cross sections the abandoned cross sections have the advantage that the front- and the backside are not covered and can therefore easily be connected.

For both preparation methods, the used abrasive paper for the last grinding step should exhibit a graining of 1 μm or beneath as a high roughness of the surface leads to bad measurement results. As a cross section is done through the pn-junction the prepared chips will always exhibit leakage currents. However, with a good preparation, they can be kept in the range of microamps and still OBIC measurements leading to good results can be done.

As it was described in 2.3.1 the surface recombination rate plays an important role in later experiments. The surface defect density will increase due to the preparation of cross sections which has to be taken into account when interpreting the measurement results, especially as the 1300 nm laser, with which most experiments on cross sections are done, has the property to create the minority charge carriers mainly at the surface.

Chapter 4

Measurements on TPMS devices

The tire pressure monitoring system (TPMS) is a micro electro mechanical system (MEMS) integrated in vehicles to warn the driver if the tire pressure is significantly outside the desired range. The sensor chip is very suitable for OBIC measurements as its structure is quite simple and consists mainly of p-doped wells (acting as conductors or piezoresistors), lying on top of, or being buried in, n-doped bulk silicon. During the fabrication process, the device is (after the p-wells are implanted and the metal lines and pads are placed) selectively etched from the backside in a way that only the desired structures remain, abandoned, in the arising cavity. The exact fabrication process takes numerous steps and will not be described in detail. The measurements shown in this chapter were all done on wafers, where the production process was stopped before the etching step was executed, so all structures are still buried in silicon. That was decided to demonstrate the power of OBIC measurements as non-destructive method to resolve buried structures.

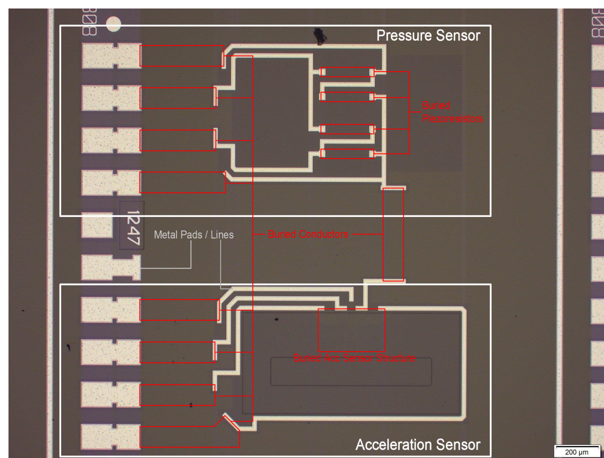

Figure 4.1: TPMS sensor chip

Figure 4.1 shows an optical image of a TPMS sensor chip as it was used for the subsequent OBIC measurements. The pressure sensor is situated on the upper- and the acceleration sensor on the under part of the chip (marked with white rectangles). The positions of the buried conductors and resistors, as well as those of the buried structures of the acceleration sensor, are marked with red rectangles. One can easily spot the metal lines and pads. On the right, the beginning of the next chip on the wafer can be seen.
Both sensors are realized by wheatstone bridges taking advantage of the fact that a mechanical deformation of the resistors leads to a change of their electrical resistivity due to the piezo-

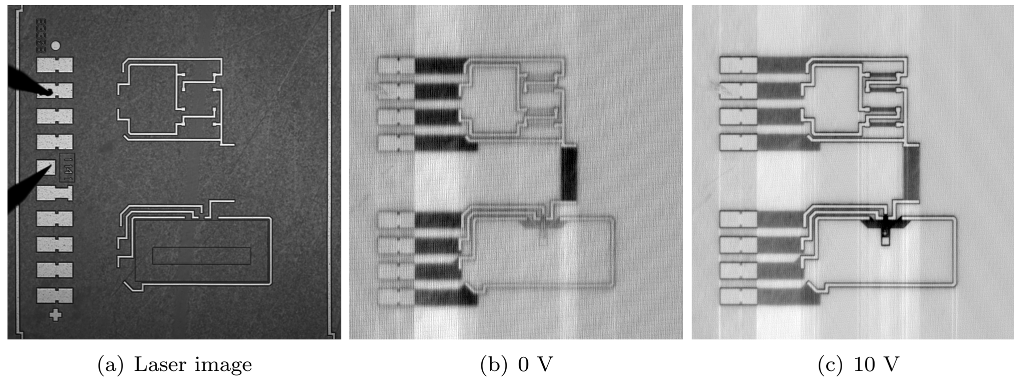

(a) Laser image (b) 0 V (c) 10 V

Figure 4.2: OBIC measurement on a TPMS sensor chip

resistive effect. While the resistors of the pressure sensor are deformed directly by the tire pressure, the piezoresistors of the acceleration sensor are connected to a rectangle where the gyrating mass will be attached later. The displacement of the mass due to an acceleration leads to a deformation of the resistors. The signal is picked up at the metal pads that can be seen on the left of the image. All pads, excluding the two pads in the middle (which are connected to the bulk) are connected to the p-wells. For gathering an OBIC signal, one metering needle has to be connected to one of the p-wells, the other one to the n-bulk.

4.1 Revealing structures

Figure 4.2 shows the result of an OBIC measurement on the chip described previously. The left image shows the laser image, while image (b) and (c) display the received OBIC signal when the device is not biased / reverse biased with 10 V. The exact measurement parameters for this and the following measurements are summarized in the appendix. Although the image was taken with only 5x magnification, the p-wells and also the buried structure in the acceleration sensor can already be identified very well. Reverse biasing the device leads to a significantly sharper signal. The metering needle, connected to the metal pads can be seen on the left of the laser image. In the case an OBIC measurement is performed in the course of failure analysis, a problem with the p doping would immediately attract attention. A more detailed view in the buried structures of the acceleration sensor is given by figure 4.4. Both the 20x and the 100x image were taken when the chip was reverse biased with 10V. Figure 4.5 shows a detail image of the pressure sensor. Image (a) shows the laser image, image (b) an overlay of the OBIC image and the laser image, where current values beyond a certain value are filtered out. The resistors forming the wheatstone bridge are marked in the overlay image. It should not go unnoticed that p wells are also situated beyond the metal lines. The data from OBIC measurements can be converted into a three dimensional image, where the z-coordinate indicates the value of the current. This was done for an overview image of the TPMS sensor chip and is shown in figure 4.3.

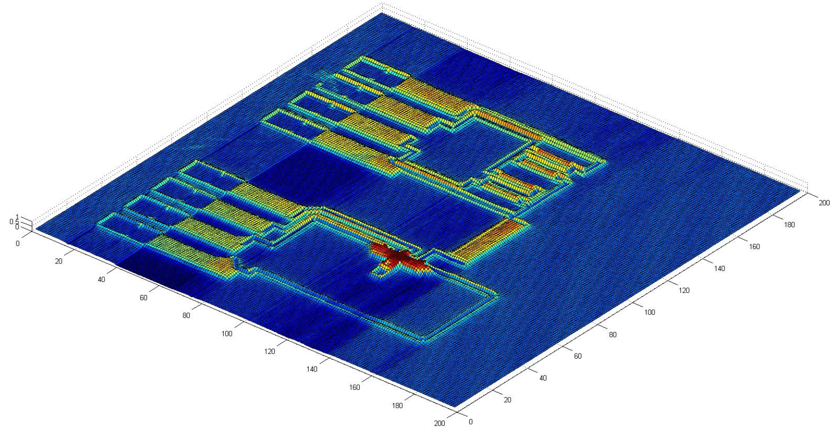

Figure 4.3: OBIC data of a measurement on a TMPS sensor chip converted into a threedimensional image

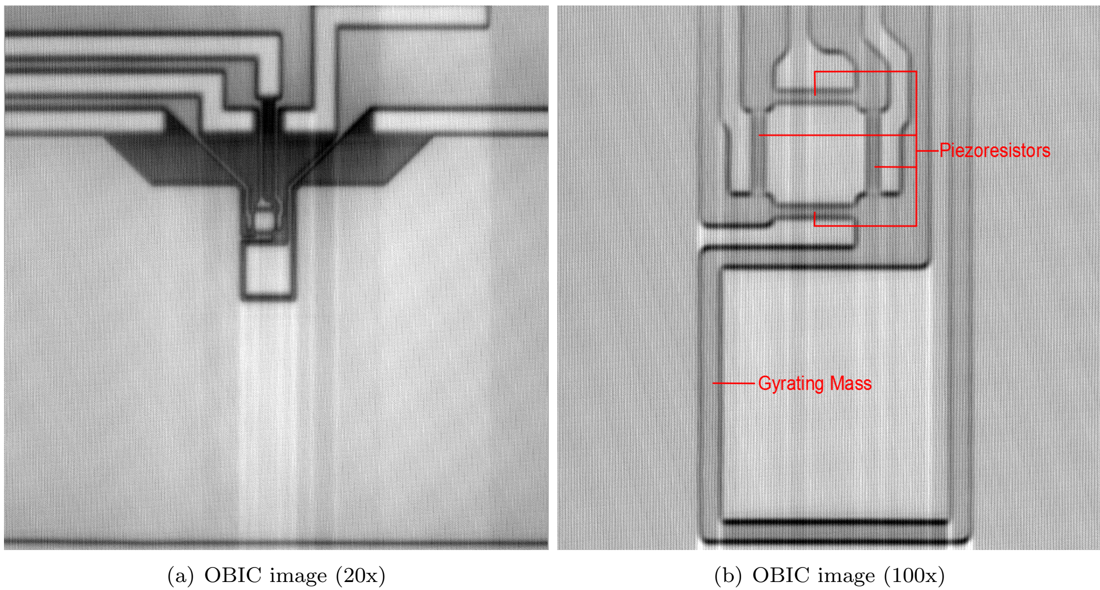

(a) OBIC image (20x)

(b) OBIC image (100x)

Figure 4.4: Detail image of the buried structure of an acceleration sensor

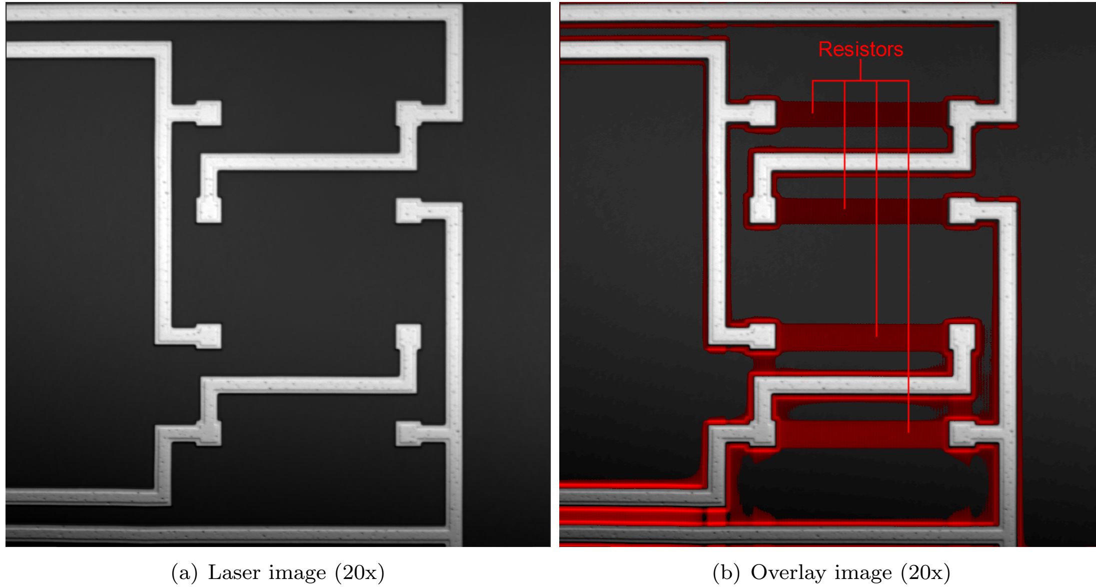

(a) Laser image (20x)

(b) Overlay image (20x)

Figure 4.5: Laser image and overlay image of the piezoresistors of a pressure sensor

4.1.1 Depth sensitive measurements

For the previous measurements, the 1300 nm laser was focused on the surface of the chip. Thus, the strongest signal will be detected when the laser scans over a pn junction which is placed directly on the surface and perpendicular to it. Buried pn junctions will deliver a significantly lower signal compared to those on the surface as the beam will be partially absorbed by the silicon above and thus its intensity will be lower. Additionally it will be out of focus. The focus, however, only needs to be considered if the pn junction is perpendicular to the surface or its dimensions in horizontal direction are smaller than the laser spot size.

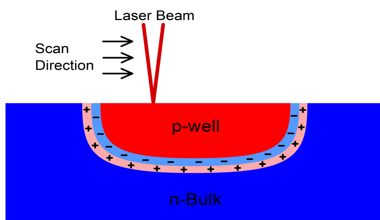

Figure 4.6: Laser scan along a p-well

Figure 4.6 shows a sketch of the cross section of a p-well in an n-bulk to illustrate what happens if the laser scans over it. The light red/blue regions indicate the depletion region. While in the middle of the well, the space charge region is located beyond the surface, it reaches to the top at the edges. This leads to peaks in the measured photocurrent when scanning over the edges. Moreover, a lower doping concentration in the n-bulk than in the p-well causes the depletion region to spread into the bulk when reverse biasing the device. As a consequence the broadening will only be detected at the edges, where the pn junction is rather vertical, while in the middle, where it is almost horizontal one will hardly see any current change.

A measurement was done on one of the p-wells acting as connections from the metal pads to the pressure sensor structures. Figure 4.7 (a) shows an overview image, where the inspected area is marked with a red rectangle. The p-wells are sketched in semitransparent red. Image (b) shows the OBIC image, obtained at 14 V reverse bias, where dark areas indicate a high current value. The results of the experiment matches the previous considerations: The strongest signal is received at the edges, while within the p-well, the photocurrent stays almost constant. A series of images demonstrating the behavior at reverse bias voltages between 0 V and 14 V can be seen in figure 4.8.

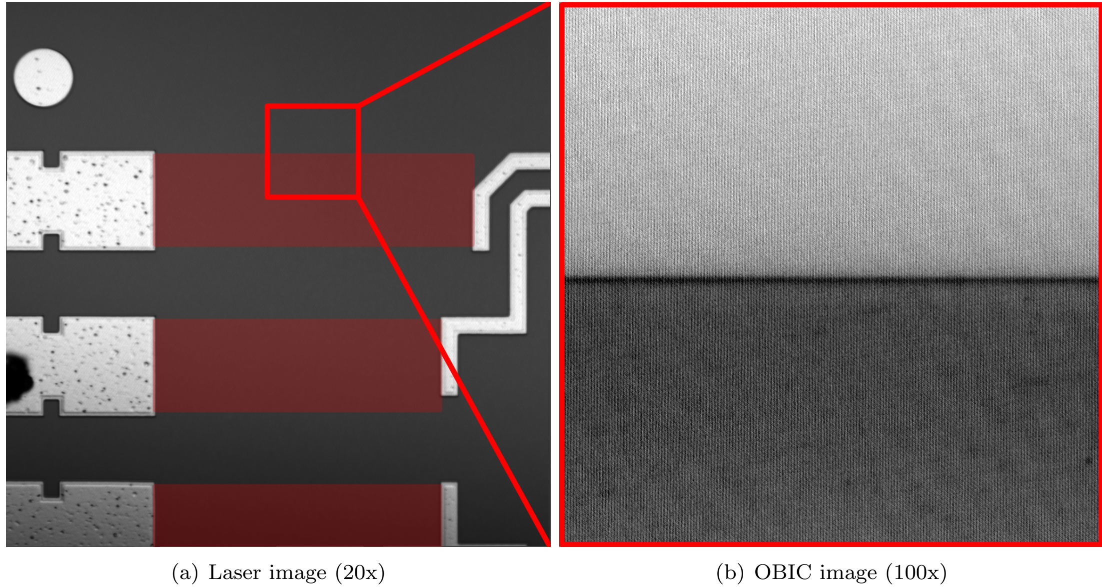

(a) Laser image (20x)　　(b) OBIC image (100x)

Figure 4.7: Detail inspection of a p-well

The results of the measurements suggest that the OBIC signal contains not only information about the position of the pn junction in xy- but also in z direction, thus information about its position inside the bulk. The prospects of an experiment to extract that data depend on the wavelength of the laser and its interaction with the silicon (2.1) and, dependent on which laser is used, the structure of the material. As mentioned before, the PHEMOS-1000 offers two lasers with wavelengths of 1064 nm and 1300 nm. The previous measurement utilizes the fact, that the 1300 nm laser heats up the sample mainly on the surface, thus charge carriers are created mainly in this region. This is why differences in the signal at the edges and the center of the p well can be seen. When executing the same experiment using the 1064 nm laser, the beginning of the p well can, indeed, be easily identified. However, the laser creates charge carriers directly through the depth of the whole substrate, which means that the difference in the signal between the edges and the middle of the well will be less. The result of the same experiment using the 1064 nm laser is shown in figure 4.9. So, in general, for experiments on structures close to the surface, the 1300 nm laser is more suitable. By contrast, when examining a structure deep in the substrate, the lower wavelength laser should be used. An experiment to determine the depth of a structure buried deep in the substrate where the 1064 nm laser was used is described below.

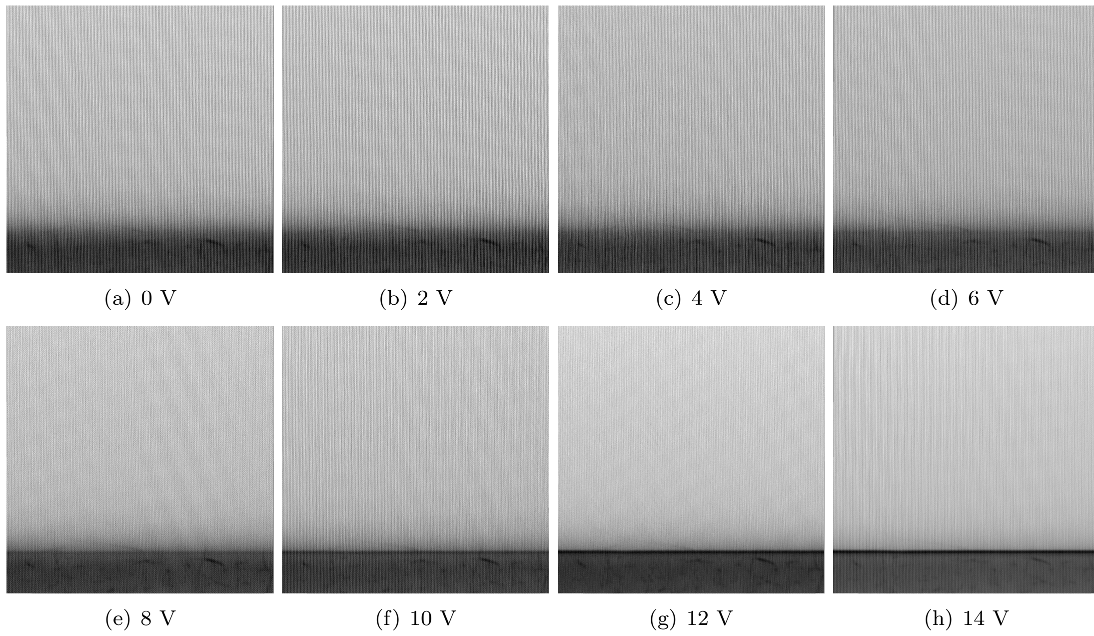

Figure 4.8: Demonstrating the peak arising at the edges of a p-well when reverse biasing the device

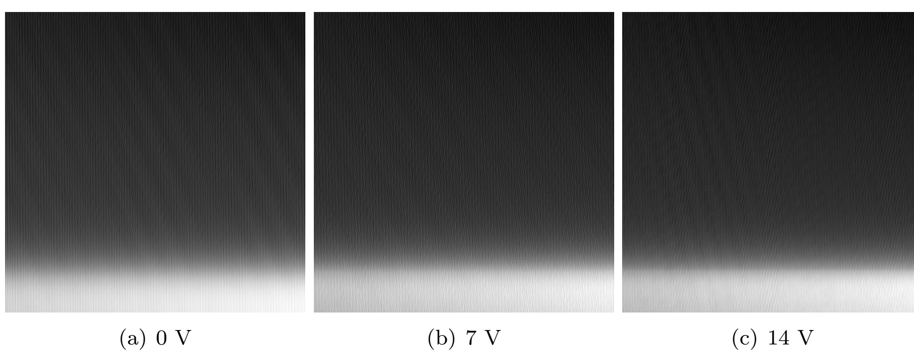

Figure 4.9: p-well, reverse bias: 0 V, 7 V, 14 V, 1064 nm laser

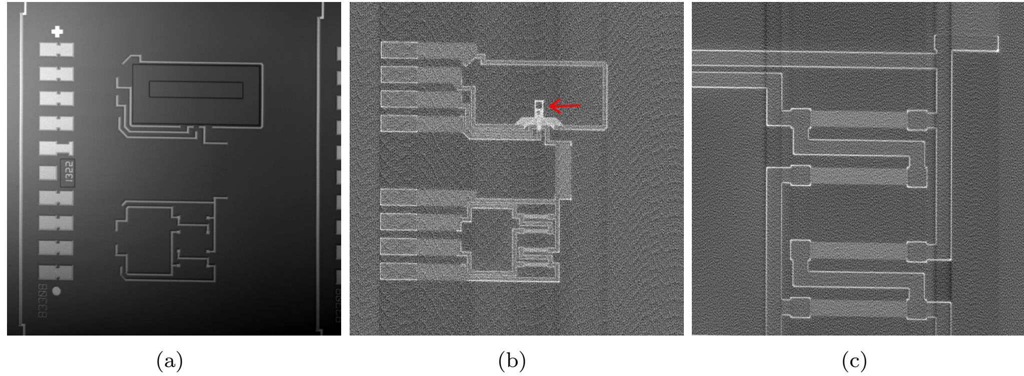

(a) (b) (c)

Figure 4.10: Backside OBIC measurement on a TPMS sensor chip: (a) Laser image, (b) OBIC image, (c) Pressure sensor detail image

Determination of the z-position of the acceleration sensor from the backside

In figure 4.4 the buried structure in the TPMS acceleration sensor was revealed. It is buried close to the surface so that, for a measurement from the front side, focussing on the surface is sufficient to receive the observed results. However, working with the 1064 nm laser beam provides the potential to reveal structures buried deep inside the silicon (assuming that the doping level of the surrounding silicon is not so high that it would lead to significant absorption of the beam) and - if the composition of the surrounding material is known - also the possibility to determine how deep inside the bulk it is located. For this purpose, the laser is focused on the backside at first. After that, the focus is moved in z-direction into the silicon, using the stage control. If the index of refraction of the material illuminated by the beam is known, one can calculate how far the focus will move as the stage is moved for a known distance. When the focus comes near the pn-junction, one will receive a blurred image of the structure at first. A sharp image will occur when the focus reaches the pn-junction - by knowing how far the stage was moved down one then can estimate in which depth of the pn-junction is located. The 1064 nm laser was originally attached to the PHEMOS-1000 to take images when emission microscopy is done from the backside. It is therefore focused through the backside silicon onto the structures on the front side. Then an image is taken from the reflected light. This image is later overlaid with the emission image to relate the received emission spot to a certain position on the chip. From this one can see that the application of the laser in this experiment doesn't differ a lot from the one it was originally intended with the only difference that instead of an ordinary reflection image, an OBIC image is taken. First, an overview OBIC image of the examined chip as well as a detail image of the pressure sensor chip were taken for a demonstration of what can be seen. See figure 4.10. The laser was therefore focused onto the front side from the backside as described above. These and the later measurements were done on a PHEMOS-1000 with a chuck that is conceived for backside analysis on wafers as described in chapter 3.

In the following experiment, the depth of the acceleration sensor structure, sketched with a red arrow in image (b) was determined. First of all the properties of the PHEMOS-1000 have to be known. The stage can be moved at minimum steps of 1 μm at a magnification of 100x. If the stage is moved down, the focal point inside silicon moves a factor 3.5 more because of the refraction of the beam, according to the data provided by the manufacturer. However this factor may change dependent on e.g. the doping concentration. To receive more detailed results, one should determine the factor for the examined sample before the actual measurement starts. For the TPMS chip, the thickness of the wafer was measured on a cross section, as it is shown in figure 4.11 by optical microscopy. It was determined to be 380 μm. Next, the laser was focused on the front side with a magnification of 100x and moved down in steps of 1 μm by counting the

steps till the backside, that had been marked with silver glue as it does not exhibit structures, was reached. Determination of the factor delivered 380/107=3.55.

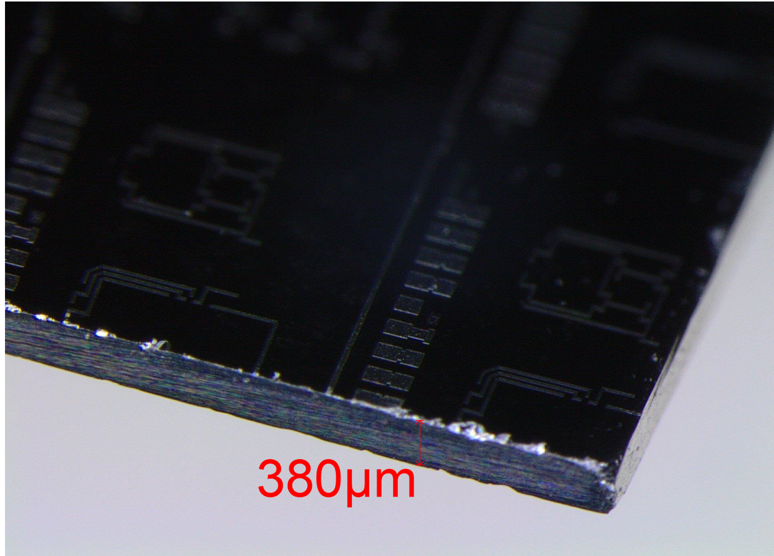

Figure 4.11: Edge of a broken wafer with TPMS sensor chips

To perform the depth sensitive measurement, the laser was moved to the desired position and focused on the surface of the backside with 100x magnification. Then the stage was moved down step by step, taking an image for every step. The result (a selection of the images) is plotted in figure 4.12. Image (a) shows the OBIC signal when the beam is focused on the backside: No structure can be seen, as well as in the next images (b) and (c), taken in a calculated depth of 71 and 142 μm. In a depth of 213 μm the contours of the buried structure can be noticed. In a depth, of 376 μm the beam is in perfect focus - this is the estimated depth of the pn-junction. When the stage is moved down deeper, the structure gets blurred again as it is seen in image (i). In contrast to the previous measurement on a p well, executed with the 1300 nm laser, this measurement does not deliver information about the shape of the p layer. It simply uses the fact that the strongest signal is measured when the laser is focused. It works well on thin layers that are small compared to the laser spot size. If the layer extends deep in z-direction a problem occurs that will be seen in chapter 7 at cross sections: While the laser is focused in a certain depth, an additional signal is detected that comes from deeper layers - one doesn't receive sharp transitions. If a p-structure larger than the spot size is examined as it is e.g. the case if a simple diode chip is observed (which consits of only a p and an n layer and a horizontal pn-junction) through the backside, the signal detected will always be the same, no matter if the beam is focused on the pn junction or not. In that case the total beam intensity reaching a pn junction stays the same no matter if the diameter of the spot gets smaller. A possibility to improve the experiment is to use a variable laser frequency. The penetration depth of the beam could then be calculated and the received signal could then be related to a certain depth. With this method, the homogeneity of a doped layer could be measured. However, this method could not be checked in practice as the equipment only offers the two mentioned lasers.

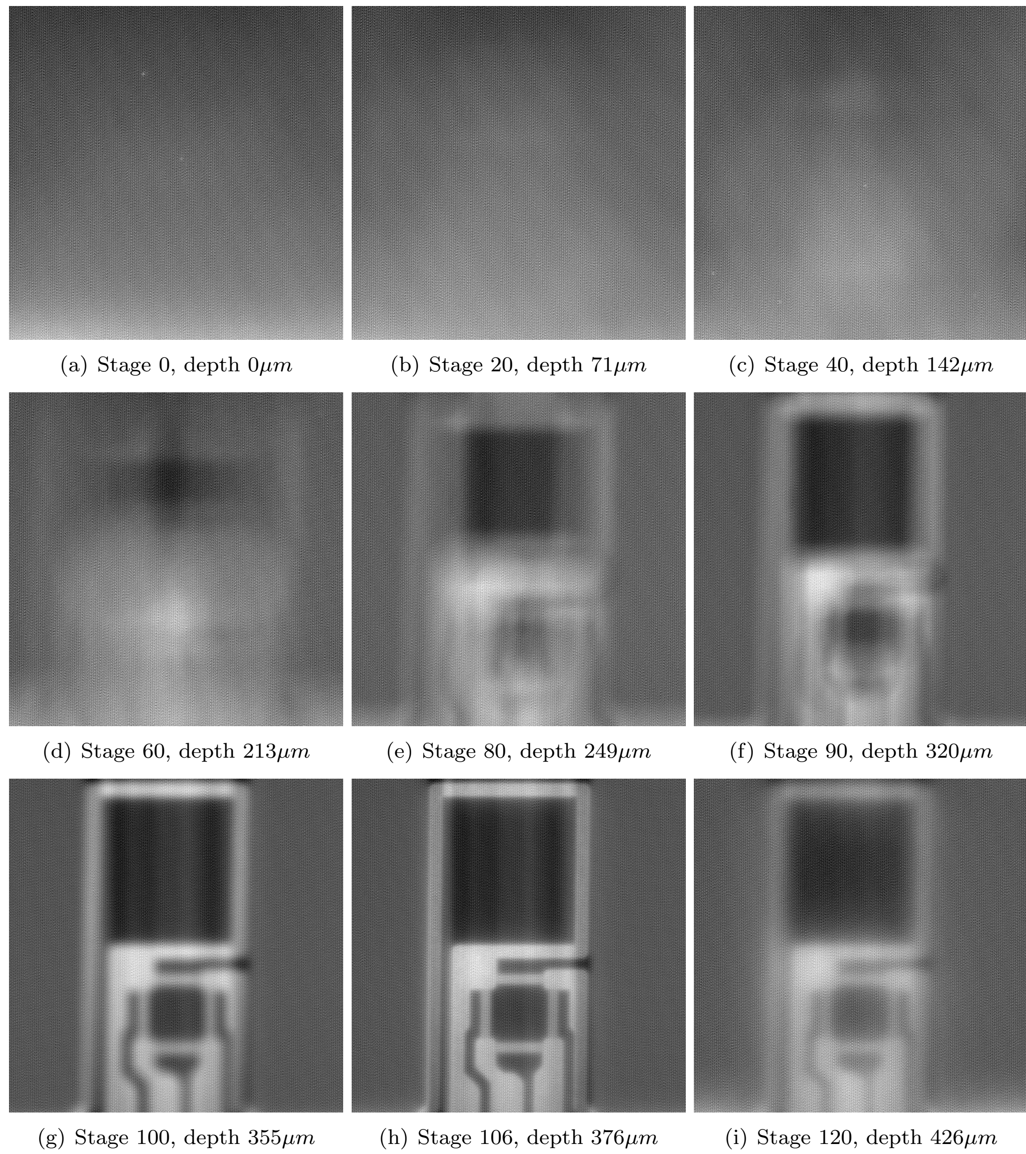

(a) Stage 0, depth $0\mu m$ (b) Stage 20, depth $71\mu m$ (c) Stage 40, depth $142\mu m$

(d) Stage 60, depth $213\mu m$ (e) Stage 80, depth $249\mu m$ (f) Stage 90, depth $320\mu m$

(g) Stage 100, depth $355\mu m$ (h) Stage 106, depth $376\mu m$ (i) Stage 120, depth $426\mu m$

Figure 4.12: Determination of the depth of the buried structure of the acceleration sensor of a TPMS sensor chip from the backside

4.2 Diffusion length measurements

There are two alternative ways to execute a line scan for a diffusion length measurement with the PHEMOS-1000 which lead to equivalent results. In the first one, the scan mode is set on point scan (see also chapter 3), in which the laser is fixed at a certain position. The current is measured with an externally connected amperemeter. The laser is then moved over the sample step by step manually using the stage control. For every step, the current is noted. This is the direct way. It delivers acceptable results, however it is very time consuming - a line scan can take a couple of hours, depending on the sample. For the second way, an ordinary image is taken as it was done in the previous experiments. This works comparatively fast, but the desired data has to be extracted from the images at first. This is done by a software that had to be specifically programmed. In contrast to the direct method, one has no access to the exact current values as the software only delivers an image in which every current value is equivalent to a certain gray level. This should not be a problem as for the parameters that shall be obtained by the subsequent analysis only the shape of the graph and not the exact current value is a matter of interest. In this thesis experiments using both methods were done.

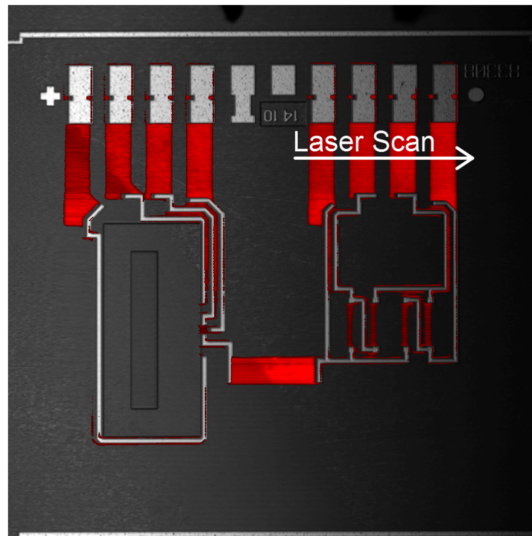

Figure 4.13: TPMS overview image for a line scan along the p-wells(conductors) between pins and the sensor structure. The scan direction is indicated with a white arrow.

Those methods are demonstrated in figure 4.14 which shows the measured current when a line scan along the p-wells acting as conductors is executed ((a) by measuring the current directly via the picoamperemeter and (b) by extracting the data from an OBIC image). In figure 4.13 an overview laser image of the TPMS sensor chip, overlaid with an OBIC image can be seen, in which it is sketched where and in which direction the line scan was performed using the first method with a white arrow.

For figure 4.14b, the data was extracted from an image taken with 5x magnification. The stage is not completely level, which explains the rising of the current minima/maxima from the left to the right in the extracted plot.

The procedure to obtain the diffusion length of the minority charge carriers from the measurement was described in chapter 2. Equation 2.4 delivers a relationship for an ideal, linear pn-junction perpendicular to the surface and parallel to the incident beam if the minority charge carriers are created in a small region close to the surface only. However, these conditions will not be present in the TPMS sensor chip. In fact the present pn-junctions are p-wells of various

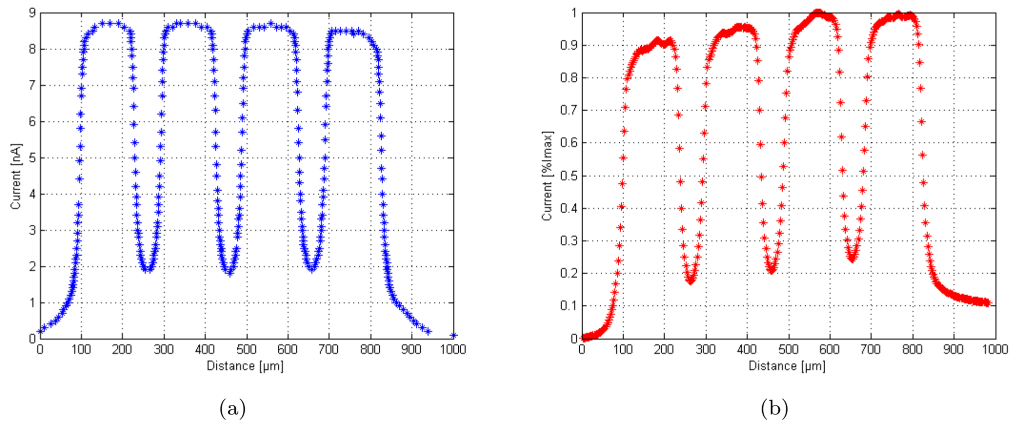

Figure 4.14: Linescan along four p-wells of a pressure sensor using an external picoamperemeter (a) / extracting data from an OBIC image (b)

depths and dimensions in n-silicon. Moreover, in contrast to theory, the laser beam will create charge carriers not only in a region near the surface (if the 1064 nm laser is used) but in a broadening cylindrical area through the whole vertical extension of the chip.

As it was described in 2.2 the intensity within a circle in this cylinder, which lies in a magnitude of μm (which is described in chapter 3), is not perfectly equally distributed within the circle and has no sharp transition at the edge, but exhibits a Gaussian intensity distribution. This creates an influence on the measurement results. While scanning over a pn junction with a perfectly sharp laser would (neglecting diffusion at first) deliver a step function which assumes a constant current value if the beam is over the depletion region and zero if it is not, scanning over a pn junction with the real laser beam delivers the integral over its Gaussian intensity-distribution function, which is the density function. When, additionally, the diffusion current is taken into account, which exhibits an exponential decrease with the distance to the depletion region, the measured total current signal will be a combination of those two contributions if the position of the beam is close enough to the pn junction so that it extends partially into the depletion region. The measured current will then always be caused by minority charge carriers created inside the space charge region and such created outside but diffusing into it. When the whole beam is outside the pn-junction, the source of the current will only be the diffusion of minority charge carriers. These considerations describe the limits of the resolution power. Diffusion lengths close to the spot size will not be detectable. The described behavior can be seen if the logarithmic current is plotted. The curve will exhibit a kink from the distance on where the effect plays a role. This is usually at a distance of about 10 - 20 μm as the standard deviation σ of the Gaussian intensity distribution is denoted with a value of about 3 μm and furthermore the interaction area within the sample will be usually bigger. For the extraction of the diffusion length the values above that distance will be fitted. If one tries to fit a function to the real measurement values the fit function for the diffusion current has to be multiplied by the fraction of the total laser beam that is outside the depletion region and afterwards the current created inside the depletion region has to be added to the function.

The relationship for the diffusion length depends on the geometry of the device and the surface recombination. The TPMS chip has a thickness of about 400 μm (as it was seen before). On the top there are p-wells in an n-region. However, most of the 400 μm is p-substrate. In the fabrication process, an n-region is implanted into the p-substrate and an additional n-region is grown epitaxial onto it. Together, the n-region exhibits a thickness of about 20 μm. The p-well conductors extend about 10 μm into the n-region. From the backside, the p-substrate is

isolated with an oxide layer. However, it is internally connected to the n-epi. The frontside is also protected by a thin oxide layer.

It is difficult to include the surface recombination velocity for this structure. The oxide layer should decrease the surface recombination at the frontside. However at the backside, the pn-junction at the transition from the n-epi to the p-substrate acts as a sink for minority charge carriers (holes) created in the n-region.

For the determination of the diffusion length, line scans were done on one of the p-wells. It is obviously that a pn-junction with no other components nearby that could affect the results is most suitable for the determination of the desired parameters. Of the eight pn-junctions available in the previous linescan in figure 4.14, one would use one of those two that are situated at the edge. In figure 4.15 the position on the chip where line scans were done is shown. The scan direction is indicated with a red arrow.

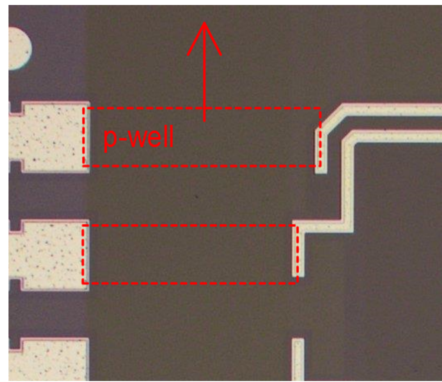

Figure 4.15: Position of the line scan for the diffusion length measurements (p-well (conductor) between pin and sensor structure on the pressure sensor).

To extract the diffusion length, the p-wells were considered as pn-junctions parallel to the incident beam, as it is idealized shown in figure 3.3. The relationship for the diffusion length for this structure was given by 2.29 where $\tilde{\alpha}$ was a fitting parameter which takes the surface recombination into account. For the present structure $\tilde{\alpha}$ equals 0.5 for infinite surface recombination velocity and 0 if the surface recombination is neglected. For all measurements a constant noise will be present. This noise is subtracted before the estimation of the diffusion length.

4.2.1 Comparison of two possibilities to obtain the diffusion length

The two possibilities to perform the measurement which have been described were compared first. This measurement intends to compare both ways to perform the measurement and therefore the surface recombination velocity was neglected at first. Figure 4.16 a and b show the result of a diffusion length measurement on a p-well of a TPMS sensor chip, executed with the 1064 nm laser, as it was indicated in 4.15. The current was measured by the use of an external picoamperemeter. If the parameter $\tilde{\alpha}$ is chosen zero the relationship for the diffusion length simplifies to equation 2.30. Image (a) shows the results of the line scan, where the x-axis is the distance to the pn-junction and in the y-axis the measured current is plotted. In image (b) $ln(I_{diff})$ is plotted versus $-\frac{r}{L}$. A linear fit was done to obtain the diffusion length of the minority charge carriers (holes) in the n-region (red line). One can see that for distances close to the pn-junction than about 20 μm the kink which is described above appears. The fit was therefore done through the current values measured more than this distance away from the junction. The obtained value for the diffusion length is $L = 44\,\mu m$.

When a line scan is performed the second way by analyzing the images delivered by the software, one has to keep in mind that the main target of the PHEMOS-1000 is the execution of optical beam induced resistance change (OBIRCH) measurements, where it is important to display the relative thermally induced current changes of points situated next to each other (e.g. on an IC[1]). Therefore, the gray levels for the intensity would not have to correlate exactly with the measured current. However, that is the most important factor for estimating the diffusion length. For the success of an experiment, the parameters, especially the laser power and the scan speed have to be well considered to receive useable results. The parameters used for the experiment are summarized in the appendix. Based on the experience from several measurements, the laser power should be set to the lowest possible level where a signal can be seen, which normally lies between 1 and 2 percent of the maximum laser power. High scan speed should be chosen to avoid side effects. One should not use the possibility the software offers to integrate over multiple images, as this can distort the measurement.

In figure 4.16c and d the result of a measurement where the diffusion length was estimated from an image taken at the same position is shown. Its value is similar to the first measurement (L=44μm). Above 50 μm a drop in the graph can be seen. Above 80 μm, which is the edge of the image, the lowest current values will be seen which correspond to color values close or equivalent to zero, which causes a drop in the graph which is cut from the plot. Once one has the program to extract the image data, this experiment is a lot faster to perform than measuring the current directly with the picoamperemeter. However, if it is desired to obtain the diffusion length exactly the use of the first method will deliver more reliable data. Especially the drop that occurs at the edge of the image is an undesired effect. All of the following diffusion length measurements on the TPMS have been done using the first method.

[1] Integrated Circuit

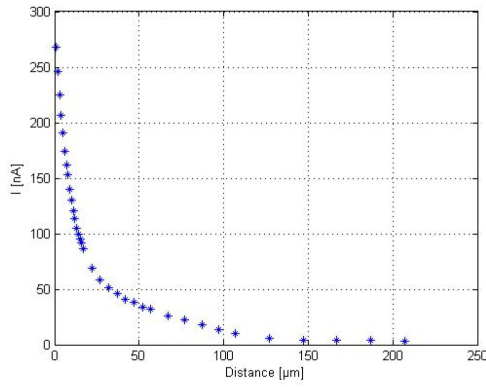

(a)

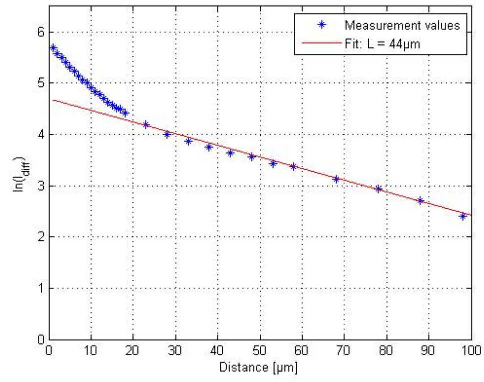

(b)

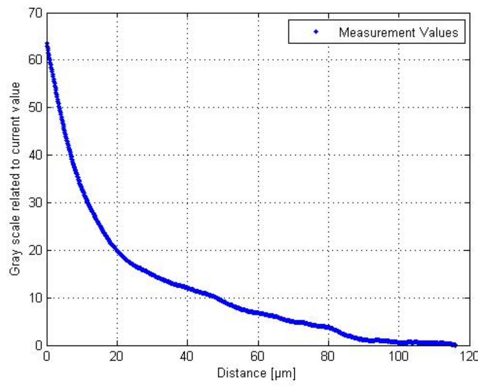

(c)

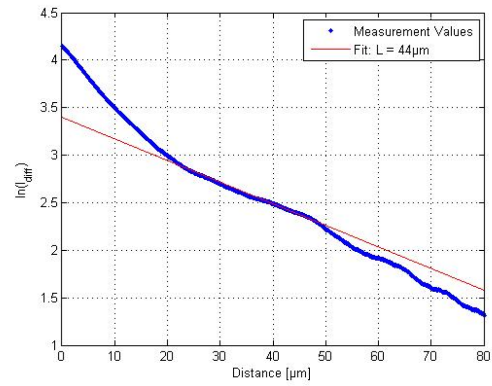

(d)

Figure 4.16: Original measurement data of a line scan perpencidular to a p-well (conductor) in a TPMS sensor chip and extraction of the diffusion length of minority charge carriers, measured with an external picoamperemeter (a,b) and measurement data and calculated diffusion length extracted from an OBIC image taken at the same position (c,d).

4.2.2 Comparison of diffusion length measurements with the 1064 nm and the 1300 nm laser

In the previous measurement the 1064 nm laser has been used. It creates charge carriers deeper in the substrate than the 1300 nm laser. The influence of the used laser to the measurement results is investigated in this section. Therefore two linescans using both lasers were done at the same position. Figure 4.17 shows the data obtained in this measurement. The graphs show the expected exponential decrease. Usually the 1300 nm laser delivers very low maximum currents also for 100 % laser power. In this measurement the maximum current value if the laser is above the depletion region was only about 3 nA. As described before, in reality the current will always be superimposed by an offset current which is almost constant over the whole sample. The offset can be seen very well in the measurement with the 1300 nm laser (4.17b) and lies at about 0.5 nA. Before the diffusion length was obtained the offset value was subtracted.

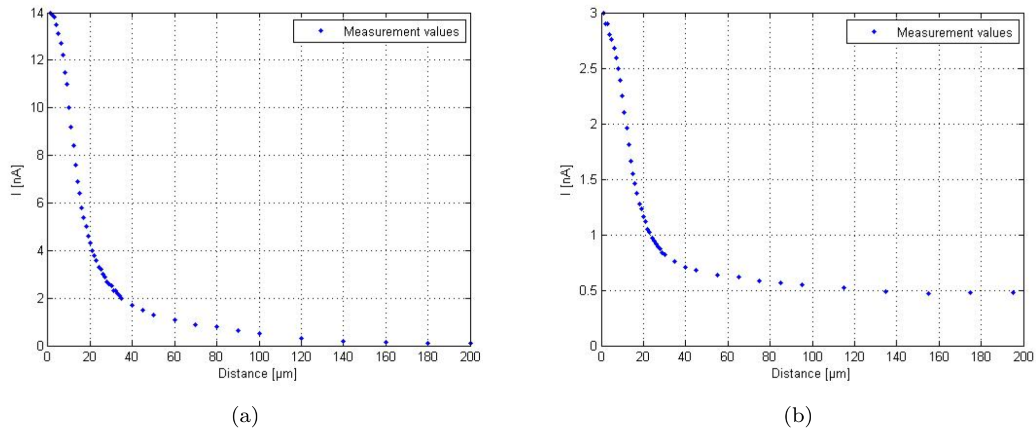

Figure 4.17: Measured current values plotted against the distance to the pn-junction for two line scans on a p-well, executed at the same position with the 1064 nm laser (a) and the 1300 nm laser (b).

The graphs with the evaluated parameters, obtained from the measurements data plotted in figure 4.17, are shown in figure 4.18. The data is plotted both for the assumption of an negligible and an infinite surface recombination velocity. It can be seen that the estimated parameters don't depend from the used laser in this particular case. As the 1300 nm laser creates charge carriers near the surface only, while the 1064 nm laser creates them also in the bulk one could have expected that the graph for the 1300 nm laser shows a sharper decline if strong surface recombination is present. Therefore, a conclusion could be that the surface recombination velocity can be neglected. This would lead to a diffusion length of 44 μm. If the surface recombination was infinite, the samples would exhibit a diffusion length of 92 μm. OBIC experiments to determine the diffusion length, found in literature research, done with a 1020 nm laser can be compared use a negligible surface recombination, based on the consideration that the laser creates charge carriers deep in the substrate ([Fl090]).

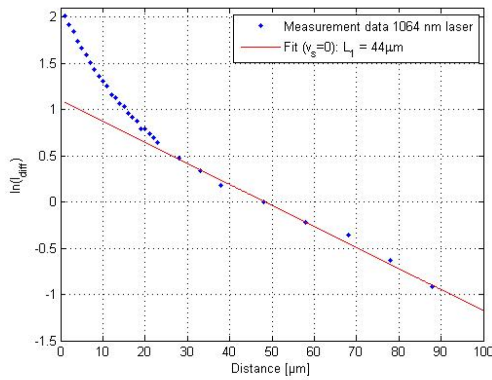

(a)

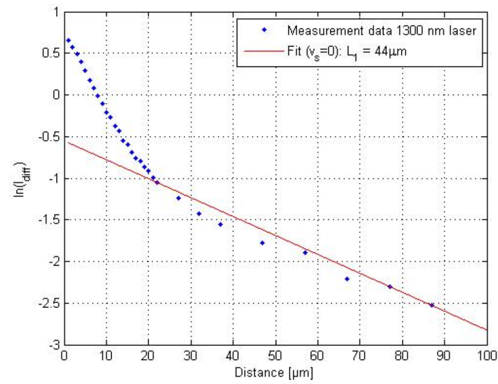

(b)

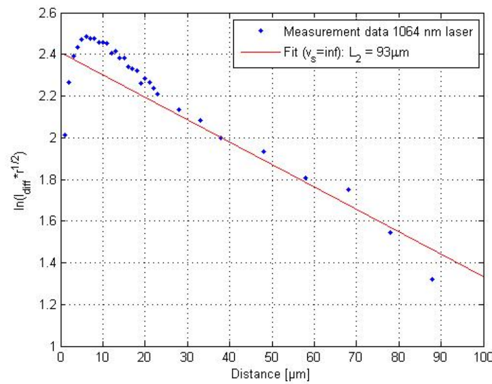

(c)

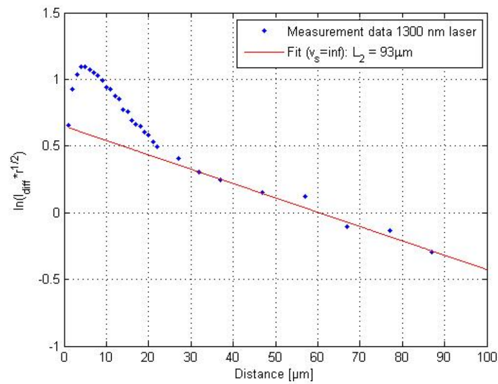

(d)

Figure 4.18: Comparison of estimated diffusion length by using the 1064 nm laser (a,c) and the 1300 nm laser (b,d) from the measurement data obtained in 4.17 for negligible surface recombination (a,b) and infinite surface recombination (c,d).

4.2.3 Line scans with various intensities

To reveal the section above 20 μm away from the pn-junction, the laser power at the 1064 nm laser can be increased. The expected result should be the same shape of the curve with a higher current and therefore a better possibility to reveal the region which has been close to zero and get useful results also in a distance more than 100 μm away from the pn-junction, where for the previous measurements the current values were too close to zero to deliver practical data. As the kink at the beginning of the graphs was explained by the laser spot size which should hardly change if the power is increased it should not change its width. The results for measurements setting the laser power to 50 %, 75 % and 100 % are plotted in figure 4.19. It can be seen in the images a-c, where the original measurement data is plotted, that the current is in the μA range in this experiment. The kink at the beginning stays the same as it was expected. Therefore the results match the interpretation. The linear shape of the curves could be revealed up to 140 μm very well and the fits deliver diffusion lengths of L=46 μm, L=47 μm and L=48 μm.

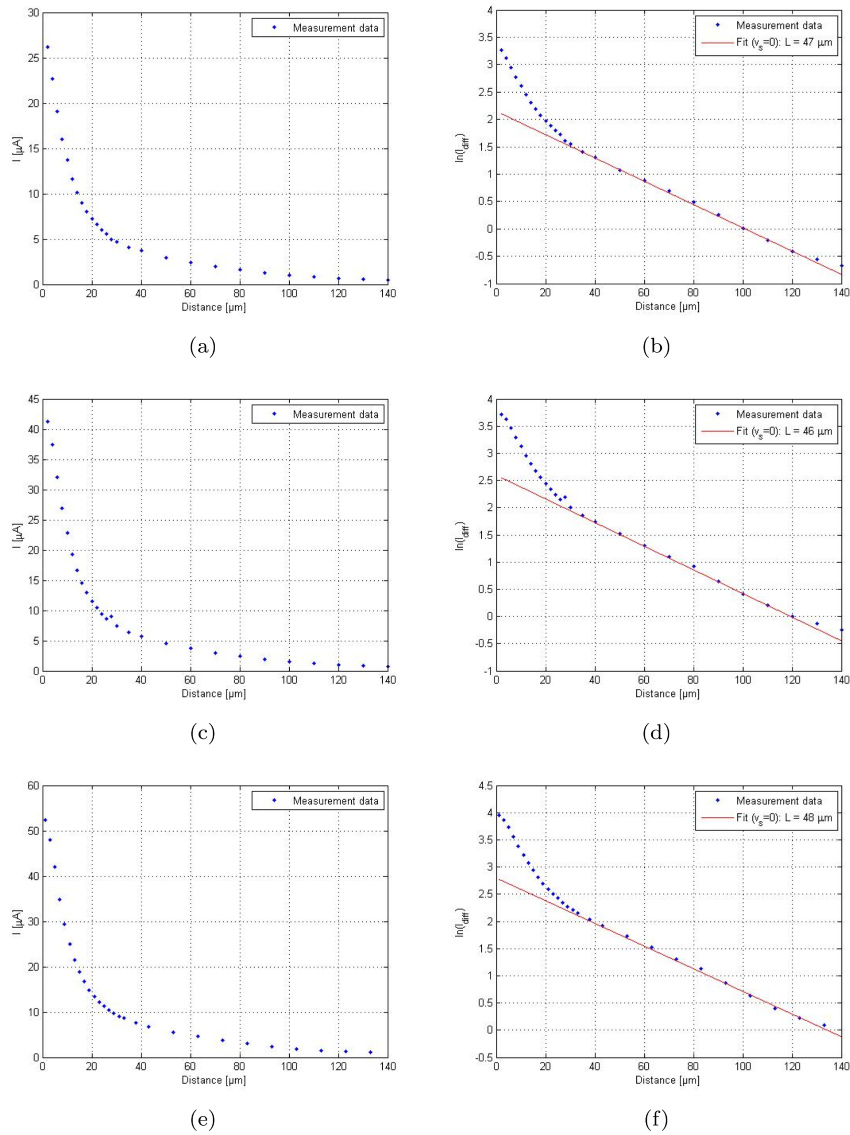

Figure 4.19: Diffusion length measurements with the 1064 nm laser for high laser powers: a,b: 50 % laser power, c,d: 75 % laser power, e,f: 100 % laser power.

4.2.4 Comparison of line scans done at different positions of the p-well

The diffusion length doesn't have to be constant over the whole sample. Additional to the diffusion length measurement at the first position, where L=44 μm was obtained under the condition of no surface recombination. The same line scan was done at two different positions on the p-well. The results are plotted in figure 4.20. Diffusion lengths of 39 μm and 47 μm were obtained.

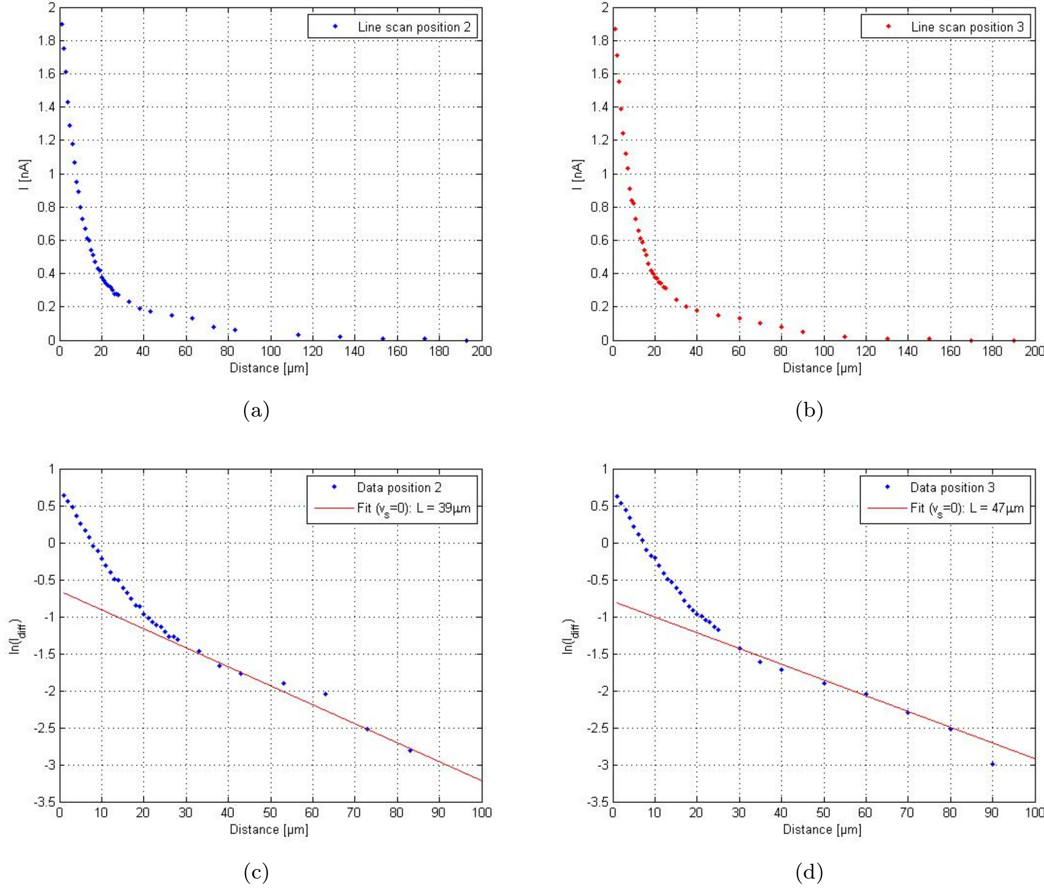

Figure 4.20: Results of diffusion length measurements at two different positions of the p-well.

4.2.5 Deriving a function including the laser spot size

The kink which appears if the current values are plotted is caused by the laser spot width. As it was mentioned several times the laser beam exhibits a Gaussian intensity distribution. If the beam is scanned over the edge of the depletion region, some of it will be inside, some of it outside the depletion region and therefore create charge carriers in- and outside. Charge carriers created inside will be separated immediately and therefore lead to a current additional to the current that comes from diffusion. Furthermore the current takes a constant value maximum value I_{max} if the laser is completely over the space charge region. Neglecting diffusion, the current detected will be dependent only on the part of the laser spot which is over the depletion region. The decrease of the current caused by the laser spot width I_{spot} is then given by the density function multiplied with the maximum current value I_{max} if the whole laser is over the depletion region:

$$I_{spot} = I_{max} \cdot \frac{1}{2} \cdot \left[1 - erf\left(\frac{r - \mu_g}{\sqrt{2 \cdot \sigma^2}} \right) \right] \tag{4.1}$$

In equation 4.1, μ_g (expected value) is the position of the edge of the depletion region, r the distance from it and σ is the standard deviation. If the diffusion length and $\tilde{\alpha}$ are known, the diffusion current I_{diff} can be calculated, as it was given in 2.29. The next step, the diffusion current has to be corrected by the part of the laser beam, which is over the depletion region. This was done by multiplying it with the inverse of the density function. It will then be zero if the whole beam is over the depletion region. As last step both current contributions are added.

This was done for the measurement values shown in figure 4.17b. In figure 4.21 the result is shown. The measurement values are plotted in blue. The green line shows the contribution to the current by minority charge carriers created directly inside the depletion region caused by the circumference of the laser beam. The standard deviation σ was chosen $6\,\mu$m. The red line is a plot of the diffusion current as it is described in equation 2.29 for L=$44\,\mu$m. Surface recombination was neglected. The function for the current caused by diffusion multiplied with the part of the laser beam which is outside the depletion region is plotted in black. The resulting values are then added to the current caused by the fraction of the laser spot which is above the depletion region. This leads to the purple curve. Both current contributions lead to a curve that fits the measurement values.

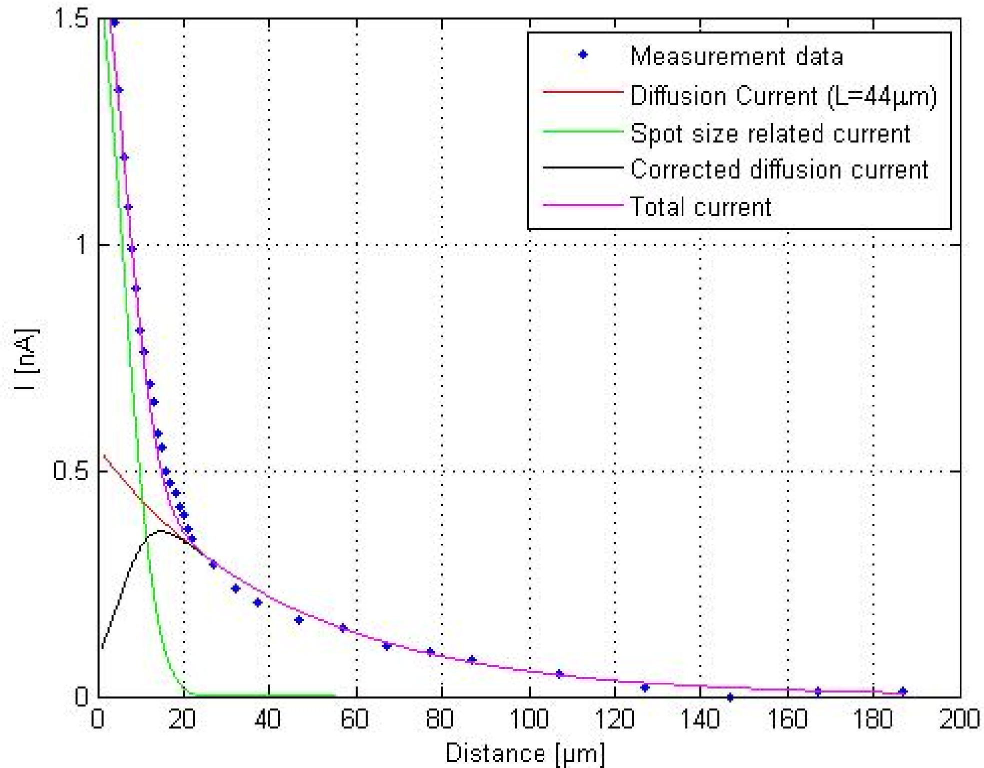

Figure 4.21: Measurement values and theoretical function when scanning over a pn-junction

Chapter 5

OBIC measurements on proton doped samples

5.1 EDMR

The measurements were performed on samples which were originally designed for electrically detected magnetic resonance (EDMR) analysis. They consist of an n doped bulk material and a thin p^+ doped layer on the front side. Additionally, except for sample 'EDMR8' which is used as reference device, the samples were implanted with protons and then annealed which leads to an n^+ region beyond the p^+ region. To execute the measurements, cross sections of the samples were prepared as described in 3.3. The exact setup for every measurement is summarized in the appendix.

5.1.1 Determination of the depletion width and the concentration of dopants of EDMR8 (not proton doped)

As OBIC measurements on a pn junction provide the current maximum if the charge carriers are created within the depletion region and as the current value for the whole depletion region is almost constant, these measurements offer a direct way to determine and visualize the space charge region. Moreover, the broadening of the depletion region when reverse bias is applied can be measured and compared to theoretical values. In the most simple, one-dimensional case, the relationship between the depletion width and the applied voltage is given by equation 2.26. For measurements on devices like that, the 1300 nm laser is chosen as these cross sections correspond compltetely to the devices shown in 3.3b.

The undoped EDMR samples is very suitable for this measurement, as it exhibits a shallow p-doped region at the frontside and a n-region with a low doping concentration. The pn-junction will therefore broaden almost only into the n-region and, moreover, the voltage that has to be applied to receive resolveable results will be quite low because, due to the lightly doping the depletion width increase will be already quite large there. When executing the measurement, one would expect a heavy increase of the current when the laser spot reaches the pn-junction (thus creating charge carriers within the space charge region) and a saturation of the current as soon as the laser beam is in its entirety above the depletion region. However, in general the depletion width at zero bias will be smaller than the laser spot size. Hence, the saturation of the current will only be observed when the applied voltage is hight enough to increase the depletion region so that it exceeds the spot size. For smaller depletion widths the maximum current value during the experiment will be lower.

For the experimental realization, a series of OBIC measurements, in which the applied voltage

was increased in 1V steps from 0V to 25V, using the parameters summarized in the appendix was performed. A selection of the obtained images can be seen in figure 5.1. The space charge region can be identified as the white stripe on top of the images. The broadening of the depletion region when reverse biasing the sample can be seen. When observing an abnormality in the depletion region one could conclude that there is a local inhomogeneity in the doping profile or, considering that the depletion width depends on the concentration of donors/acceptors a fluctuation of the doping concentration. However, these fluctuations may also occur as a result of the preparation of the sample as a cross section which causes inhomogeneities on the surface, which is also the region where most of the charge carriers are created that contribute to the signal, as the experiments are in executed using the 1300 nm laser.

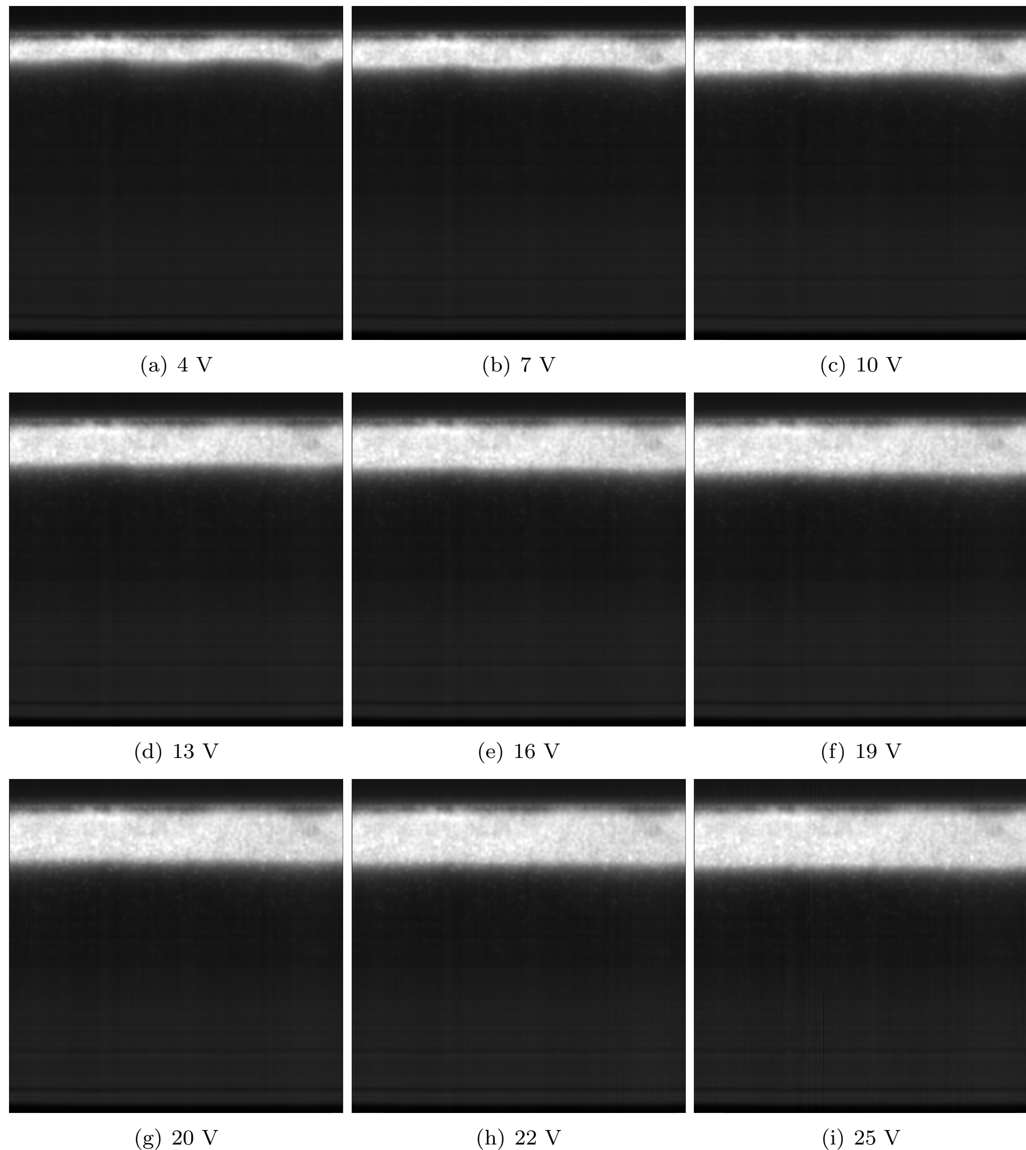

(a) 4 V (b) 7 V (c) 10 V

(d) 13 V (e) 16 V (f) 19 V

(g) 20 V (h) 22 V (i) 25 V

Figure 5.1: OBIC images demonstrating the broadening of the depletion region of sample EDMR8 (reference, no proton implantation)

To obtain the depletion width from the OBIC images, the current values were averaged parallel to the pn junction to get a linear representation of the measured data. Moreover, the offset

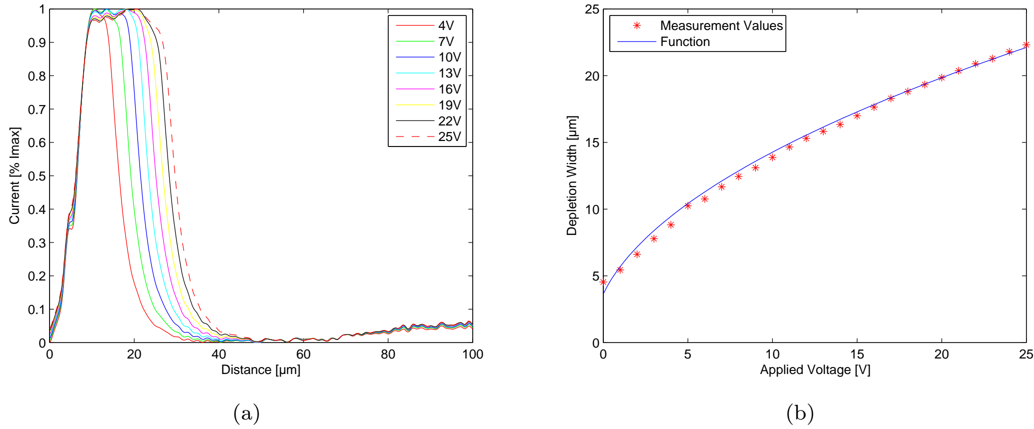

Figure 5.2: (a) Broadening of depletion region (b) Depletion width as a function of voltage compared to calculated values using equation 2.26

was substracted and the data was plotted in terms of the maximum current value in figure 5.2 (b). Afterwards, the width of the observed peak was measured at a current value of 0.6 (as the laser spot is not negligible small) and plotted in 5.2. One would chose the current value at 0.5 if there was no diffusion as it is the point where half of the laser beam is above the space charge region and thus the exact position of the pn-junction. In reality, additionally, charge carriers created outside the depletion region diffuse into the pn-junction and cause a diffusion current. The width of the depletion region must then be smaller as it is at a peak width of half of the maximum. As the contribution of these charge carriers decreases fast when the peak of the gaussian beam has passed the pn-junction, the actual value must be slightly above 0.5 and was chosen 0.6.

As implied previously, equation 2.26 contains information about the concentration of dopants. When the depletion width is determined experimentally at a pn-junction where the concentration in one region (in this case the n-region) exceeds the concentration in the other region by far, the doping concentration can be obtained. This was achieved by overlaying figure 5.2b with the calculated values using equation 2.26, adjusting the parameter N_D to the measurement values with $V_{bi} = 0.7\,V$.

$$N_D = 7.5 \cdot 10^{13} cm^{-3}$$

This matches the results of measurements done by spreading resistance profiling (SRP) and summarized in the appendix. SRP measurements deliver the majority charge carrier concentrations and therefore the doping concentration as it is almost equal at room temperature as was described in 2.14 and can therefore be used to compare the results. If the built-in voltage is not known, it can be determined from the data too. It is the intercept if the depletion width W is plotted versus $\sqrt{V}$.

5.1.2 Determination of the diffusion length of minority charge carriers on EDMR8 (not proton implanted)

The broadening of the depletion region could be estimated from the image data very well. However, to measure the diffusion length, one has to perform line scans using the external connected picoamperemeter as it was described in chapter 4. The structure is a pn-junction parallel to the incident beam as it was shown in figure 3.3. The 1300 nm laser is used which means that the minority charge carriers are created near the surface and determined as described in chapter 2 using equation 2.28. Therefore and according to the sample preparation infinite surface recombination was considered, as the surface itself is a grinded cross section and will therefore exhibit lots of defects.

The result can be seen in figure 5.3. As one can see in figure (a), where the measured current is plotted versus distance, the current decreases very fast when the laser beam is outside the depletion region and then takes a value close to zero (at about 15 μm). This makes it very difficult to obtain the diffusion lenght. The low currents deliver unreliable results, a current amplifier or a laser with higher power would have to be used. Again, as in the previous diffusion length measurements a kink is seen related to the laser spot size till about 15 μm. Above that the values are very noisy as the corresponding current is close to zero. Therefore, no linear fit is done. This experiment depicts the limits of a diffusion length measurement using this method: If the induced current is very low it cannot be revealed any more.

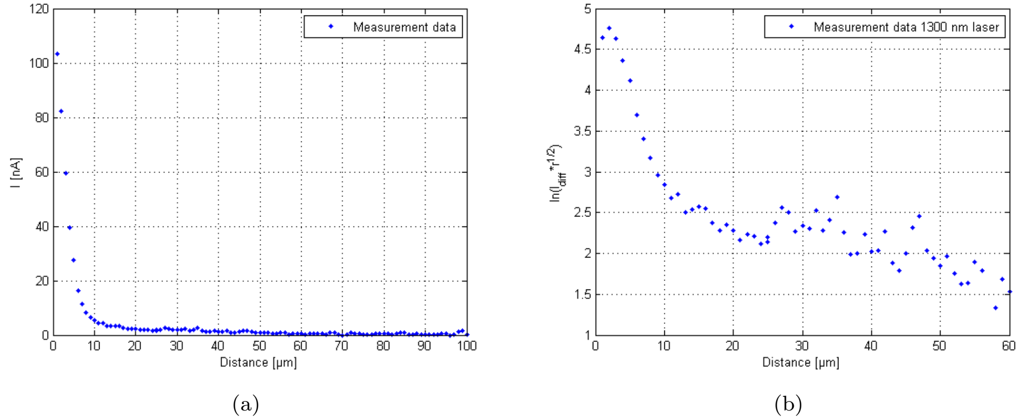

Figure 5.3: Current versus distance in a linescan along EDMR8 (not proton doped) (a) and extraction of the diffusion length of minority charge carriers, measured with the picoamperemeter (b)

Also the use of a different laser could probably deliver better results here. As it was described in chapter 3 the 1064 nm laser cannot be used in this experiment. A laser suitable for this experiment should be able to create charge carriers by interband absorption till a certain depth, but should be absorbed stronger than the 1064 nm laser to avoid the undesired side effects. As could be seen in figure 2.1a laser with a lower wavelength and variable intensity would fulfill these conditions.

5.1.3 Determination of the depletion width and the concentration of dopants of proton doped samples

As mentioned above the proton doped samples exhibit a shallow n+ doped region at the pn junction, which can be also seen in the SRP measurements. The expected effect on the experiment would be a more narrow space charge region as long as it doesn't extend into the more lightly doped region (as the doping concentration is the important parameter). If it extends into the more lightly doped region, the increase should be stronger again when it is reverse biased even more. The PHEMOS-1000 offers the possibility to apply a maximum voltage of 25 V. If the critical voltage lies above that, which is dependent on the width of the n+ region, it will not be possible to reveal this effect and therefore not possible to determine the doping concentration.

In this measurement, the behavior of of three proton doped samples was investigated. They differ in the width of the proton implanted n+ region which is located next to the p-region on the frontside of the chip. According to SRP measurements, the widthsof the n+ region of EDMR4 ($\approx 2\,\mu$m), EDMR5 ($\approx 2,5\,\mu$m) and EDMR6 ($\approx 3\,\mu$m) are between 2 and 3μm. For every sample, OBIC measurements done with the 1300 nm for a reverse bias of 5 V, 15 V and 25 V are shown in figure 5.4.

Again, the white stripe on top of the images indicates the depletion region. There is hardly any broadening seen for the maximum voltage of 25 V, which means that in this case an estimation of the concentration of dopants was not possible due to the highly doped n+ layer. According to the SRP measurements the concentration of dopants is about $10^{16}cm^{-3}$ in the n+ region. This would lead to a depletion width of below 5 μm and matches the result of the measurement.

However, those samples showed an unexpected behavior. As can be seen a bright, blurred region appears next to the depletion region. As the region next to the depletion region is more heavily doped one would rather expect a decrease even sharper as in the reference sample EDMR8.

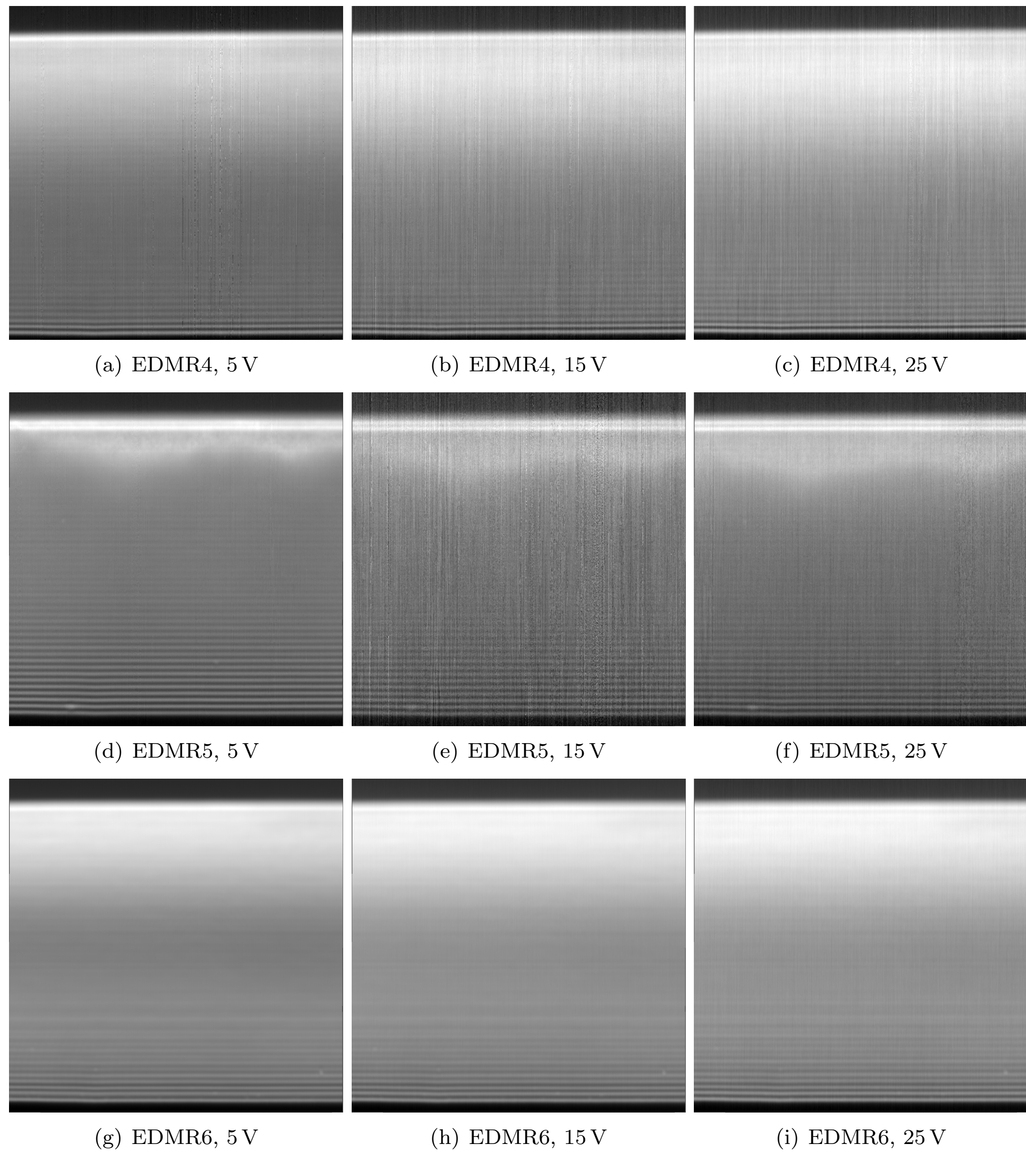

Figure 5.4: Behavior of proton implanted EDMR samples under reverse bias (5 V, 15 V and 25 V). (a-c) EDMR4, (d-f) EDMR5, (g-i) EDMR6.

Line scans on proton implanted samples

From the results of the diffusion length measurement on the reference sample EDMR8, which does not exhibit a proton implantation, one could conclude that measurements on the proton implanted samples, which exhibit an additional n+ layer near the pn-junction, will not deliver useful information: The decrease of the current outside the depletion region is already too sharp to extract the diffusion length for minority charge carriers properly and for the proton implanted samples it should be even sharper because of the additionally implanted n+ layer. However, as it was already seen in figure 5.4 the images show the unexpected result that beneath a narrow white stripe on the top of the images, which is the depletion region, a blurred white region occurs beyond it. For this reason line scans using the 1300 nm laser and the picoamperemeter were done. The result of a line scan on EDMR6, where the effect is strongest is shown in figure 5.5a, where in the y-axis the current and in the x-axis the distance to the pn-junction is plotted. The point of origin is set to the edged of the depletion region. The first three measurement values near zero show the fast decrease as it was expected. After that, however, the curve exhibits the shape of a density function. To explain this behavior one would have to perform additional experiments. A possible explaination would be that the 1300 nm laser can create minority charge carriers directly inside the proton doped region. Therefore, this region would have to exhibit states that can be excited with the laser beam energy of 0.92 eV (which is below the silicon band gap). The result would then be similar to a scan of the 1064 nm laser along a pn-junction parallel to the laser beam, where the curve gets blurred due to the broadening of the laser spot within the sample. As can be seen in 5.5b, the density function fits the measurement values. Another indication for this is that the signal was gathered with a laser power of only 2 %. The exact explaination of the behavior of these samples would require further analysis like absorption spectroscopy in the n+ region.

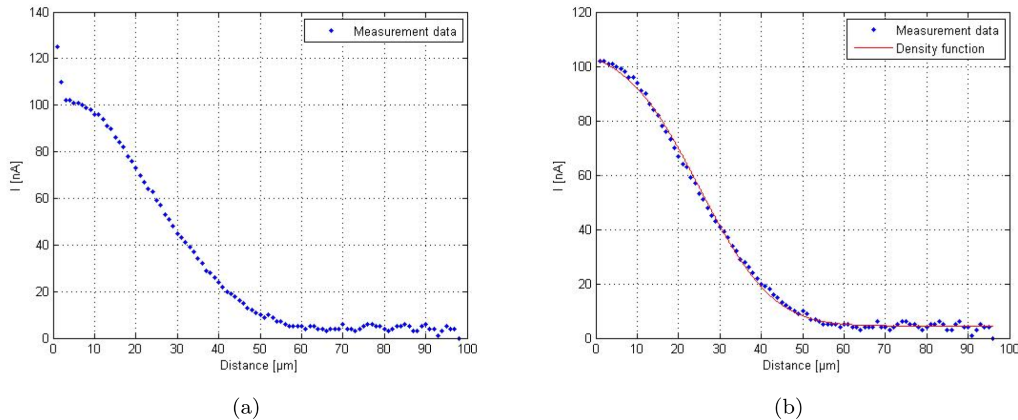

(a) (b)

Figure 5.5: Current versus distance in a linescan along EDMR6 (a). Fit of the density function to the curve (b).

5.2 P116

P116 is a diode which is additionally double proton implanted, which means that it exhibits a large pn-junction at about 80 μm and furthermore two implanted n-layers into the p-region, which leads to three more pn-juntions. In figure 5.6 the result of a line scan over a cross section of this structure is plotted. Image (a) shows the EBIC, image (b) the OBIC line scan, performed with the 1300 nm laser. EBIC exhibits a better spacial resolution. Therefore all transitions can be seen very well. Due to the spot size of the laser, the peaks at the junctions are wider in the OBIC measurements. The small peaks can hardly be resolved. Mostly the small peaks are overlaid by the most significant peak 80 μm away from the chip edge.

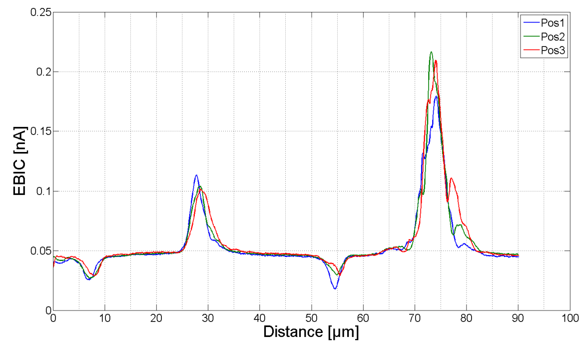

(a)

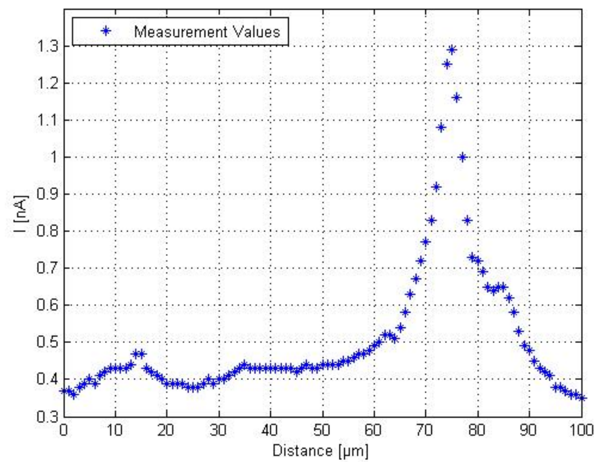

(b)

Figure 5.6: Comparison of a line scan along a cross section of a proton implanted sample. (a) EBIC data, (b) OBIC data.

Chapter 6

OBIC measurements on an EMCON diode

Similar to the experiments on the proton implanted EDMR samples previously described in chapter 5.1.1, measurements of the broadening of the depletion region when reverse bias is applied and also the estimation of the concentration of dopants were done on an emitter controlled (EMCON) diode.

An EMCON diode is characterized by an improvement in the reverse recovery time compared to common diodes [Sch06]. Bad reverse recovery times can come from the fact that in reality the charge carrier distribution inside a diode is not homogeneous. A higher carrier density in the peripheral zones of the pn-junction than at the edges (e.g. at the n^-n^+ interface) leads to the undesired reverse recovery behavior. In an EMCON diode this distribution is inverted so that the carrier concentration is higher at the n^-n^+ interface. This can be achieved by a reduction of the surface of the emitter by a change in its structure, or, like in the EMCON diode by the same emitter surface but a p-zone with high recombination. This is achieved by a reduction of the concentration of acceptors N_A. This leads to a higher density of minority charge carriers inside the p-region which increases the recombination and therefore reduces the charge carrier density.

The preparation of the sample and the execution of the experiment was done the same way as for the EDMR diode and is summarized in the appendix. It has to be considered that the sample is broken and ground during the preparation process. This will certainly affect the electrical properties of the device which influence the OBIC experiment. To be more precise, leakage currents will appear when the diode is reverse biased, differing from sample to sample in their level. For the EDMR8 diode those leakage currents were e.g. insignificantly low between 0 and 25V. For the EMCON sample, however, a significant leakage current already appeared right at the beginning. Figure 6.1 shows the OBIC images when the diode was reverse biased with 0 to 10V, showing the depletion region as white line on top of the image. Between 6 and 10V it can be observed that the edges at the transition from the space charge region to the substrate are not clearly defined and the structure cannot be resolved in a satisfying way anymore, an effect which is clearly caused by the leakage current. For the measurements of the depletion width, only measurement values beyond 5V were considered. Figure 6.2a shows the broadening of the depletion region due to the applied voltage, while in figure 6.2b one can see the values for the depletion width, estimated from graph (a), compared to the theoretical function (2.26). Due to the leakage current the aberration of the measured values is higher than for the EDMR diode. It is obvious that for a significant value for the doping concentration the leakage current should be as low as possible. However, the doping concentration can still roughly be approximated. Concentration of donors N_D:

$$N_D = 8.5 \cdot 10^{13}\ \text{cm}^{-3}$$

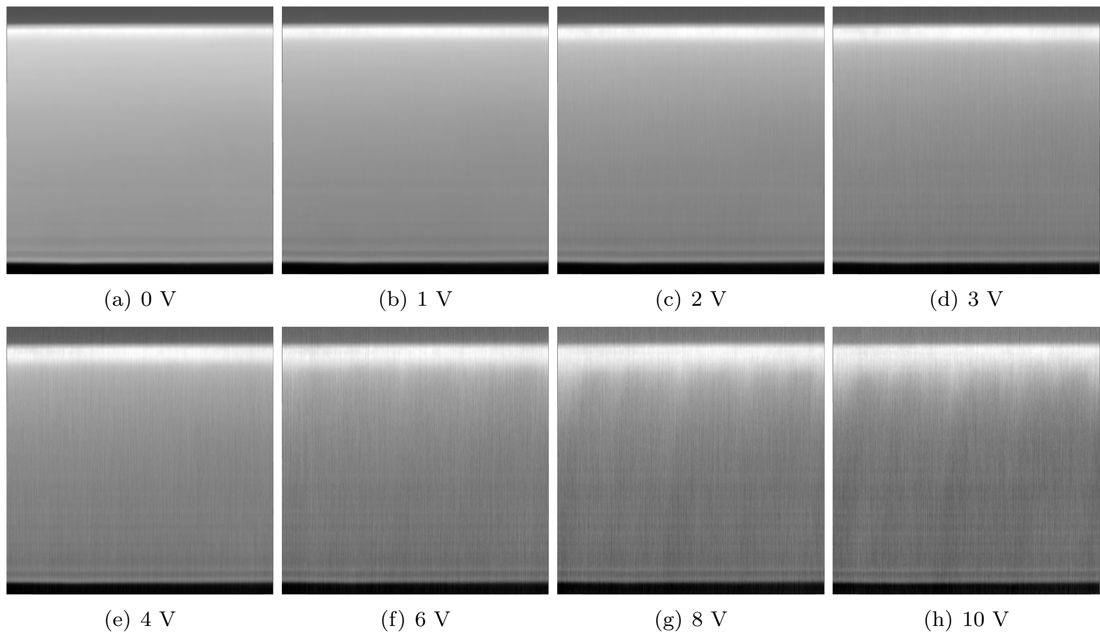

(a) 0 V (b) 1 V (c) 2 V (d) 3 V

(e) 4 V (f) 6 V (g) 8 V (h) 10 V

Figure 6.1: OBIC images demonstrating the broadening of the depletion region in an EMCON diode)

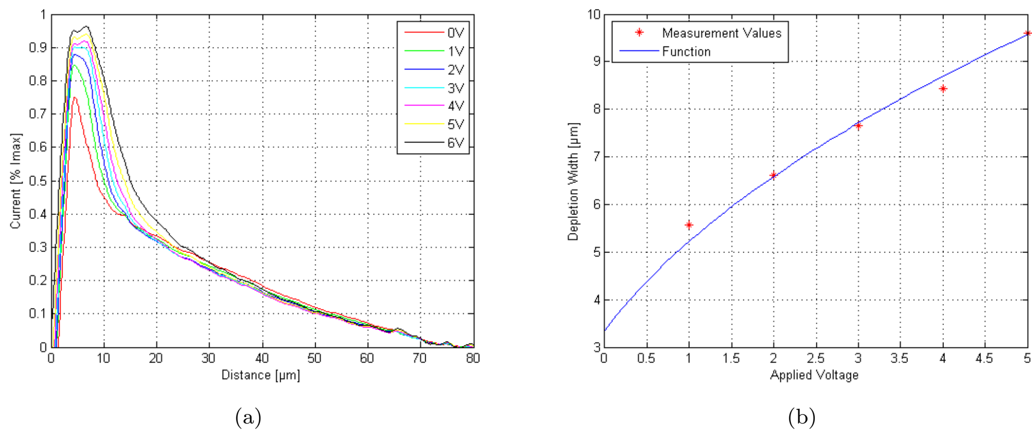

(a) (b)

Figure 6.2: (a) Broadening of depletion region (b) Depletion width as a function of voltage of and EMCON diode compared to calculated values using equation 2.26

Chapter 7

Structure visualization on various devices using OBIC

7.1 CoolMOS^{TM}

A CoolMOS^{TM} is a MOSFET conceived for high power applications. Compared to conventional MOSFETs (like e.g. the SFET described in 7.3) highly doped p-columns are placed beneath the p-body of the cells and connected to them. In between the columns an n$^-$ drift area is located. These columns are usually constructed by repeating steps of epitaxial growth of the n$^-$ layer and doping. This step by step process leads to the formation of 'bubbles' as will be seen in the OBIC images. The substrate is usually n^+ doped. The p-columns lead to a feature of the device designed to block high voltages (up to 1200V) as the columns will form a wide depletion region if the device is reverse biased as the depletion region of the columns will extend into the n^- region perpendicular to them and will combine with the depletion region of the neighboring columns. As the substrate is doped n^+ the broadening of the depletion region into the substrate will be lower. The thick depletion layer which can block high voltages is called a super-junction.

OBIC measurements were performed on CoolMOS^{TM} devices both from the backside and on cross sections. For the analysis, source and drain (front- and backside) were connected to the measuring instrument. Looking at the cross sections, the p-columns, which are acting as extended body, are revealed (figure 7.1). Figure 7.1 (a) shows the laser-, (b) the OBIC-image. In image (c) an overlay of a laser image and an OBIC image, where current values below a certain value were filtered out, was done.

Furthermore, OBIC analysis from the backside was done. For this purpose, the backside metallization was removed in the desired area. The 1064 nm laser was focused on the front layer through the silicon. To perform an analysis like this, the sample has to fulfill the properties discussed in chapter 2.

The results are shown in figure 7.3. 7.3 (a) shows the laser image taken when the laser was focused through the substrate onto the frontside. The OBIC images are shown in (b)-(f). The contours are becoming more sharp when the device is reverse biased. It is not possible to adjust the wafer fragment absolutely planar, which leads to intensity differences in the OBIC image, as the laser is not perfectly focused over the whole area. This leads to the dark stripe on top of the images. However, for both the analysis on cross sections and from the backside, the formation of the superjunction could not be revealed as the voltage of 25 V which is the maximum voltage that can be applied due to the tool parameters is not sufficient. If a very high voltage was applied, the red columns would combine to a continuous white area in the OBIC images. Figure 7.4 shows OBIC images from the backside of the alternative designed CoolMOS^{TM} at 0 V, 10 V

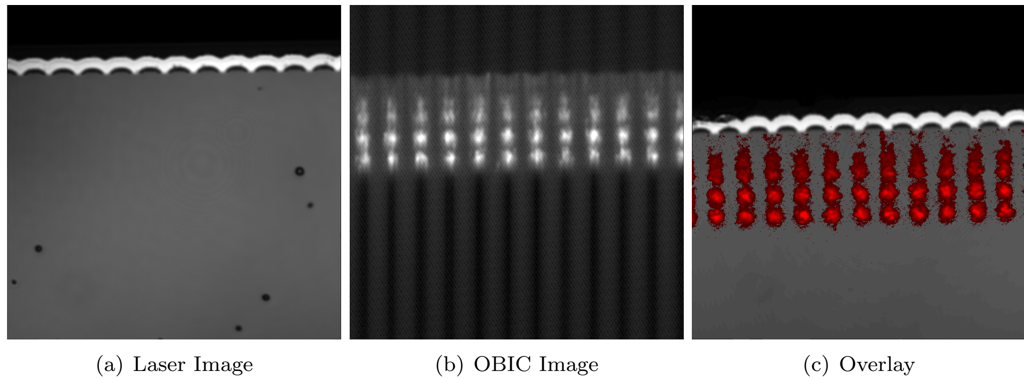
(a) Laser Image (b) OBIC Image (c) Overlay

Figure 7.1: OBIC measurement on a cross section of a CoolMos^{TM}.

and 25 V. The doped regions appear white.

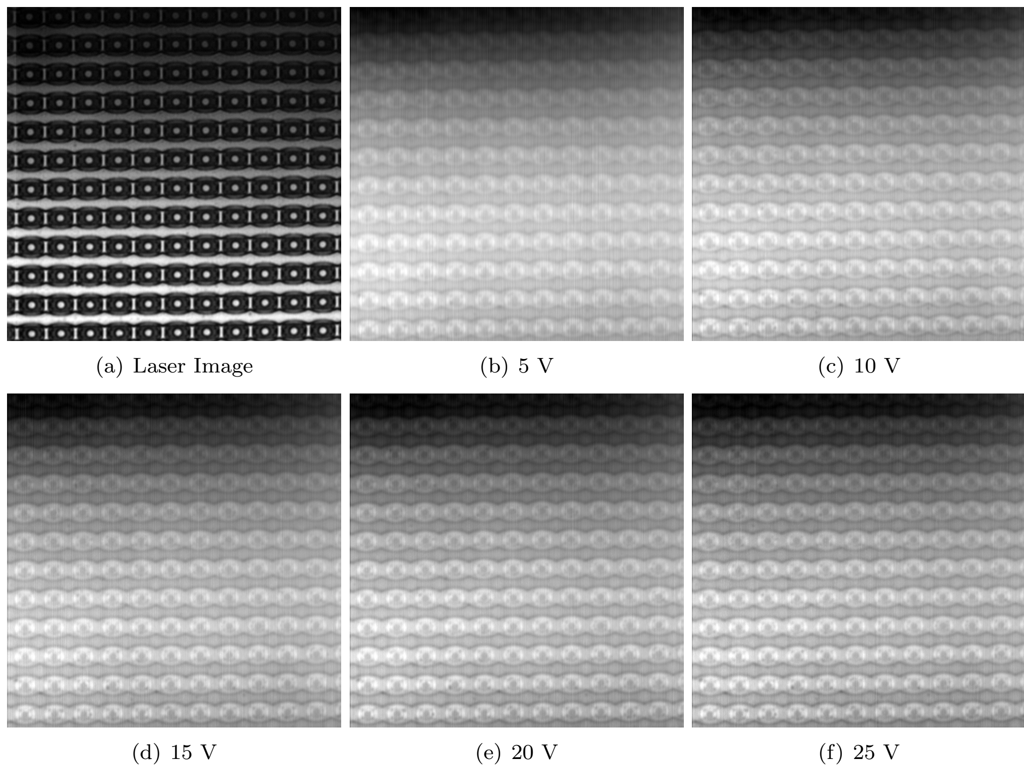
(a) Laser Image (b) 5 V (c) 10 V
(d) 15 V (e) 20 V (f) 25 V

Figure 7.2: Backside OBIC images of a CoolMos^{TM} (b-f) and laser image (a).

7.2 Insulated gate bipolar transistor (IGBT)

The structure of two different insulated gate bipolar transistors (IGBT) was visualized by preparing cross sections and performing OBIC analysis. The IBGTs are Infineon devices of the 3rd and 4th generation, respectively and therefore denoted IGBT3 and IGBT4. Figure 7.5 shows an optical image and an OBIC image of an IGBT3. The pn junctions between n-substrate and p-body, p-body and n-bulk and floating p-well and n-bulk can be seen very well, although electrical contacts are only applied on the front- and backside of the device. Of course, the most significant signal can be observed between n-source and p-body, which are directly connected to the frontside. Also for the other layers (Poly, FOX[1], ZWOX[2]) a current change can be seen.

Figure 7.6 shows an IGBT4 which exhibits an alternative design. As well as described for IGBT3, the structures can be resolved and indicated in the image. Similar to what was done on simple diodes (e.g. section 5.1.1), it is possible to apply voltage between front- and backside and monitor the behavior of the pn-junctions. Figure 7.7 shows this experiment and reveals the broadening of the depletion region. However, as before, the results strongly depend on the preparation of the sample or, more precisely, how high the leakage current caused by the cross section is. The leakage current is already quite high in the last image, so that no good images above 12V could be taken.

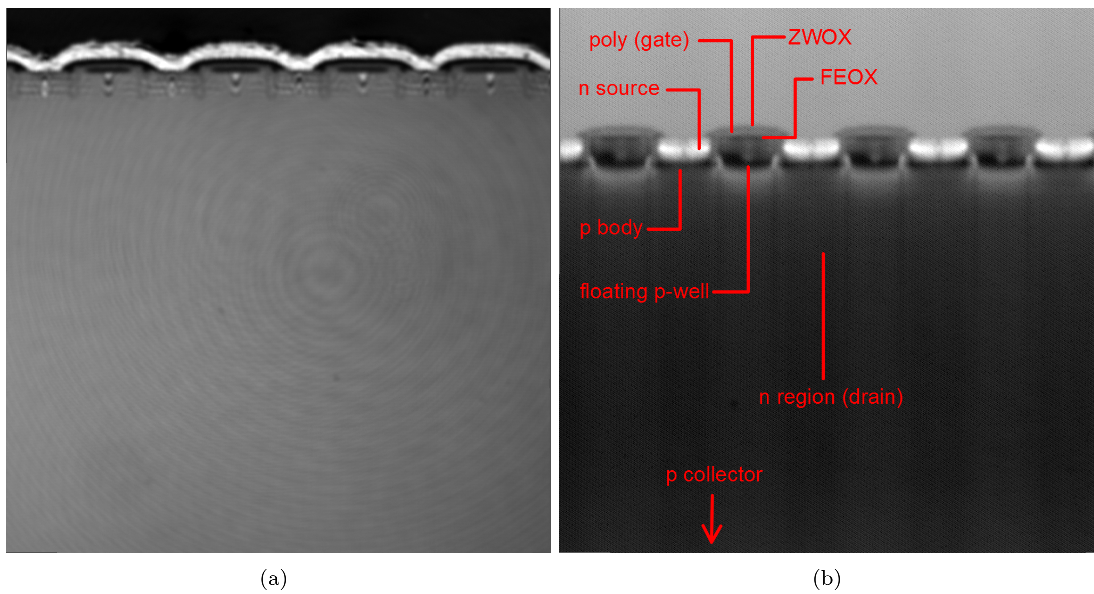

Figure 7.3: OBIC image of IGBT3 cross section (b) and laser image (a)

[1] Fieldoxide

[2] Interlayer Dielectric, 'Zwischenoxid'

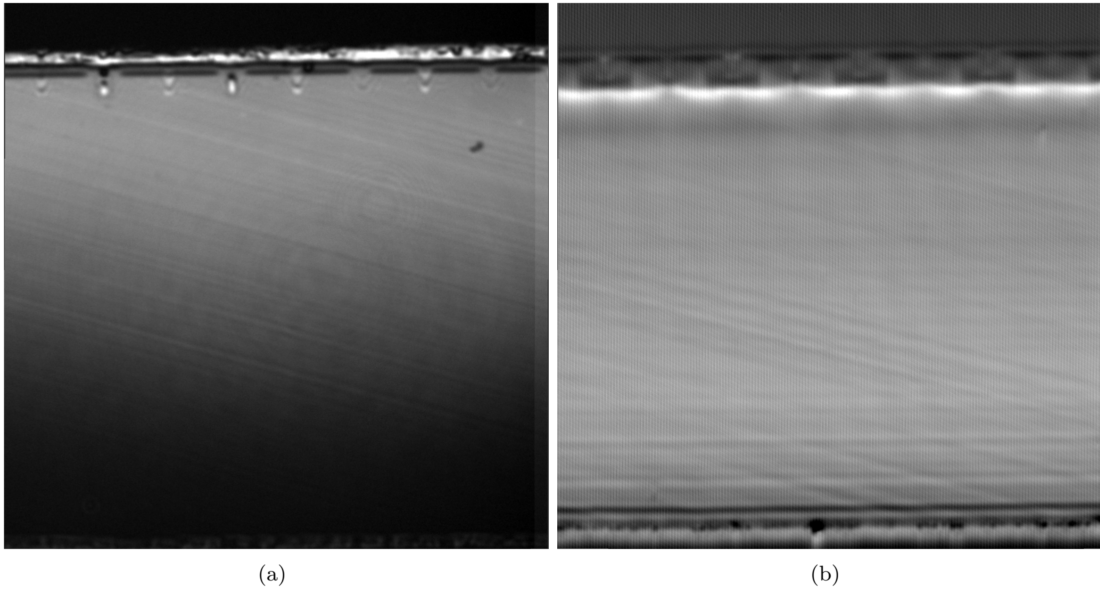

Figure 7.4: OBIC image of IGBT4 cross section (b) and laser image (a)

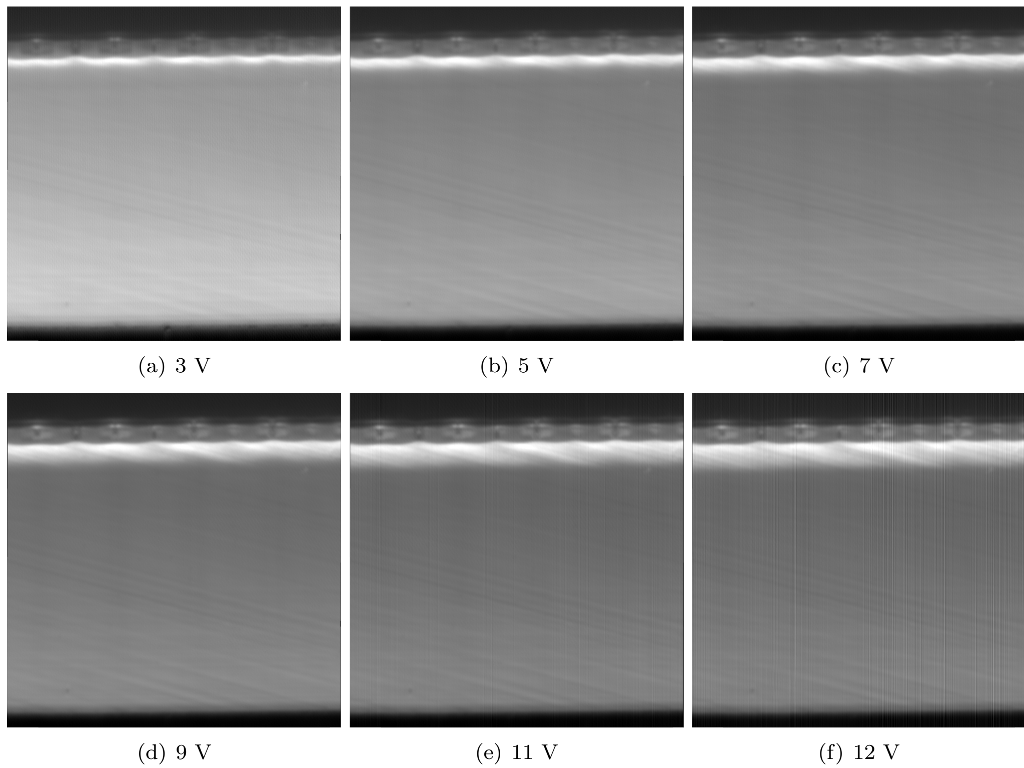

Figure 7.5: Broadening of the depletion region of the pn-junction between emitter and base in an IGBT

7.3 S-FET2

OBIC measurements were done on cross section of an S-FET2, as well as measurements from the backside through the substrate. The S-FET2 is a single chip field effect transistor. The chip is designed vertically, on the front side there is the source as well as the gate contact, on the backside the drain is placed. When turning the transistor on, current will flow from the front- to the backside. It exhibits a cell technology, which means that numerous cells, of which each is a fully functional single transistor but which are connected to act like one, are arranged.

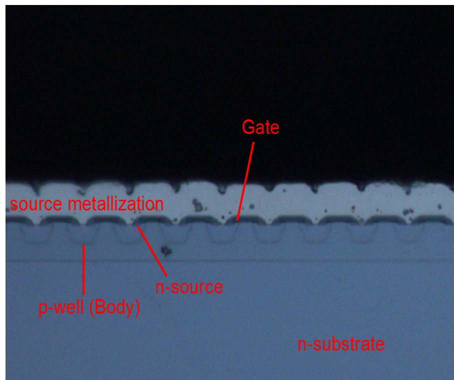

Figure 7.6: Cross section of an S-FET2

The design of every cell is easily explained: circular p-wells (body) are doped into the n-substrate (drain) at first, while in a later step an n-ring, which later will act as source, is doped into the p-wells. The p-wells are acting as body. Looking at it from the top would reveal a p-area (body contact) in the center, surrounded by an n-ring (source), surrounded by another p-ring (body), surrounded by the n-substrate (drain). The p-well and the n-ring in the center are connected to the frontside metal. Above the p-ring between source and the substrate (drain), the gate is placed. Figure 7.8 shows an optical image of a cross section of an S-FET2, where a pn-etch was done - a method with which it is possible to visualize p- and n-areas on a chip, using the fact that the etch affects p and n areas in a different way. In contrast to an OBIC measurement, however, it is not possible to reveal buried layers or analyze devices where a voltage is applied. The described body-, source-, gate- and drain areas are marked in the image. The p-wells shall be visualized both from the front and from the backside. For the front side measurements, cross sections of several chips were prepared. The investigated chips exhibit a front- and backside metallization, which made it easy to connect: One metering needle had to be connected on the front-, the other one on the backside, which corresponds to source and drain.

Figure 7.9 shows a laser image and an overlay (OBIC + laser) image of a cross section of an S-FET2. One can spot the p-wells. An OBIC image through the backside was taken as well. It is shown, that the data from OBIC images taken with the PHEMOS-1000 can be used to receive three dimensional images over a certain area, where the value in z-direction indicates the current value. This is shown in image 7.10. It can be observed, that the cells are hexagonal arranged over the chip. The highest current value is measured when the laser scans over the center of a the p-well. The image exhibits a slight slope which is due to tool parameters of the PHEMOS-1000 and the fact that the stage is not perfectly plane. The p-wells exhibit a circumference of only about 5μm, which is only slightly above the laser spot size of about 3μm. A close look into the p-wells shows a slightly drop in the current around the p-wells, which can be related to the source ring. However, it can hardly be resolved as the width of the ring is in the range of the laser spot size.

As for the other measurements of cross sections and backside images, the cross section images were obtained with the 1300 nm-, the backside images with the 1064 nm laser. It should not go unnoticed, that the images through the backside with the 1064 nm laser exhibit an advantage of OBIC over EBIC, as it can the executed through the backside substrate, while for EBIC analysis the backside of the device would have to be thinned at first.

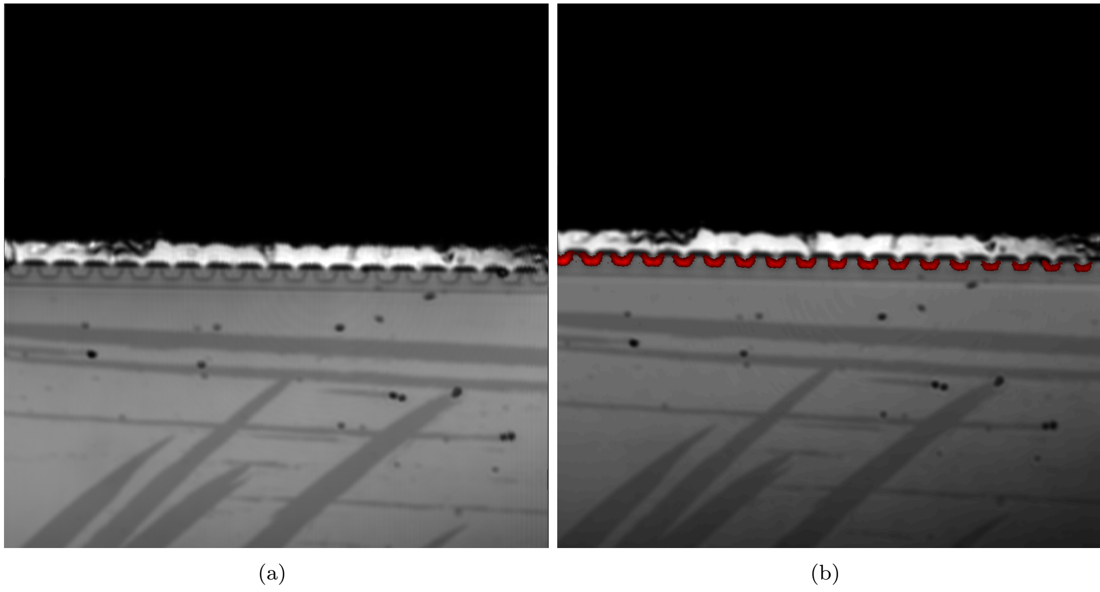

(a) (b)

Figure 7.7: OBIC image of S-FET2 cross section (b) and laser image (a)

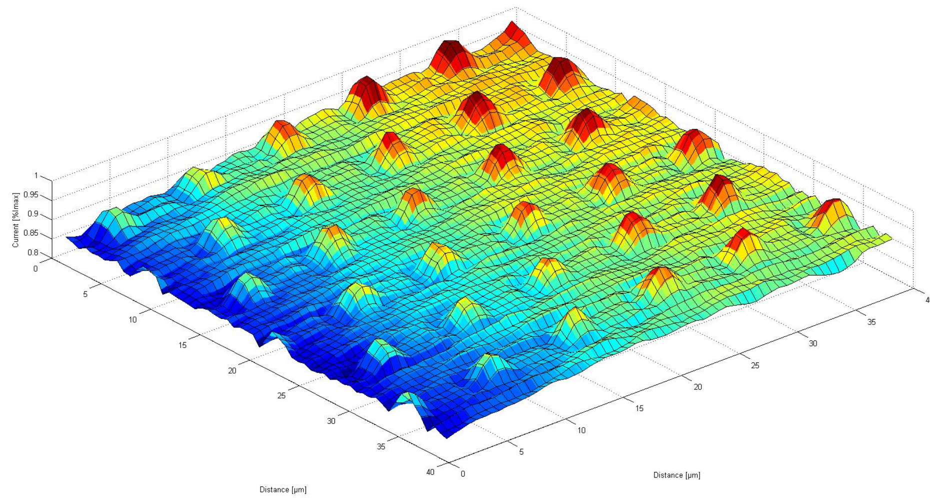

Figure 7.8: 3D Plot of an S-FET2 OBIC image from the backside

7.4 S-FET3

It has been previously mentioned that the 1064 nm Laser in the PHEMOS-1000 is originally included into the system to obtain a laser images when doing photo emission microscopy (PEM) from the backside in failure analysis to relate an emission spot to a structure on the chip. However, if the substrate exceeds a certain thickness or exhibits a doping concentration that is too high, it sometimes is not possible to obtain such an image. As a consequence, the device then has to be thinned by e.g. mechanical grinding or plasma etching which takes an additional, time consuming, working step which has the risk that, in the worst case, the device gets damaged and/or the failure disappears or cannot be revealed any more. Sometimes it is possible to take an OBIC image from the backside when it is not possible to get a laser image. An example is shown in this section. It was not possible to obtain a laser image on an S-FET3, another version of a field effect transistor like the one that has been already shown in section 7.3, which, however, is a further development and doesn't consist of cells, but exhibits trenches. Figure 7.11 shows that, even though it was not possible to obtain a laser image, it was possible to obtain an OBIC image. Images (a), (b) and (c) show the OBIC image with 5x, 20x and 100x magnification. On images (a) and (b) the gate can be observed at the left side of the chip. On the 100x detail image even the trenches can be observed perpendicular to the gate. However, if one wants to overlay the received OBIC image with an image that shows a PEM spot later, the equipment has to be calibrated exactly. This is absolutely necessary, especially when further physical analysis, e.g. focused ion beam (FIB) analysis, are done on the chip to investigate the correct position. If this method is applicable varies from sample to sample. It is clear that, if the thickness of the substrate is extraordinary high or the doping concentration is so high that the beam gets totally absorbed, it will not be possible to avoid the thinning step.

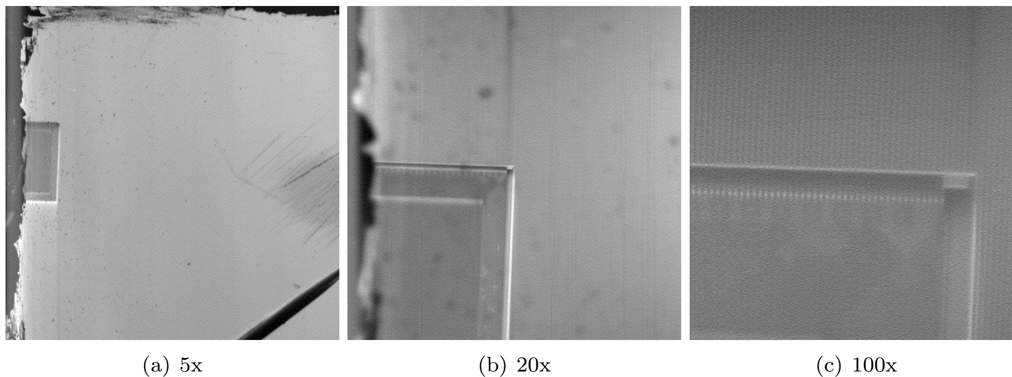

(a) 5x (b) 20x (c) 100x

Figure 7.9: OBIC Measurement on an S-FET3 from the backside

Chapter 8

Conclusive discussion and perspectives

8.1 Structural analysis of semiconductor devices

The OBIC experiments, executed with the PHEOMS-1000 by Hamamatsu, showed that both the 1064 nm and the 1300 nm laser - although its energy is beyond the silicon band gap - can be used to visualize structures in silicon semiconductor devices by inducing a current, taking advantage of the photovoltaic effect. For the 1300 nm laser, the effect was explained by surface states and therefore charge carrier creation near the surface. As the lasers differ in their interaction with the illuminated material the examined structure and the parameters which shall be obtained determine which laser is more suitable for a certain experiment. Considerations which laser should be chosen were made in 3.2.2.

Experiments to determine structures were done on the sensor chip of a tire pressure monitoring system (TPMS) in chapter 4, on diodes in chapter 5, on MOSFETs in the chapters 7.1, 7.3 and 7.4 and on IGBTs in chapter 7.2.

The measurements on the TPMS showed that both lasers are suitable to visualize the p-doped structures at the surface and buried in the n-silicon (4.1). Furthermore the 1300 nm laser exhibits a depth sensitivity to pn-junctions close to the surface as it creates charge carriers mainly in this region. This was shown on a p-well of a surface conductor, where the value of the measured current was determined by the distance of the pn-junction to the surface (4.1.1). However to show this behavior qualitativ the system would have to deliver the actual current value and the surface of the device would have to be prepared completely planar to avoid side effects. In contrast, the 1064 nm laser did not show this kind of depth sensitivity as the creation of charge carriers is not limited to the surface. However, it delivers a possibility to determine the depth of pn-junctions buried deep in the silicon. This is shown in 4.1.1, where the position of the p-doped structure of an acceleration sensor in the substrate was determined from the backside.

In other devices like MOSFETs and IGBTs, the main matter of interest lies in the vertical structures, these are mainly seen in cross sections of the chips. In the case of cross sections it could be found that the use of the 1064 nm laser is not productive. However, the advantages of the 1300 nm laser were used to visualize the desired regions. Chapter 7 shows structures of several MOSFETs and IGBTs which are visualized on cross sections. Furthermore, a demonstration for experiments from the backside was given in this chapter. It was shown that the high transmittance for the 1064 nm laser makes it possible to take OBIC images also for thick substrates. This could be useful not only to localize failures directly with this method but also as additional possibility in backside failure analysis methods like photo emission microscopy to

relate a received spot, which indicates an irregularity, to a certain position on the chip for further analysis (7.4).

It was demonstrated in 5.1.1 and 6 that reverse biasing a sample during the OBIC measurement allows to a visualization of the broadening of the depletion region of pn-junctions. It was shown that a set of measurements of the depletion width at constantly increased reverse bias can be used to determine the concentration of dopants if the sample fulfills the requirement that the extension of the depletion region is large enough to be resolved. If one region is furthermore doped by magnitudes higher than the other region the experiment is simplified as the depletion region spreads into the lightly doped region only. If both sides are doped with similar concentrations, the doping concentration for both regions can be measured. Moreover these experiments are limited to the maximum voltage value that can be applied with the PHEOMS-1000. It could be seen that, if the experiment is done on cross sections, the achievable quality of the results strongly depends on the preparation of the samples and the choice of the measurement parameters.

8.2 Determination of charge carrier properties

From OBIC linescans, the diffusion length of minority charge carriers can be obtained. Experiments to determine the parameter were done on a p-well of a TPMS in 4.2 and on a cross section of a diode in 5.1.2.

Diffusion length measurements were done using an external connected picoamperemeter and by the extraction of data from OBIC images provided by the PHEMOS-1000. For the extraction from the images a software program was designed. Both methods were compared in 4.2.1. They show that both methods deliver similar results. However, as only the use of the external picoamperemeter delivers current values directly, it was recommended to use this method for further analysis.

Line scans at the same position of a p-well of a TPMS sensor chip were done to determine the influence of the used laser on the obtained diffusion length (4.2.2). It was shown that the estimated value is independent of the wavelength used in this experiment. Surface recombination plays an important role for diffusion length measurements. The measurement results were evaluated both for infinite and negligible surface recombination rate. As the 1064 nm laser creates charge carriers throughout the whole substrate and the result for the diffusion length doesn't differ to the measurement with the 1300 nm laser, the surface recombination rate was neglected. As the diffusion length is usually not constant over the whole material, diffusion lengths estimated from two additional line scans were compared to the first one (4.2.4). Furthermore a line scan was done with various intensities in 4.2.3. As the laser spot is not perfectly sharp the graphs showed a kink. In 4.2.5 this factor was considered and a function that includes it was derived. The plot of the function fit the measurement results.

While the specific design of the TPMS sensor chip was very suitable for OBIC measurements using the available lasers the measurements on cross sections of diodes did not deliver comparable good results. Because of the structure only the 1300 nm laser could be used. Through the preparation process the surface is less planar and exhibits more defects. Therfore, the measrued diffusion current was very low and could hardly be measured. In 5.1.2 the result of a diffusion length measurement was shown. The low current values lead to a very noisy signal. The examination of the proton implanted samples delivered unexpected results that were summarized in 5.1.3. The graph exhibited the shape of a density function as it would be observed if a laser of a Gaussian intensity distribution which can create charge carriers by interband absorption scans over a pn-junction. The behavior could not be explained qualitative but it was suspected that

the 1300 nm can excite electrons directly in this region which then are collected by the space charge region nearby. However, the behavior of those samples would require further analysis with additional methods.

In section 5.2 line scans on a double proton implanted sample were done and compared to an EBIC line scan at the same device. It could be seen that due to the lower spacial resolution, the additional pn-junctions can be hardly seen using OBIC. For such experiments EBIC measurements should be preferred.

In summary it can be said that the available laser can be used to determine the diffusion length if devices exhibit structures like they are found on the sensor chip. The experiments on cross sections of diodes showed limitations for this method. These could be solved by the use of a laser with higher energy to achieve a lower penetration depth. Then, a higher current could be induced and the same time the spot size related blurring of the images could be reduced.

Appendix

References

[Ash88] *Solid State Physics*, N.W. Ashcroft and N.D. Mermin, 1988

[Bar99] *FLIP-chip and 'backside' techniques, Microelectronics Reliability 39*, D.L. Barton, K. Bernhard-Hfer, E.I. Cole Jr., 1999

[Ein05] *Ueber einen die Erzeugung und Verwandlung des Lichtes betreffenden heuristischen Gesichtspunkt, Annalen der Physik*, Albert Einstein, 1905

[Fac13] *Spacial resolved measurements of charge carrier properties in proton doped silicon*, M. Facinelli, 2013

[Fl090] *Determination of the spatial variation of the carrier lifetime in a proton-irradiated Si n^+-n-p^+ diode by optical-beam-induced current measurements*, T. Flohr, R. Helbig, 1990

[Glo10] *Expanding the scope of laser stimulation techniques for functional analysis and reliability of semiconductor devices by in-depth investigation of the optical interaction with the devices*, Arkadiusz Glowacki, 2010

[Hab06] *Moderne Fehleranalyse Methoden: Untersuchungen zur Wirkung des 1064/1320 nm Lasers an ausgewaehlten Strukturen*, S. Habicht, 2006

[Hal52] *Electron-hole recombination in germanium*, R.N. Hall, 1952

[Hec02] *Optics, Fourth Edition*, Eugene Hecht, 2002

[Kit04] *Introduction to Solid State Physics, Eighth Edition*, Charles Kittel, 2004

[Ong94] *A direct and accurate method for the extraction of diffusion length and surface recombination velocity from an EBIC line scan*, V.K.S. Ong, J.C.H. Phang and D.S.H. Chan, 1994

[Pan10] *Optical Processes in Semiconductors, Second Edition*, Jacques I. Pankove, 2010

[Pie96] *Semiconductor Device Fundamentals*, Robert F. Pierret, 1996

[Sch06] *Leistungselektronische Bauelemente, 2. Auflage*, Dierk Schroeder, 2010

[Sho52] *Statistics of the recombinations of holes and electrons*, W. Shockley, W.T. Read, 1952

[Sin01] *Semiconductor Devices, Basic Principles, Edition*, Jasprit Singh, 2001

[Sor87] *Electrooptical effects in silicon, IEEE Journal of Quantum Electronics*, R.A. Soref, B.R. Bennett, 1987

[Sze85] *Semiconductor Devices Physics and Technology*, S.M. Sze, 1985

List of figures and tables

List of figures

2.1 Transmission through silicon for various doping concentrations
2.2 Intensity distribution of a Gaussian beam, broadening in the propagation direction
2.3 States localized within the band gap of silicon
2.4 Generation- and recombination process in a semiconductor
2.5 Scheme of a pn-junction
2.6 Photovoltaic effect in a pn-junction
2.7 OBIC measurement
2.8 Scheme of a MOSFET
2.9 Scheme of an IGBT
3.1 PHEMOS-1000 overview
3.2 PHEMOS-1000 measurement principle
3.3 Laser beam interactions with different structures
3.4 Measurements of the laser power on a parallel pn-junction
3.5 PHEMOS-1000 scan modes
3.6 PHEMOS-1000 objective system detail view
3.7 Ambandoned and embedded cross section of a chip
4.1 Optical overview image of a TPMS sensor chip
4.2 Overview laser- and OBIC images of a TPMS sensor chip
4.3 Threedimensional overview OBIC image of a TPMS sensor chip
4.4 Detail OBIC images of an acceleration sensor
4.5 Detail OBIC images of a pressure sensor
4.6 Scheme of a buried p-well in n-substrate
4.7 Overview OBIC image of a conducting p-well
4.8 OBIC images demonstrating the arising of current maxima at the edges of a p-well
4.9 OBIC images showing no current maxima for the 1064 nm laser
4.10 Overview OBIC image of a TPMS sensor chip taken through the backside
4.11 Edge of a broken wafer with sensor chips
4.12 Determination of z-position of an acceleration sensor
4.13 Line scan position marked in a laser image
4.14 Line scan executed with picoamperemeter, extracted data from an OBIC image
4.15 Detail position for a diffusion length measurement
4.16 Comparison of methods to execute diffusion length measurements
4.17 Line scans at the same position using the 1300 nm and the 1064 nm laser
4.18 Demonstrating the influence of the laser on diffusion length measurements
4.19 Line scans at various intensities
4.20 Line scans at various positions
4.21 Plot including the spot size related current
5.1 Demonstrating the broadening of the depletion region under reverse bias
5.2 Calculation of the doping concentration
5.3 Diffusion length measurement on EDMR8
5.4 EDMR4, EDMR5 and EDMR6 under reverse bias
5.5 Line scan along EDMR6

5.6 Line scan along P116
6.1 Broadening of the depletion region under reverse bias on an EMCON diode
6.2 Determination of concentration of dopants
7.1 OBIC on a CoolMOS^{TM} cross section
7.2 OBIC of a cross section of a differently designed CoolMOS^{TM}
7.3 OBIC on a CoolMOS^{TM} through the backside
7.4 OBIC on a CoolMOS^{TM} through the backside (alternative)
7.5 OBIC on a cross section of an IGBT3
7.6 OBIC on a cross section of an IGBT4
7.7 Broadening of the depletion region (reverse bias), visualized on an IGBT
7.8 Pn-etch on a cross section of an S-FET2
7.9 OBIC on a cross section of an S-FET2
7.10 3D plot of an OBIC image taken through the backside of an S-FET2
7.11 OBIC images of an S-FET3 in 5x 20x and 100x magnification through the backside

List of tables

3.1 Maximum laser power of 1300 nm and 1064 nm laser
3.2 Microscope ojectives and laser characteristics
3.3 Current amplifier characteristics

List of measurement parameters

OBIC measurements with external connected picoamperemeter

Fig	Sample	FS/BS	Laser	Power	OL	Mode	Voltage
3.4a	TPMS	FS	1064 nm	0-50 %	100x	Point	0 V
3.4b	TPMS	FS	1064 nm	0-2 %	100x	Point	0 V
3.4c	TPMS	FS	1300 nm	30-100 %	100x	Point	0 V
4.14a	TPMS	FS	1064 nm	1.5 %	100x	Point	0 V
4.16a-b	TPMS	FS	1064 nm	2 %	100x	Point	0 V
4.17a	TPMS	FS	1064 nm	1.5 %	100x	Point	0 V
4.17b	TPMS	FS	1300 nm	100 %	100x	Point	0 V
4.18a-b	TPMS	FS	1064 nm	1.5 %	100x	Point	0 V
4.18a-b	TPMS	FS	1300 nm	100 %	100x	Point	0 V
4.19a-b	TPMS	FS	1064 nm	50 %	100x	Point	0 V
4.19c-d	TPMS	FS	1064 nm	75 %	100x	Point	0 V
4.19e-f	TPMS	FS	1064 nm	100 %	100x	Point	0 V
4.20a,c	TPMS	FS	1300 nm	100 %	100x	Point	0 V
4.20b,d	TPMS	FS	1300 nm	100 %	100x	Point	0 V
4.21	TPMS	FS	1300 nm	100 %	100x	Point	0 V
5.3a-b	EDMR	FS	1300 nm	50 %	100x	Point	0 V
5.5a-b	EDMR	FS	1300 nm	2 %	100x	Point	0 V
5.6b	P116	FS	1300 nm	100 %	100x	Point	0 V

PHEMOS-1000 OBIC images measurement parameters

Fig	Sample	FS/BS	Laser	Power	OL	CA	Speed	Frames	Voltage
4.2b	TPMS	FS	1300 nm	10 %	5x	HS	16	2	0 V
4.2c	TPMS	FS	1300 nm	10 %	5x	HS	16	2	10 V
4.3	TPMS	FS	1300 nm	10 %	5x	HS	16	5	10 V
4.4a	TPMS	FS	1300 nm	20 %	20x	HS	16	2	10 V
4.4b	TPMS	FS	1300 nm	100 %	100x	HS	16	2	10 V
4.5b	TPMS	FS	1300 nm	20 %	100x	HS	16	2	10 V
4.7b	TPMS	FS	1300 nm	100 %	100x	HS	16	2	14 V
4.8a-h	TPMS	FS	1300 nm	30 %	100x	HS	16	3	0-14 V
4.9a-c	TPMS	FS	1064 nm	1.6 %	100x	HS	16	3	0-14 V
4.10b	TPMS	BS	1300 nm	100 %	5x	HS	16	10	14 V
4.10c	TPMS	BS	1300 nm	100 %	20x	HS	16	10	14 V
4.12a-i	TPMS	BS	1064 nm	5 %	10x	HS	16	1	0 V
4.13	TPMS	FS	1064 nm	1.6 %	5x	HS	16	2	0 V
5.1	EDMR8	FS	1300 nm	100 %	100x	HS	16	2	4-25,V
5.2a-b	EDMR8	FS	1300 nm	100 %	100x	HS	16	2	0-25,V
4.16c-d	TPMS	FS	1064 nm	2 %	100x	HS	16	2	0 V
5.4a-c	EDMR4	FS	1300 nm	20 %	100x	HS	16	2	5-25,V
5.4d-f	EDMR5	FS	1300 nm	100 %	100x	HS	16	2	5-25,V
5.4g-i	EDMR6	FS	1300 nm	10 %	100x	HS	16	2	5-25,V
6.1	EMCON	FS	1300 nm	100 %	100x	S	16	2	0-10,V
6.2	EMCON	FS	1300 nm	100 %	100x	S	16	2	0-10,V
7.1	CoolMOS	FS	1300 nm	100 %	100x	HS	16	3	0,V
7.2a	CoolMOS	FS	1300 nm	100 %	20x	S	72	1	0,V
7.2b	CoolMOS	FS	1300 nm	100 %	100x	S	72	1	0,V
7.3	CoolMOS	BS	1064 nm	1.8 %	100x	HS	16	2	5-25,V
7.4	CoolMOS	BS	1064 nm	2 %	100x	HS	16	2	0-25,V
7.5b	IGBT3	FS	1300 nm	100 %	100x	HS	16	2	0,V
7.6b	IGBT4	FS	1300 nm	100 %	100x	HS	16	3	0,V
7.7a-f	IGBT4	FS	1300 nm	100 %	100x	HS	16	3	0-12,V
7.9b	S-FET2	FS	1300 nm	100 %	100x	HS	8	5	0,V
7.10	S-FET2	BS	1064 nm	100 %	100x	HS	8	5	0,V
7.11a	S-FET3	BS	1064 nm	10 %	5x	HS	16	2	25,V
7.11b	S-FET3	BS	1064 nm	40 %	20x	HS	16	2	25,V
7.11c	S-FET3	BS	1064 nm	100 %	100x	HS	16	2	25,V

SRP-Data for EDMR Samples

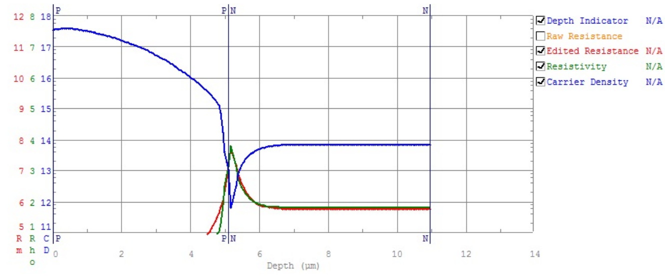

(a) EDMR6

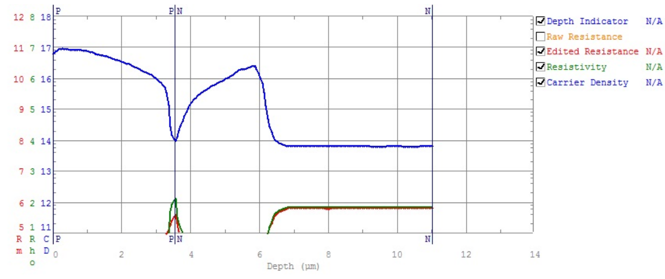

(b) EDMR4

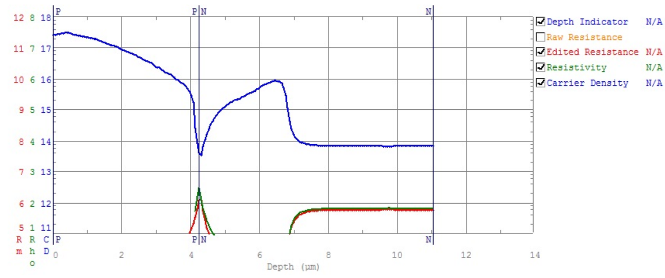

(c) EDMR5

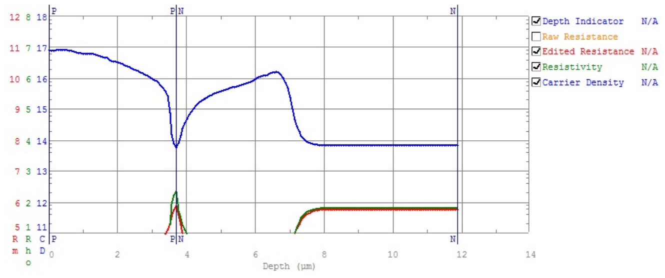

(d) EDMR6